Iowa State University Digital Repository

1976

Nonlinear analysis of reinforced concrete beams, beam-columns and slabs by finite elements

Kadambi Ramaswami Rajagopal
Iowa State University

www.manaraa.com

76-18,288

RAJAGOPAL, Kadambi Ramaswami, 1943-
  NONLINEAR ANALYSIS OF REINFORCED CONCRETE
  BEAMS, BEAM-COLUMNS AND SLABS BY FINITE
  ELEMENTS.

  Iowa State University, Ph.D., 1976
  Engineering, civil

Nonlinear analysis of reinforced concrete beams,

beam-columns and slabs by finite elements

by

Kadambi Ramaswami Rajagopal

A Dissertation Submitted to the

Graduate Faculty in Partial Fulfillment of

The Requirements for the Degree of

DOCTOR OF PHILOSOPHY

Department: Civil Engineering
Major: Structural Engineering

Approved:

Signature was redacted for privacy.

In Charge of Major Work

Signature was redacted for privacy.

For the Major Department

Signature was redacted for privacy.

For the Graduate College

Iowa State University
Ames, Iowa

1976

TABLE OF CONTENTS

LIST OF FIGURES

LIST OF TABLES

LIST OF SYMBOLS

a	x dimension of the finite element
a_{ij}, a'_{ij}	elements of the compliance matrix in the material modeling
A_s	area of the steel reinforcement per inch width of the composite layer
b	y dimension of the finite element
c_{ij}, c'_{ij}	elements of the constitutive matrix in the material modeling
C	matrix relating nodal displacements to the generalized displacement parameters
d	total displacement gradient matrix
$^i d$	total displacement gradient matrix at the ith displacement configuration
dA	elemental area
dv	elemental volume
D	matrix relating displacement gradients to the generalized displacement parameters
E_0	initial tangent modulus of concrete
E_s^c	secant tangent modulus of concrete at the point of maximum stress in the Saenz's curve
E_i	tangent modulus of concrete in the ith principal direction
E_s	tangent modulus of steel reinforcement
f'_c	cylinder strength of concrete
f_t	tensile strength or the modulus of rupture of concrete
G_{12}, G'_{12}	shear modulus of concrete
h_j, hm_j, h_{j+1}	jth layer distances from the middle surface

H_i	symmetric matrix used to form the nonlinear part of the strain-displacement relationships
K_0	basic stiffness matrix of the element
K_T	tangent stiffness matrix of the element
$\hat{K}_0$	matrix used in the generation of K_0
K_σ	the initial stress matrix of the element
$\hat{K}_\sigma$	matrix used in the generation of K_σ
K_D	the initial displacement matrix of the element
$\hat{K}_1$, K_1, $\hat{K}_2$, K_2	matrices used in the generation of K_D
K1	matrix used as work space in the generation of stiffness matrices
L_i	matrix used to form the linear part of strain-displacement relationships
M_x, M_y	bending moment per unit width in the x and y directions respectively
M_{xy}	twisting moment per unit width
N_x, N_y	normal force per unit width in the x and y directions respectively
N_{xy}	shearing force per unit width in the direction of y axis perpendicular to x axis
P	applied nodal loads
r	nodal displacements
R	nodal loads in equilibrium with the internal stresses
R_{ic}	factor used in calculating equivalent uniaxial failure strains for concrete
t_j	thickness of the jth layer
T, $\bar{T}$	transformation matrices
u, v, w	displacements in the x, y and z directions respectively

$u_{,x}$, $u_{,y}$ etc.	lower case subscript following a comma denotes partial differentiation, with the subscript indicating the coordinate with respect to which the quantity is differentiated
z	distance from the midsurface of the element
α	the generalized displacement parameters
α_c	ratio of the principal stress, $\dfrac{\sigma_1}{\sigma_2}$
δ	symbol denoting virtual quantities
$\triangle$	symbol denoting incremental quantities
ϵ_i, ϵ_i'	ith strain component in the element and inclined axes respectively
${}^1\epsilon_i$, ${}^2\epsilon_i$	ith strain component in the displacement configuration 1 and 2 respectively
ϵ_i^L, ϵ_i^{NL}	linear and nonlinear ith strain component respectively
ϵ_{iu}	equivalent uniaxial strain in the ith direction
ϵ_{ic}	failure equivalent uniaxial strain in the ith direction
ϵ_{cu}	failure uniaxial strain
θ	angle measured counterclockwise from the element x axis to the axis under consideration
ν_i	Poisson's ratio in the ith principal direction
ν	effective Poisson's ratio
σ_i, σ_i'	ith stress component in the element and inclined axes respectively
σ_i^{ex}	excess ith stress component

CHAPTER 1. INTRODUCTION

General

Ultimate strength design of structures which includes postelastic effects has gained importance in recent years. Ultimate strength design of reinforced concrete building frames and slabs is based on semi-empirical methods using results from extensive laboratory testing programs. Reinforced concrete is also beginning to be used in special structures such as nuclear containment structures and pressure vessels. Stringent safety requirements of such special structures have given additional incentives to the development of accurate analytical methods which can predict the behavior of reinforced concrete structures from zero to failure load.

An accurate analysis of reinforced concrete structures is complicated by a number of factors. The material properties of concrete is an area that is still not well understood. As an example, there is no universally accepted failure criterion for concrete for a general state of stress. The inherent variability of concrete, its cracking, creep, and shrinkage behavior, nonhomogenous character and the complex composite action between the steel reinforcement and the concrete are some additional complicating factors. Difficulties in analysis procedures are compounded when realistic boundary conditions and loading history are considered. Thus the only practical approach to a realistic nonlinear analysis of

reinforced concrete structures is the use of approximate
methods rather than a rigorous approach using continuum
mechanics.

The success of the finite element method in solving com-
plex linear elastic problems is well known. A great deal of
progress has taken place in recent years in the application
of the finite element method as an analytical tool. Many
applications of the finite element method considering material
and geometric nonlinearity in the static and dynamic analysis
of structures can be found in recent literature (1). In the
last eight years, the finite element method has also been
applied to the analysis of reinforced concrete structures.

Previous Work

One of the early applications of the finite element
method to the study of reinforced concrete structures was made
by Ngo and Scordelis (2). They performed linear elastic
analyses of reinforced concrete beams with predefined cracks
and also included special bond link elements between the steel
reinforcement and the concrete to simulate bond-slip charac-
teristics. However, a linear elastic analysis is unsuitable
for the study of the behavior of reinforced concrete structures
over the entire range of loading. Nilson (3) introduced non-
linear material properties and nonlinear bond-slip relation-
ships in the analysis of reinforced concrete beams. The loads
were introduced incrementally but the computer analysis had to

be stopped at the end of each increment and a new set of up-
dated input to the computer program was necessary. Later de-
velopments in the nonlinear analysis made the above approach
obsolete.

Franklin (4) considering nonlinear material properties
analyzed reinforced concrete frames with or without infilled
walls over the entire range of loading. Rashid (5) performed
a nonlinear analysis of axisymmetric prestressed concrete
pressure vessels and studied the response of the structure
covering the entire range of loading. His advanced work con-
sidered concrete cracking, creep of the concrete, temperature
stresses and the influence of unbonded prestressing reinforce-
ment together with the bonded steel reinforcement. Cervenka
and Gerstle (6) made an inelastic analysis of reinforced con-
crete panels. They added the stiffness of the steel to the
stiffness of the concrete at the constitutive matrix level and
modeled the reinforced concrete as a composite finite element.
This eliminated the necessity of modeling the reinforcement
as separate finite elements. The composite material approach
has been extensively used by later researchers and is also used
in this investigation.

Yuzugullu and Schnobrich (7) studied the inelastic be-
havior of shear wall-frame systems treating the concrete as an
elastic-plastic material much along the same lines as Cervenka
and Gerstle (6). Yuzugullu calculated a hypothetical crack
width using the strain as a measure. The cracks were allowed

to open and close during the redistribution of stress and loading. Opening and closing of the cracks though possible is not generally considered for monotonically increasing loads but may be of significance under cyclic loadings. Most of the above investigations used plane stress finite elements or modifications thereof.

With the development of efficient bending finite elements, several investigators modeled the nonlinear bending behavior of reinforced concrete slabs using bending elements. Jofriet and McNeice (8) analyzed a number of reinforced concrete slabs using an empirical flexural plate rigidity matrix. Bell and Elms (9) also made a nonlinear analysis of slabs using a similar approach. The use of a specific nonlinear moment-curvature relationship can be considered as a macroscopic "modified EI" approach.

Nonlinear bending behavior of reinforced concrete slabs can also be modeled by dividing the slab into a number of layers along the depth and assuming different elastic moduli for each layer as a function of layer strains. Scanlon and Murray (10) used such an approach to predict time dependent reinforced concrete slab deflections. Dotreppe, Schnobrich and Pecknold (11) used a layered finite element procedure for the inelastic analysis of reinforced concrete slabs. The layering technique results in the coupling of membrane and bending effects for anisotropic reinforced concrete slabs. Scanlon and Murray (10) and Dotreppe et al. (11) introduced simplifying

assumptions to eliminate the element inplane nodal degrees of freedom. Hand, Pecknold and Schnobrich (12, 13) did not make any such simplifying assumptions and included both inplane and bending stiffness matrices in their investigation. Hand et al. analyzed a number of slabs and a shell up to failure load and compared the theoretical results with the experimental results. Lin and Scordelis (14, 15) analyzed the nonlinear response of slabs, a hyperbolic paraboloid shell and a cylinderical shell in a manner similar to Hand et al. (12). Lin used a flat triangular element to approximate the curved shells. Bell and Elms (16) used the macroscopic "modified EI" approach to study the nonlinear behavior of thin reinforced concrete cylindrical shells.

It is thus evident that the present degree of sophistication in nonlinear analysis using high speed digital computers far exceeds the present day knowledge of the actual stress-strain relationships of concrete under multiaxial stress states. Consequently, basic experimental research in the mechanical properties of concrete is under way at many research institutions. Kupfer, Hilsdrof and Rusch (17) extensively studied the behavior of concrete under biaxial stresses. Liu, Nilson and Slate (18, 19, 20) studied the stress-strain relationship and fracture of concrete in biaxial compression. Based on the experimental results, they also developed orthotropic constitutive matrix equations suitable for use in plane stress finite elements. Kupfer and Gerstle (21) proposed matrix constitutive

equations for a biaxial stress state in concrete using variable shear and bulk moduli. Darwin and Pecknold (22) developed an inelastic concrete model for cyclic biaxial loading of concrete. All of the research investigations cited earlier considered the nonlinearity introduced in the analysis of the structure due to the degradation of material stiffness. Berg, Bergan and Holland (23, 24) extended the analysis of reinforced concrete slabs to include the nonlinear effects due to change in geometry. Aldstedt (25) performed a material and geometric nonlinear analysis of frames.

The versatility of the finite element method has resulted in an explosion of research involving its application. Application of the finite element method to the analysis of reinforced concrete structures are too numerous to cover completely here. Significant amounts of research work is being done at the University of Stuttgart (26), the University of Wales, Swansea (27) and by the nuclear reactor industry. The works of Valliappan and Nath (28), Valliappan and Doolan (29), Suidan and Schnobrich (30), Colville and Abbasi (31), Salem and Mohraz (32), Wanchoo and May (33) deserve mention. A review of the various aspects of the finite element analysis of reinforced concrete structures can be found in a paper by Scordelis (34).

Object and Scope

The purpose of this study is to develop a method of analysis using finite element techniques which is applicable to reinforced concrete structures and which incorporates material nonlinearity and also geometric nonlinearity. Biaxial failure criteria for concrete that closely fit with the experimental results are used. Concrete is treated as an orthotropic material and constitutive relationships that closely duplicate experimentally observed biaxial stress-strain responses of concrete are used. The analytical load-deflection response, internal stress distribution, cracking and crushing of the concrete, yielding of the steel are studied under monotonically increasing loads. A layered rectangular flat plate element with axial and bending stiffness is used. The flat plate element used is capable of modeling beams, slabs, columns, and shells.

An incremental and iterative procedure is used for the solution of the nonlinear problem. Tangent stiffness matrices considering material nonlinearity alone are used to study the behavior of slabs and beams. Nonlinear effects due to change in geometry are considered for beam-columns. Initial stress and initial displacement matrices are developed for the layered element using the total Lagrangian approach. The effects of bond-slip between the concrete and the steel reinforcement, time dependent creep strains and load reversals are not con-

sidered as a part of this study.

Finally, several numerical examples are studied. The analytical results for beams, beam-columns and slabs are compared with actual experimental results. The analytical results are also compared with results obtained by other researchers who used different idealizations to study the same basic problem.

CHAPTER 2. MATERIAL MODELING

General

This study uses the finite element method as the basis of an analysis of reinforced concrete structures from zero to failure load. The accuracy of the final results will closely depend upon the capability of the material model to duplicate the important characteristics of the structural material. One important aspect of this study is the modeling of short term stress-strain relationship and failure criteria for concrete in the biaxial stress state. The model to be used will closely follow the works of Kupfer and Gerstle (21) and Darwin and Pecknold (22).

Biaxial Failure Criteria for Concrete

Several experimental investigations (17) of the biaxial strength of concrete can be found in literature. The wide discrepancy found in the strength results can be attributed to unintended support restraints provided by the bearing plates. It is well known that the details of transferring the load to the test specimen can considerably alter the stress-state in the specimen. In this respect, two recent experimental investigations of Kupfer et al. (17) and Liu (18) are significant. Their test apparatus was carefully designed to minimize the lateral restraints on the specimen. Thus the experimental results obtained by Kupfer et al. (17) will be used as the

basis for material modeling of concrete in this study.

Compression-compression region

The experimental failure stresses for concrete for different ratios of principal stresses are plotted in Fig. 1. The observed increase in biaxial compressive strength in the compression-compression region over the uniaxial compressive strength can be attributed to the effect of confinement. The maximum experimentally observed increase in biaxial strength over the uniaxial strength is 27 percent. An empirical equation closely fitting the experimental results in the compression-compression region was proposed by Kupfer and Gerstle (21) and will also adopted in this study.

If σ_{1c} and σ_{2c} are the failure stresses in the principal stress directions 1 and 2 respectively and f'_c is the cylinder strength of concrete, an equation defining the failure envelope can be written as

$$(\frac{\sigma_{1c}}{f'_c} + \frac{\sigma_{2c}}{f'_c})^2 - \frac{\sigma_{2c}}{f'_c} - 3.65 \frac{\sigma_{1c}}{f'_c} = 0 \qquad (2.1)$$

In the above equation $\sigma_{1c} \geq \sigma_{2c}$ by algebric sign convention. The algebric sign convention (tension positive) will be used in this text throughout the development. Defining the ratio of principal stress as $\alpha_c = \frac{\sigma_{1c}}{\sigma_{2c}}$, equation 2.1 is rewritten as

$$\sigma_{2c} = \frac{1 + 3.65 \, \alpha_c}{(1 + \alpha_c)^2} \cdot f'_c \qquad (2.2)$$

Thus, for a given α_c, f'_c and σ_{2c} (equation 2.2), σ_{1c} can be

$$\sigma_{2c} = \frac{1 + 3.65\alpha_c}{(1 + \alpha_c)^2} \cdot f'_c \quad ; \quad 0 \le \alpha_c \le 1$$

$$\sigma_{1c} = \alpha_c \sigma_{2c}$$

$$\alpha_c = \frac{\sigma_1}{\sigma_2}$$
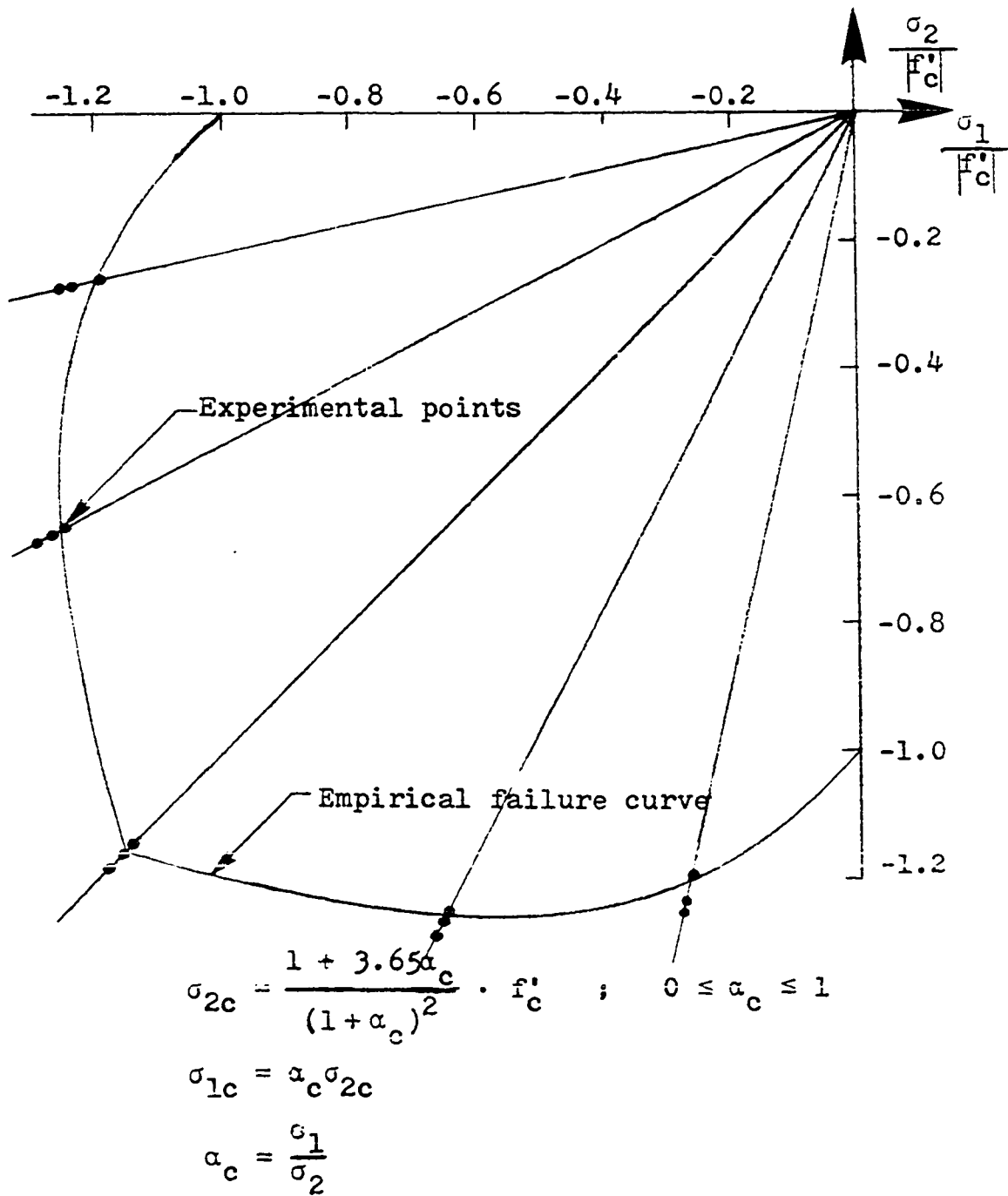
Fig. 1. Failure envelope for concrete in biaxial compression

obtained as follows:

$$\sigma_{1c} = \alpha_c \cdot \sigma_{2c} \qquad (2.3)$$

where $0 \leq \alpha_c \leq 1$ in this region.

Tension-compression region

Due to the difficulties in introducing tensile forces into concrete specimens, very limited experimental data are available concerning the failure strength of concrete in the tension-compression and tension-tension regions. The experimental failure stresses obtained by Kupfer et al. (17) are plotted in Fig. 2 for three different strengths of concrete.

The failure envelopes suggested by Kupfer and Gerstle (21) and Darwin and Pecknold (22) are shown in Fig. 3. Darwin used a combination of a straight line of constant tensile strength and a curved line to define the failure envelope in the tension-compression region (Fig. 3). Kupfer proposed a straight line reduction in tensile strength with an increase in compressive stress (Fig. 3). Though the straight line equation suggested by Kupfer agrees well with the experimental results it introduces an undesirable discontinuity in the failure envelope when $\alpha_c = 0$. The possibility of a discontinuity in the failure envelope at $\sigma_{2c} = -0.65 |f'_c|$ also exists in the model proposed by Darwin and Pecknold (22). A slightly modified failure envelope is proposed in this study.

The failure envelope in the tension-compression region is defined by a straight line of the form
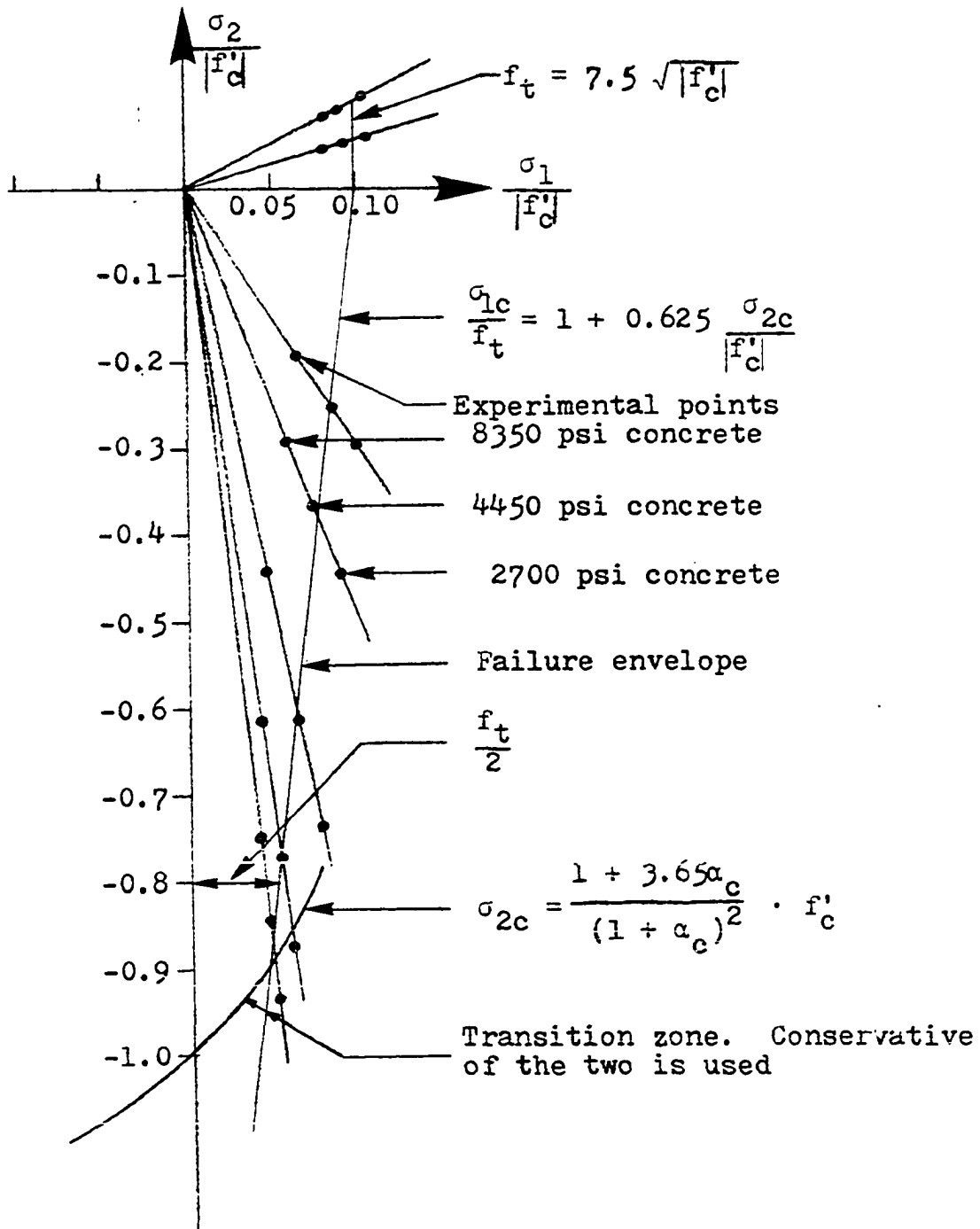
Fig. 2. Failure envelope for concrete in biaxial tension-compression and tension-tension regions
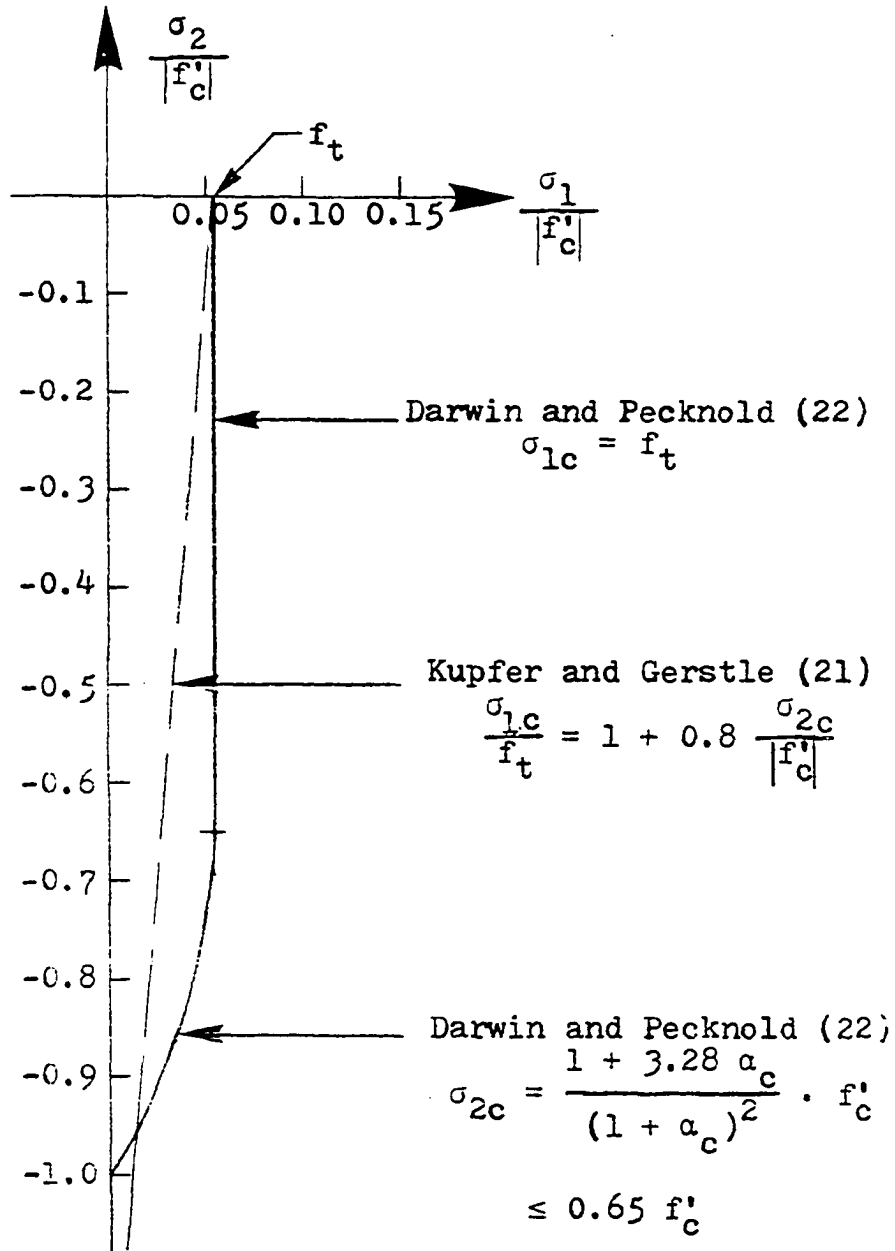
Fig. 3.   Failure envelopes proposed by Kupfer and Gerstle (21) and Darwin and Pecknold (22) for the tension-compression region

$$\frac{\sigma_{1c}}{f_t} = 1 + 0.625 \frac{\sigma_{2c}}{|f'_c|} \qquad (2.4)$$

and by the extension of the failure envelope of the compression-compression region (equation 2.2) into the tension-compression region until it intersects the straight line given by equation 2.4 (Fig. 2). In equation 2.4 when $\sigma_{2c} = 0$, σ_{1c} takes on the value of f_t and when $\frac{\sigma_{2c}}{|f'_c|} = -0.8$, σ_{1c} has the value of $\frac{f_t}{2}$, where f_t is the tensile strength of concrete. At high compressive stresses the failure envelope used to define compression-compression region (equation 2.2) is extended to also define the tension-compression region.

Tension-tension region

Experimental results (Fig. 2) indicate that the failure stresses in this region are not significantly affected by the biaxial state of stress. Hence it is assumed that the failure envelope in this region is a rectangle and the failure stress is always equal to f_t, independent of α_c (Fig. 2).

Short Term Biaxial Stress-Strain Relationship of Concrete

General

While modeling and implementing an empirical biaxial failure criteria of concrete into the analysis is comparatively simple, an accurate modeling of the biaxial stress-strain relationships of the concrete is more complex. A study of the uniaxial stress-strain diagram of concrete in compression

illustrates many important features. The stress-strain curve
is initially straight and then becomes increasingly nonlinear
as the internal microcracking develops and propagates. The
stress-strain curve after reaching a peak value has an un-
loading portion which is machine or strain rate dependent.
The shape of the stress-strain diagram in tension is more
nearly linear than the comparable diagram obtained for com-
pression. A good review of the several empirical equations
suggested to model the uniaxial concrete compressive stress-
strain relationship is given by Popovics (35).

Several previous studies of reinforced concrete structures
using the finite element method have used a variety of models
to describe the stress-strain relationship of concrete. Ngo
and Scordelis (2) considered concrete to be an isotropic
linear elastic material having different tensile and compres-
sive strengths. Nilson (3) used a curved uniaxial stress-
strain relationship in compression based on Saenz's equation
and assumed the material to be linearly elastic in tension.
Franklin (4) used a piecewise linear stress-strain diagram to
model more closely the experimental uniaxial curves. In a
number of recent studies (6, 7, 14, 32) concrete was modeled
as a linearly elastic-perfectly plastic material in compres-
sion. A more refined model than the above was used by Hand
et al. (12). Hand et al. (12) used a bilinearly elastic-
perfectly plastic model for concrete in compression. None of
the above studies considered the effect of the biaxial stress

field on the stress-strain curve of the concrete other than through the use of the Poisson's effect.

A typical stress-strain response of concrete under biaxial compression for $\alpha_c = 1$ is shown in Fig. 4. The observed reduction in strain cannot be entirely explained by the Poisson's effect alone. Liu et al. (19) attribute the large strain reduction to the confinement of the microcracking due to the presence of biaxial stresses. Thus, the stress intensity in one direction also affects the material stiffness in the perpendicular direction. This then led to modeling of concrete as a stress induced orthotropic material by Liu et al. (20) and Darwin and Pecknold (22). This study also considers concrete to be an orthotropic material and the material model used will be the same as that developed by Darwin and Pecknold (22) except as modified in the tension-compression region.

Orthotropic constitutive relationships

The nonlinear problem is solved using incremental and iterative techniques. The load is applied to the structure in small increments and iterations are performed within each increment of load until equilibrium convergence is obtained. The material is assumed to be linearly elastic within each iteration. As the analysis proceeds, the degradation in the material stiffness is accounted for by continuously updating the material stiffness based on the accumulated total strains.
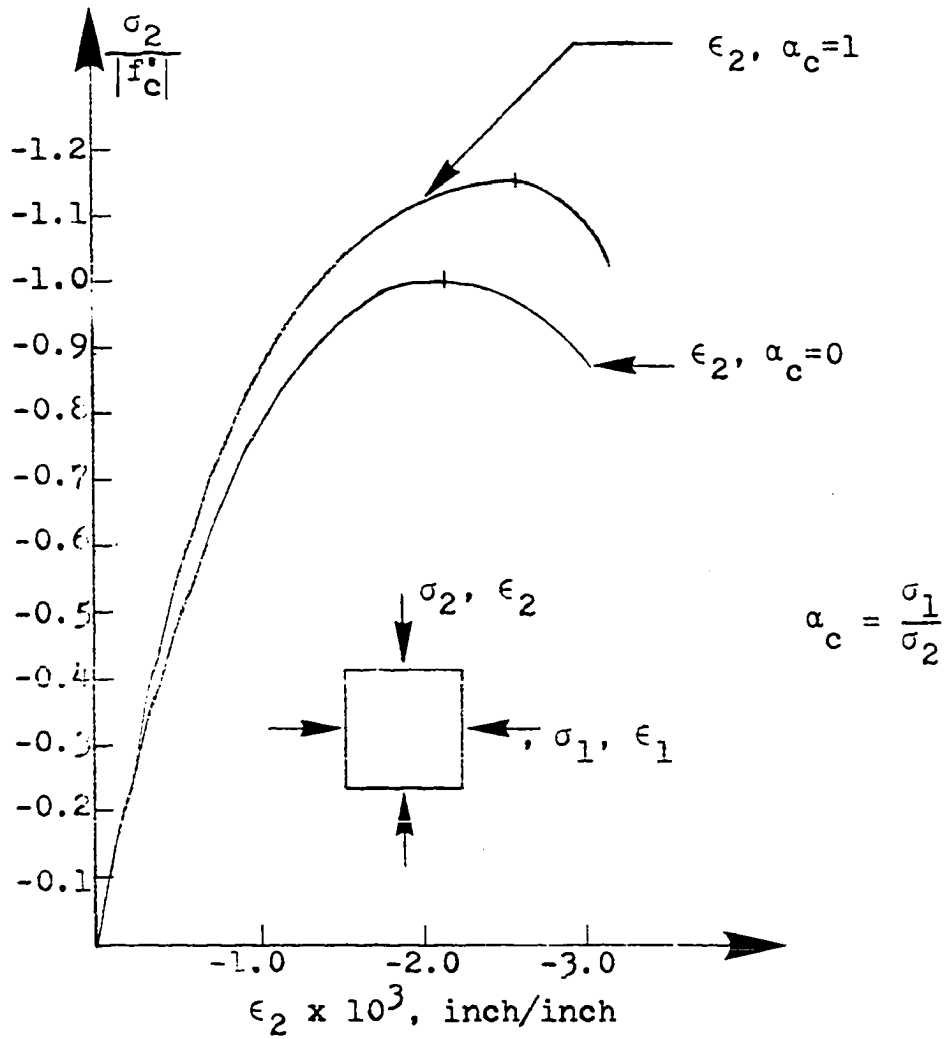
Fig. 4. Experimental uniaxial and biaxial curves for concrete in compression

The generalized Hooke's law for a continuous material is

$$\sigma_i = c_{ij} \epsilon_j \tag{2.5}$$

where σ_i are the stress components, c_{ij} are constants for the material and ϵ_j are the strain components. The summation convention of the repeated index is implied in the equation. Using the symmetry of stresses and strains and by assuming the existence of a strain energy density function it can be shown that the number of independent elastic constants for the most general anisotropic body is 21 (36). For the case of a two-dimensional orthotropic elastic problem the number of elastic constants can be further reduced to four (37). In the case of uncracked concrete, the orthotropic material directions are always assumed to coincide with the principal stress directions. Let E_1, ν_1 and E_2, ν_2 be the elastic moduli and Poisson's ratios in directions 1 and 2 respectively and G_{12} be the shear modulus associated with directions 1-2. It should be noted that of the five constants E_1, E_2, ν_1, ν_2, and G_{12}, only four are independent.

Considering first the principal stresses the relationship between the incremental stresses and the incremental strains can be written as follows:

$$\begin{bmatrix} \Delta\sigma'_1 \\ \Delta\sigma'_2 \end{bmatrix} = \frac{1}{1-\nu_1\nu_2} \begin{bmatrix} E_1 & \nu_2 E_1 \\ \nu_1 E_2 & E_2 \end{bmatrix} \begin{bmatrix} \Delta\epsilon'_1 \\ \Delta\epsilon'_2 \end{bmatrix} \tag{2.6}$$

where $\nu_1 E_2 = \nu_2 E_1$ and thus ν_1 and ν_2 are not independent. Defining an effective Poisson's ratio

$$\nu^2 = \nu_1 \nu_2 \tag{2.7}$$

Equation 2.6 can be rewritten as

$$\begin{bmatrix} \Delta\sigma_1' \\ \Delta\sigma_2' \end{bmatrix} = \frac{1}{1-\nu^2} \begin{bmatrix} E_1 & \nu\sqrt{E_1 E_2} \\ \nu\sqrt{E_1 E_2} & E_2 \end{bmatrix} \begin{bmatrix} \Delta\epsilon_1' \\ \Delta\epsilon_2' \end{bmatrix} \qquad (2.8)$$

Expanding the constitutive matrix to include the shear effect under a general state, we get,

$$\begin{bmatrix} \Delta\sigma_1' \\ \Delta\sigma_2' \\ \Delta\sigma_{12}' \end{bmatrix} = \frac{1}{1-\nu^2} \begin{bmatrix} E_1 & \nu\sqrt{E_1 E_2} & 0 \\ \sqrt{E_1 E_2} & E_2 & 0 \\ 0 & 0 & (1-\nu^2)G_{12}' \end{bmatrix} \begin{bmatrix} \Delta\epsilon_1' \\ \Delta\epsilon_2' \\ \Delta\epsilon_{12}' \end{bmatrix} \qquad (2.9)$$

where $\Delta\sigma_{12}'$, $\Delta\epsilon_{12}'$ and G_{12}' are the shear stress, the engineering shear strain and the shearing modulus in direction 1-2 respectively. It should be noted that when the concrete has cracked, the principal stress directions do not necessarily correspond to the principal material directions. Equation 2.9 can also be written in matrix notation as

$$[\Delta\sigma'] = [c_{ij}'][\Delta\epsilon'] \qquad (2.10)$$

where $[c'_{ij}]$ is the constitutive matrix in the principal material directions.

In general, the material directions will not coincide with the element reference axes. Thus, the constitutive matrix in the material directions must be transformed to element reference axes using the transformation,

$$[c_{ij}] = T^T [c_{ij}'] T \qquad (2.11)$$

where

$$T = \begin{bmatrix} c^2 & s^2 & cs \\ s^2 & c^2 & -cs \\ -2cs & +2cs & c^2-s^2 \end{bmatrix} \quad \text{and} \quad \begin{array}{l} c = \cos\theta \\ s = \sin\theta \end{array} \qquad (2.12)$$

and, $[c_{ij}]$ is the constitutive matrix along element reference axes and θ is the angle measured counterclockwise from element x-axis to material axes.

Shear modulus

When concrete is treated as an orthotropic material the shear modulus is an independent elastic constant which must be determined experimentally. No experimental data is presently available for such a determination of the shear modulus. Franklin (4), Liu (18) and Darwin and Pecknold (22) proposed approximate expressions for the shear modulus knowing the elastic moduli in the principal directions. The approximate expression for the shear modulus assumes importance when the concrete to be considered is cracked in a single direction.

All of the approximate expressions (4, 18, 22) use some form of an isotropicity assumption. Darwin and Pecknold (22) considered the constitutive matrix at an angle θ from the material principal axes. If a transformation is made using equation 2.11 then the c_{33} element of the transformed matrix is

$$c_{33} = [E_1 - 2\nu\sqrt{E_1 E_2} + E_2]c^2 s^2 + (1-\nu^2)G'_{12}(c^2-s^2)^2 \qquad (2.13)$$

Now, if an __assumption__ that c_{33} is constrained to be independent of θ is made ($G_{12} = G'_{12}$), then the following expression for

G_{12} or G'_{12} is obtained.

$$G'_{12} = G_{12} = \frac{1}{4(1-\nu^2)} (E_1 + E_2 - 2\nu\sqrt{E_1 E_2}) \qquad (2.14)$$

The expression for G_{12} as given by equation 2.14 is used in this study. It must be noted that the expression for G_{12} as given in equation 2.14 can also be obtained by considering a value of $\theta = 45°$ in equation 2.13. Franklin (4) used this idea of apparent isotropicity at $45°$ angle to arrive at equation 2.14 for the shear modulus.

It is also possible to form an approximate expression for the shear modulus using the inverse form of the equation 2.9.

$$\begin{bmatrix} \Delta\epsilon'_1 \\ \Delta\epsilon'_2 \\ \cdot \\ \Delta\epsilon'_{12} \end{bmatrix} = \begin{bmatrix} \frac{1}{E_1} & -\frac{\nu}{\sqrt{E_1 E_2}} & 0 \\ -\frac{\nu}{\sqrt{E_1 E_2}} & \frac{1}{E_2} & 0 \\ 0 & 0 & a'_{33} \end{bmatrix} \begin{bmatrix} \Delta\sigma'_1 \\ \Delta\sigma'_2 \\ \Delta\sigma'_{12} \end{bmatrix} \qquad (2.15)$$

Rewriting equation 2.15 in matrix form,

$$[\Delta\epsilon'] = [a'_{ij}] [\Delta\sigma'] \qquad (2.16)$$

where $[a'_{ij}]$ is the compliance matrix along the material axes. The compliance matrix along the element axes can be calculated using the transformation

$$[a_{ij}] = \bar{T}^T [a'_{ij}] \bar{T} \qquad (2.17)$$

where

$$\bar{T} = \begin{bmatrix} c^2 & s^2 & 2cs \\ s^2 & c^2 & -2cs \\ -cs & cs & c^2-s^2 \end{bmatrix} \quad \text{and} \quad \begin{matrix} c = \cos\theta \\ s = \sin\theta \end{matrix} \qquad (2.18)$$

and θ is measured counterclockwise from the element reference axes to the material axes.

The a_{33} element in the transformed compliance matrix is found to be

$$a_{33} = \left(\frac{1}{E_1} + \frac{1}{E_2} + \frac{2\nu}{\sqrt{E_1 E_2}} - a_{33}'\right) 4c^2 s^2 + a_{33}' \qquad (2.19)$$

Now, if an __assumption__ that the element a_{33} is constrained to be independent of θ is made, then the following expression for a_{33} is obtained.

$$a_{33} = a_{33}' = \frac{1}{E_1} + \frac{1}{E_2} + \frac{2\nu}{\sqrt{E_1 E_2}} \qquad (2.20)$$

Liu (18) obtained the same expression for the shear modulus using a different approach.

Summarizing, the constitutive matrix used in this study along the material axes is

$$
\begin{bmatrix} \Delta\sigma_1' \\ \Delta\sigma_2' \\ \Delta\sigma_{12}' \end{bmatrix} = \frac{1}{1-\nu^2}
\begin{bmatrix} E_1 & \nu\sqrt{E_1 E_2} & 0 \\ \nu\sqrt{E_1 E_2} & E_2 & 0 \\ 0 & 0 & \frac{1}{4}(E_1+E_2-2\nu\sqrt{E_1 E_2}) \end{bmatrix}
\begin{bmatrix} \Delta\epsilon_1' \\ \Delta\epsilon_2' \\ \Delta\epsilon_{12}' \end{bmatrix} \qquad (2.21)
$$

and along the element axes is

$$
\begin{bmatrix} \Delta\sigma_1 \\ \Delta\sigma_2 \\ \Delta\sigma_{12} \end{bmatrix} = \frac{1}{1-\nu^2}
\begin{bmatrix} E_1 c^2 + E_2 s^2 & \nu\sqrt{E_1 E_2} & \frac{1}{2}(E_1-E_2)cs \\ & E_1 s^2 + E_2 c^2 & \frac{1}{2}(E_1-E_2)cs \\ \text{Symmetric} & & \frac{1}{4}(E_1+E_2-2\nu\sqrt{E_1 E_2}) \end{bmatrix}
\begin{bmatrix} \Delta\epsilon_1 \\ \Delta\epsilon_2 \\ \Delta\epsilon_{12} \end{bmatrix} \qquad (2.22)
$$

Equivalent uniaxial curves and elastic tangent moduli in compression

Material nonlinearity is introduced in the analysis by considering the current values of the tangent moduli of elasticity of the material in the formation of the stiffness matrix of the structure. The off diagonal elements in the constitutive matrix defined by equation 2.21 introduce the Poisson's effect in the stress-strain relationships. Therefore, the tangent modulus used in the formation of the constitutive matrix must be devoid of any Poisson's effect. One way of calculating such a tangent stiffness modulus is through the concept of equivalent uniaxial strains suggested by Darwin and Pecknold (22). This provides a convenient way of separating the Poisson's effect from the total strains in a nonlinear material and can be extended to include cyclic loading.

The incremental equivalent uniaxial strain is defined by the equation

$$\Delta \epsilon_{iu} = \frac{\Delta \sigma_i}{E_i}$$

(2.23)

where $\Delta \epsilon_{iu}$ is the incremental equivalent uniaxial strain in the ith direction, $\Delta \sigma_i$ is the incremental stress in the ith direction and E_i is the tangent modulus at the beginning of the increment in the ith direction. The important point to be noted in equation 2.23 is the omission of the effect of stress acting in the perpendicular direction. Modeling the nonlinear

material using an incremental linear approach allows equation 2.23 to be extended in order to calculate the total equivalent uniaxial strain given by the equation

$$\epsilon_{iu} = \sum_{\substack{All \\ increments}} \frac{\Delta\sigma_i}{E_i} \tag{2.24}$$

where ϵ_{iu} is the total equivalent uniaxial strain in the ith direction.

In a general analysis of a structure an increment in principal stresses is also associated with a possible rotation of the principal axes. Thus, $\Delta\epsilon_{iu}$ is then calculated as

$$\Delta\epsilon_{iu} = \frac{\sigma_{i,new} - \sigma_{i,old}}{E_i} \tag{2.25}$$

where $\sigma_{i,new}$ is the new principal stress in the new ith direction, $\sigma_{i,old}$ is the old principal stress in the old ith direction at the beginning of the increment and E_i is the tangent modulus in the old ith direction at the beginning of the increment. The incremental strain $\Delta\epsilon_{iu}$ is then added to old total ϵ_{iu} to give the new total ϵ_{iu} oriented in the new direction of the principal axes. Thus, in uncracked concrete, E_1 and E_2 are tangent moduli always oriented along the principal stress directions 1 and 2 respectively.

The equivalent uniaxial strains are used to construct the equivalent uniaxial curves. The equivalent uniaxial curves are then used to calculate the tangent modulus of elasticity and the stress for the material for a given ϵ_{iu}. Equivalent

uniaxial curves are defined by the equation

$$\sigma_i = \frac{E_0 \epsilon_{iu}}{1 + (\frac{E_0}{E_s^c} - 2) \frac{\epsilon_{iu}}{\epsilon_{ic}} + (\frac{\epsilon_{iu}}{\epsilon_{ic}})^2} \qquad (2.26)$$

where E_0 is the initial tangent modulus, E_s^c is the secant modulus at the point of maximum stress σ_{ic}, and ϵ_{ic} is the equivalent uniaxial strain at the point of maximum stress. Since σ_{ic} and ϵ_{ic} are different for different ratios of principal stresses (α_c), a family of equivalent uniaxial curves exist as shown in Fig. 5.

To construct the uniaxial curves it is necessary to know the values of E_0, σ_{ic} and ϵ_{ic}. The value of the initial tangent modulus can either be determined experimentally or the value as suggested by the ACI Code (38) can be used. The value of the failure stress σ_{ic} can be obtained from the failure criteria discussed earlier. The value of the ϵ_{ic} must be selected such that the analytical biaxial stress-strain curves agree closely with the experimental results. Some of the elegance of the method is lost in using a long expression for ϵ_{ic} obtained by interpolation from experimental results. Darwin and Pecknold (22) proposed two expressions for ϵ_{ic} when $\sigma_{ic} \geq f_c'$ and when $\sigma_{ic} < f_c'$. This study uses the two expressions suggested by Darwin and Pecknold for the biaxial compression region. For the tension-compression region a different method of constructing the equivalent uniaxial curve is
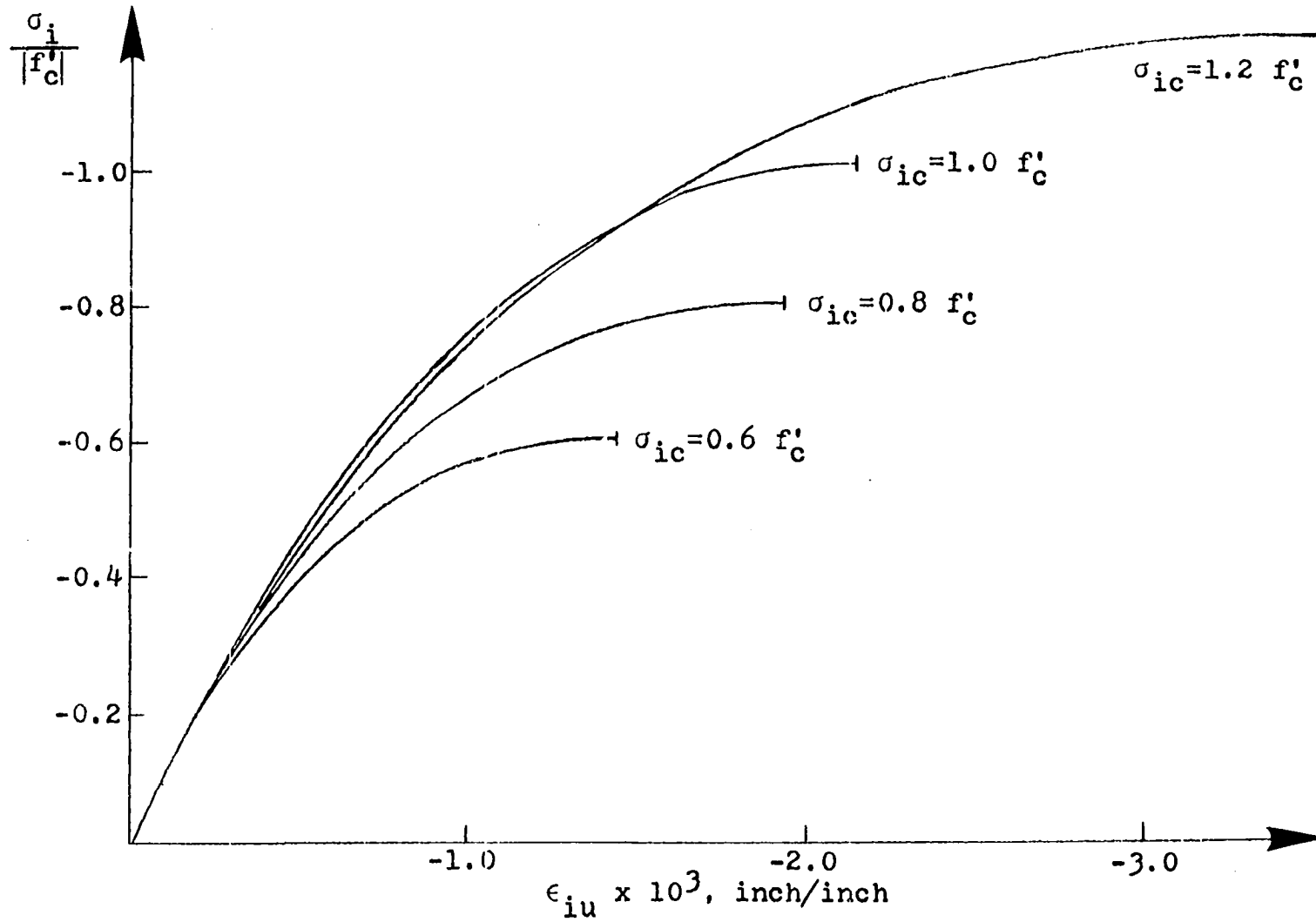
Fig. 5. Equivalent uniaxial curves for the compression-compression region

proposed.

Biaxial compression region   In this region there is an
increase in failure strength over the cylinder strength due to
microcrack confinement. For failure stresses greater than f'_c
in absolute magnitude, failure strains greater than the uniaxi-
al failure strain were observed in spite of Poisson's effect.
Darwin and Pecknold (22) use the experimental stress-strain
curve for equal biaxial compression to estimate ϵ_{ic} when $\sigma_{ic} \leq$
f'_c . The value of ϵ_{ic} for $\alpha_c = 1$ can be found by dividing the
experimental failure strain by $(1 - \nu)$. The value of ϵ_{ic} for
the uniaxial case is the experimentally observed ϵ_{cu}. Assuming
ϵ_{ic} varies linearly with the increased compressive strength the
following equation can be obtained.

$$\epsilon_{ic} = \epsilon_{cu}[\frac{\sigma_{ic}}{f'_c} R_{ic} - (R_{ic} - 1)] \qquad (2.27)$$

where ϵ_{cu} = uniaxial failure strain and

$$R_{ic} = \frac{\dfrac{\epsilon_{ic} (\alpha_c = 1)}{\epsilon_{cu}} - 1}{\dfrac{\sigma_{ic} (\alpha_c = 1)}{f'_c} - 1} \qquad (2.28)$$

The value of R_{ic} is to be calculated from experimental biaxial
test data. A value of $R_{ic} = 3.15$ was used throughout this
study.

When $\sigma_{ic} > f'_c$ the value of ϵ_{ic} is given by

$$\epsilon_{ic} = \epsilon_{cu}[-1.6(\frac{\sigma_{ic}}{f'_c})^3 + 2.25(\frac{\sigma_{ic}}{f'_c})^2 + 0.35(\frac{\sigma_{ic}}{f'_c})] \qquad (2.29)$$

In order to prevent the equivalent uniaxial curve (Eq. 2.26) from becoming concave upward, ϵ_{ic} must have a minimum value such that the ratio $\dfrac{E_0}{E_s^c} \geq 2$.

Tension-compression region   When the uniaxial curves in the tension-compression region were constructed along the lines suggested for the biaxial compression-compression region, it was found that the theoretical model overestimated the strains in the compressive stress direction for high negative values of α_c. This difficulty is due to the fact that the ratio $\dfrac{E_0}{E_s^c} \geq 2$ to prevent the stress-strain curve from becoming concave upward. Hence, the equivalent uniaxial curves in the tension-compression region are constructed differently from the biaxial compression-compression region. After several trial and errors, an expression for ϵ_{ic} given by the following equation gave good correlation with experimental results.

$$\epsilon_{ic} = \epsilon_{cu}[4.42 - 8.38(\frac{\sigma_{ic}}{f'_c}) + 7.54(\frac{\sigma_{ic}}{f'_c})^2 - 2.58(\frac{\sigma_{ic}}{f'_c})^3] \quad (2.30)$$

Equivalent uniaxial curves in this region are constructed using the cylinder strength f'_c as the peak stress and using ϵ_{ic} as given by equation 2.30. The equivalent uniaxial curves are then truncated corresponding to the failure stresses as shown in Fig. 6. This procedure gave very satisfactory agreement with the experimental results.
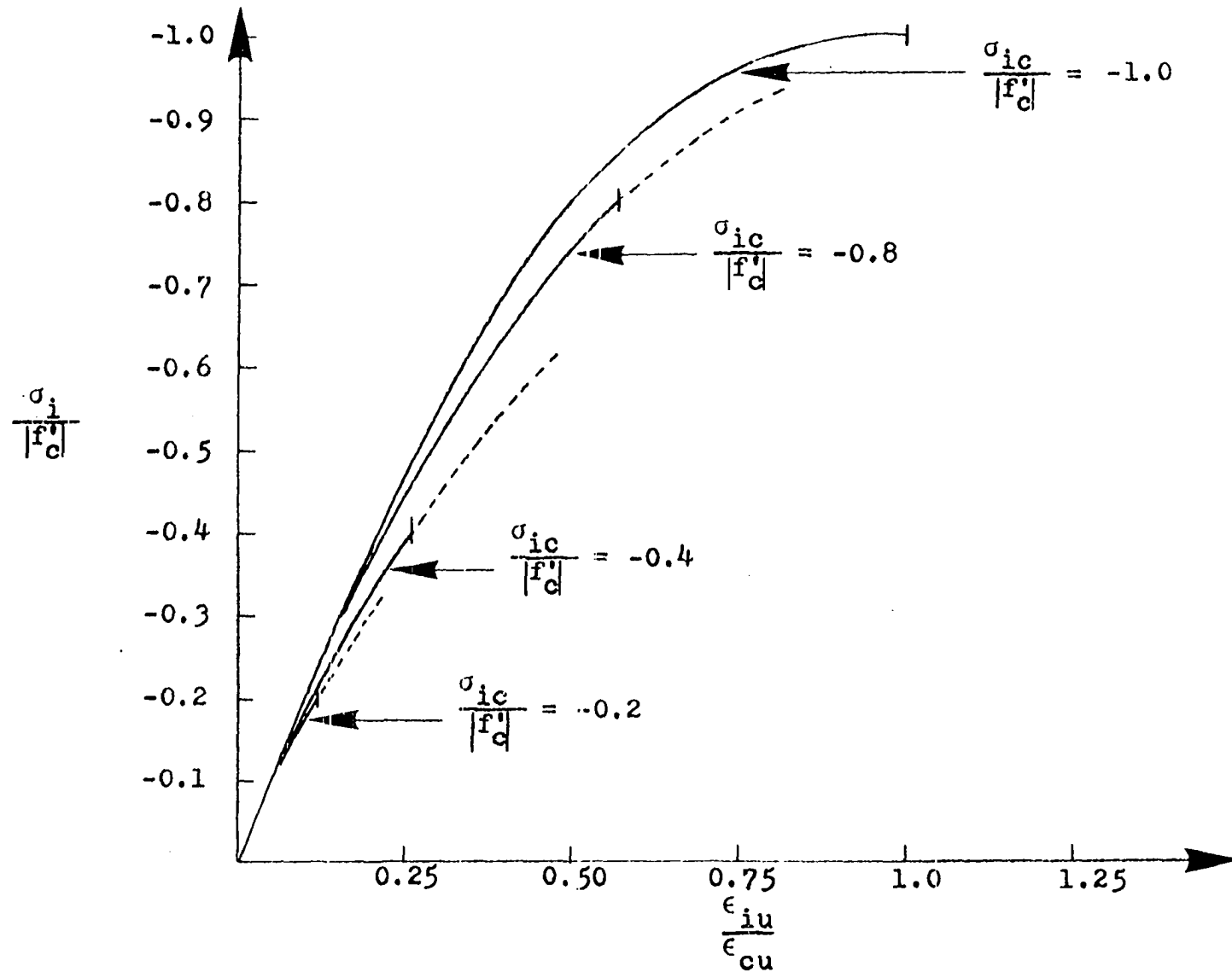
Fig. 6. Truncated uniaxial curves for the tension-compression region

Elastic tangent modulus in tension

The response of concrete in tension is comparatively
linear. Therefore, the tangent modulus of concrete in ten-
sion is assumed to be constant until fracture occurs and is
equal to the initial tangent modulus E_0.

Effective Poisson's ratio

The value of the effective Poisson's ratio was assumed
to be 0.2 for the entire load range in all the three regions
(compression-compression, tension-compression and tension-
tension). The experimentally observed Poisson's ratios vary
from 0.18 to 0.2 below the elastic limit (17). A study of the
experimental uniaxial curve (17) indicates that ν increases
significantly when the stress level is greater than about 80
percent of the failure stress. Darwin and Pecknold proposed
a varying value of ν for the uniaxial and tension-compression
region. In the expression they proposed, the value of ν for
certain values of α_c can vary from 0.2 to as high as 0.99.
In the analysis of slabs, numerical difficulties were en-
countered in using such high Poisson's ratios. Hence in this
study a constant value of $\nu = 0.2$ was used for the effective
Poisson's ratio. This resulted in the analytical stress-
strain curves deviating from the experimental curves on the
tension side in the tension-compression region at high stresses
(Fig. 10).

Comparison of the analytical stress-strain curves with experimental results

The analytical stress-strain curves for plain concrete were compared with experimental results obtained by Kupfer et al. (17). A comparison was made for three different ratios of α_c in each of the tension-tension, tension-compression and compression-compression regions as shown in Fig. 7 through Fig. 10. The model gives good results in the cases illustrated.

Modeling the Cracking of Concrete

An important characteristic of concrete is its cracking behavior at low tensile stresses. The cracking of concrete is a major factor contributing to the nonlinear behavior of reinforced concrete structures. Realistic theoretical analyses consider the cracking of concrete even under service loads. With reference to finite element idealization of a structure two approaches to the modeling of the cracking of concrete have been made in the past. The first approach separated the nodes of the finite element mesh when the tensile stress reached a critical value. This approach has been used by Ngo and Scordelis (2) and Nilson (3). This method of modeling the cracking of concrete has certain advantages. It can simulate a single crack and can give an estimate of crack width. Possibilities exist in this analysis to include the shear transfer through aggregate interlock as a function of crack width and
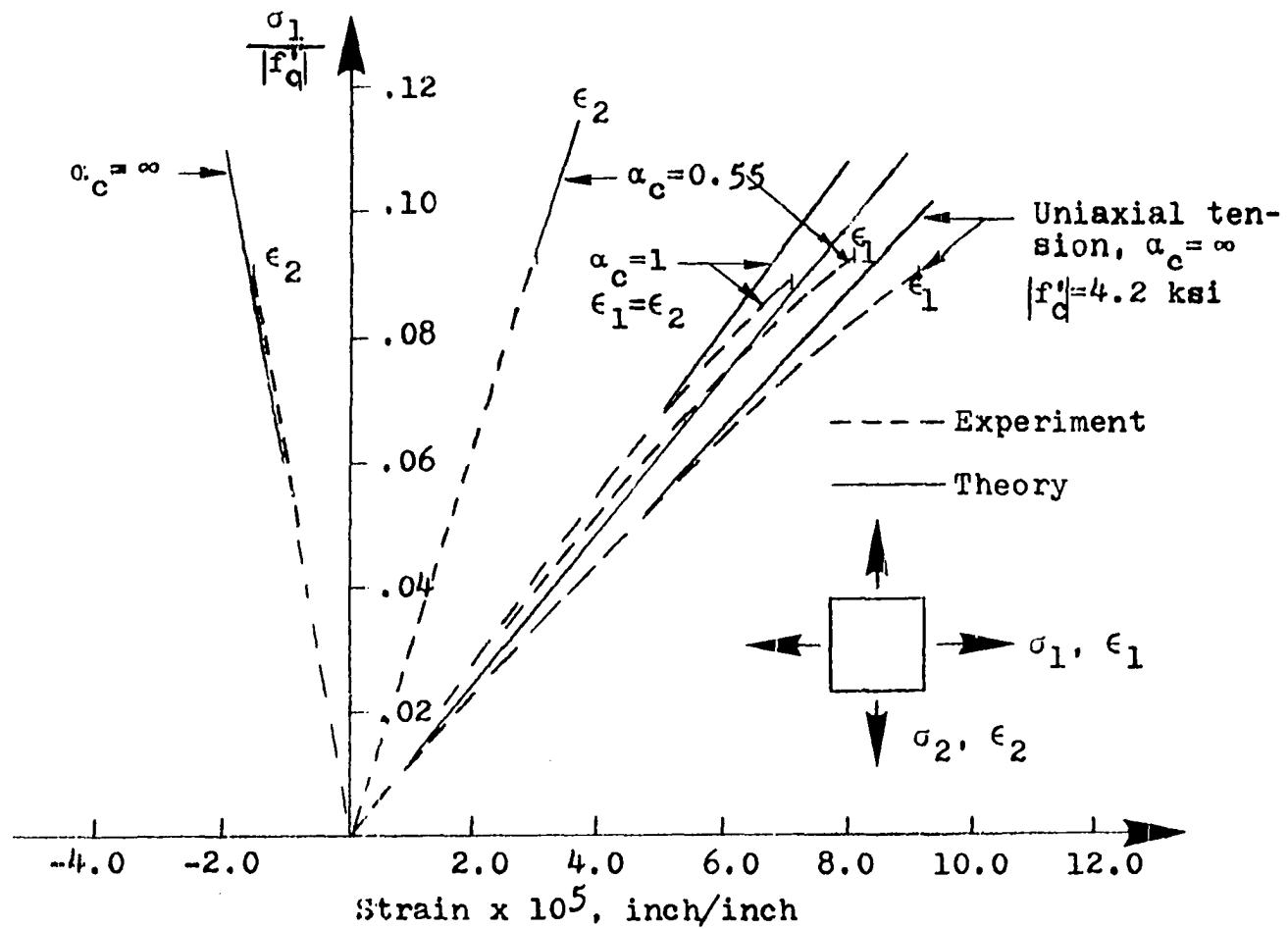
Fig. 7. Stress-strain curves for the tension-tension region
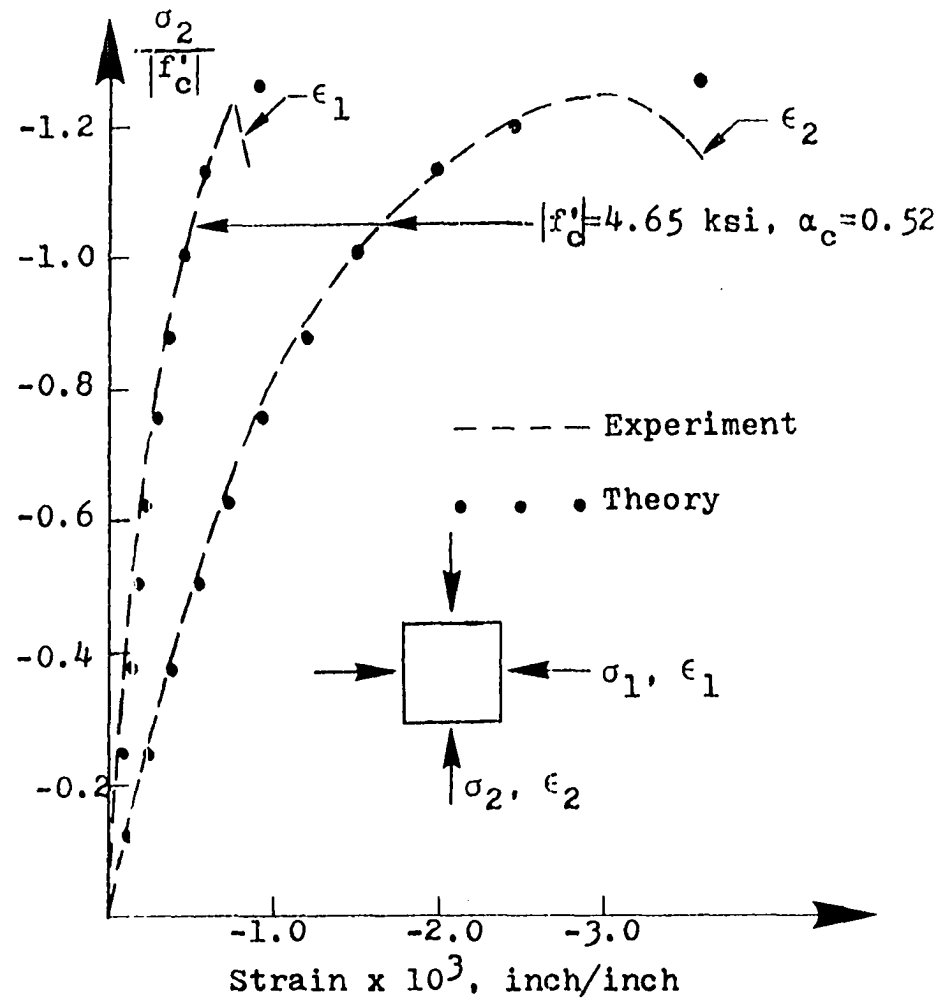
Fig. 8. Stress-strain curves for the biaxial compression region for $\alpha_c = 0.52$
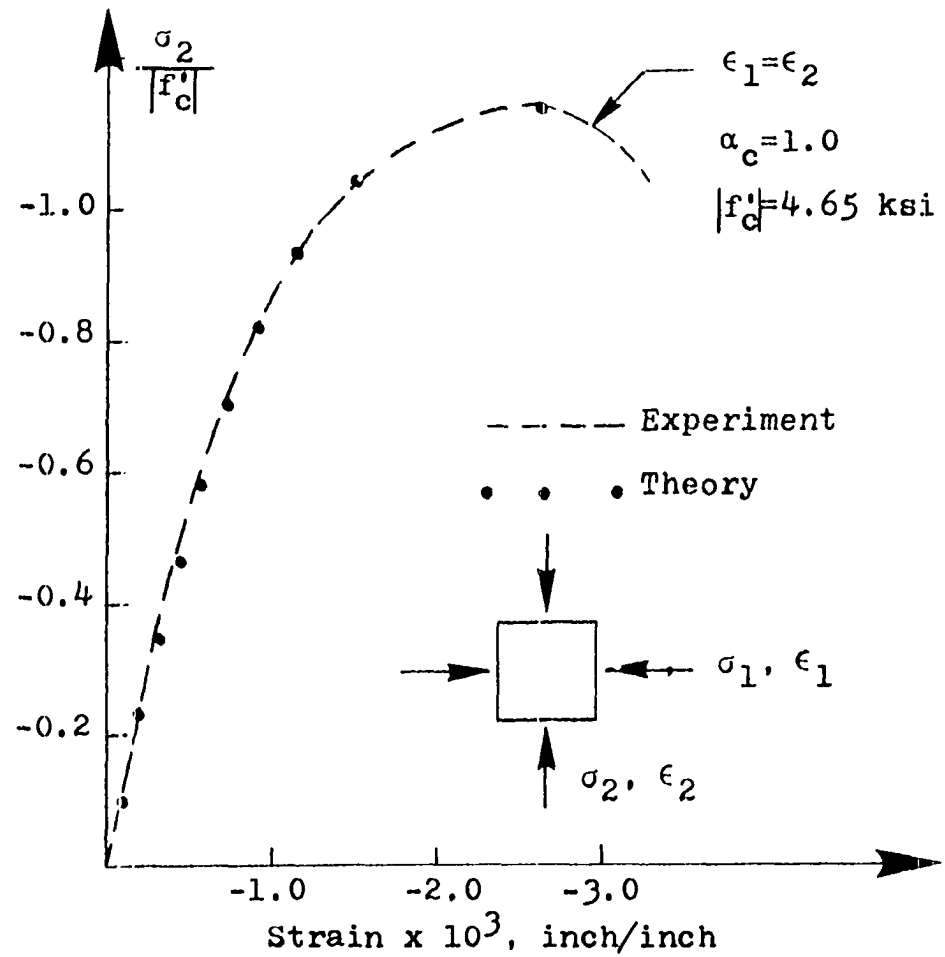
Fig. 9.   Stress-strain curve for the biaxial compression region for $\alpha_c = 1.0$

σ₂ axis label: $\frac{\sigma_2}{|f_c'|}$

Uniaxial compression
$|f_c'| = 4.65$ ksi

$\alpha_c = -0.052$

— — — Experiment

• • • Theory

$\alpha_c = -0.103$

$\alpha_c = -0.204$

σ_1, ϵ_1

σ_2, ϵ_2

ϵ_1 ϵ_2

Strain x 10^3, inch/inch
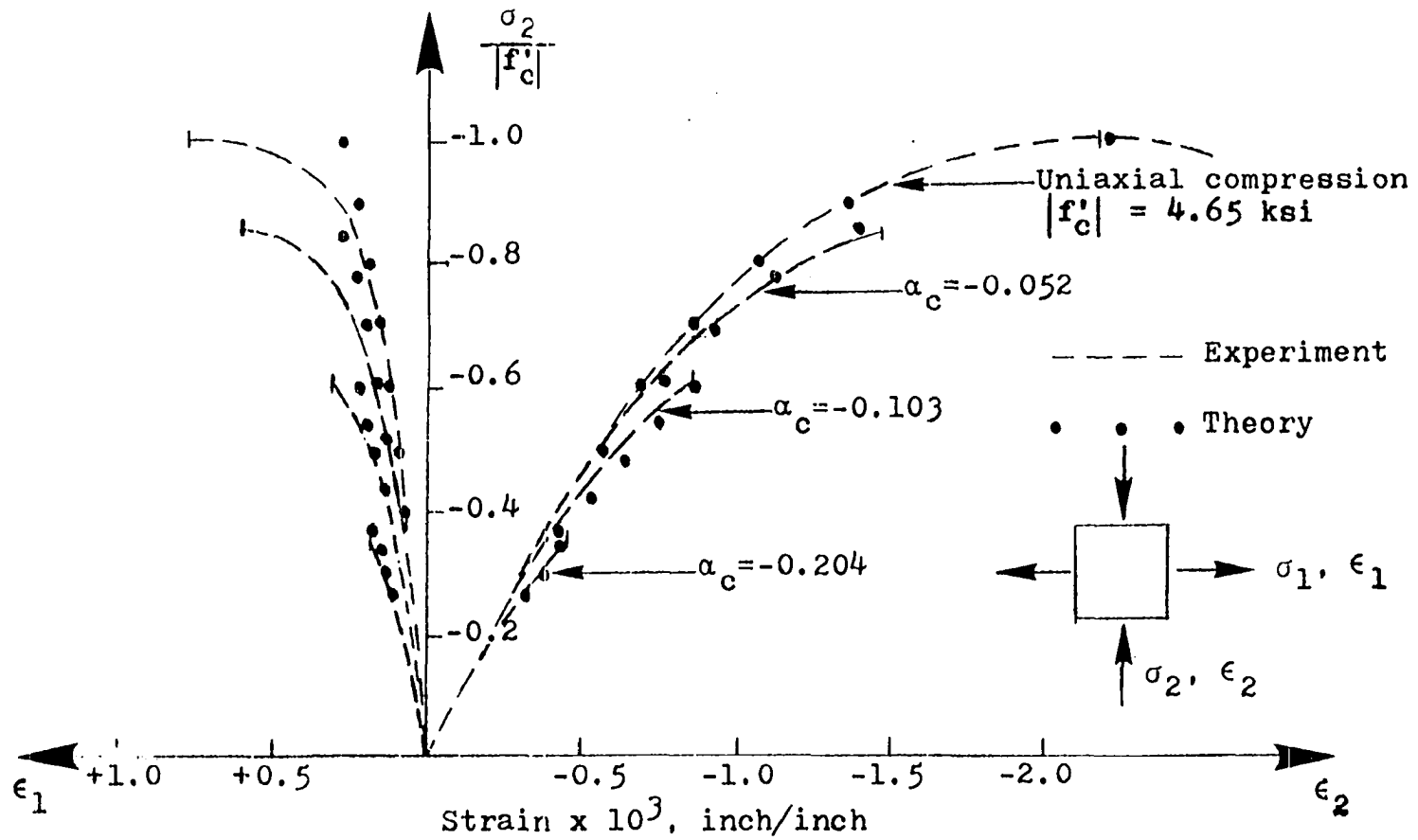
Fig. 10.   Stress-strain curves in the tension-compression region for different ratios of α_c

also to estimate the increase in stress in the vicinity of
the crack provided a sufficient number of elements near the
cracks have been used. The contribution of the uncracked con-
crete in between the cracks to the structural stiffness is
automatically included. However, this approach has some
serious disadvantages when implementing these assumptions
into a computer program. The separation of nodes results in
an increased number of nodes, an increased size of the system
equations and also would lead to increased bandwidth in the
stiffness matrix unless a proper renumbering of nodes is
accomplished. The above approach is difficult to implement in
an automated program that would analyze the structure from zero
to failure load in one continuous run. In addition, the path
of propagation of the cracks would be influenced by the finite
element mesh layout used.

The disadvantages of this method led to the modeling of
the cracking of concrete at the constitutive matrix level.
The modeling of cracking is simply achieved by assuming the
elastic tangent modulus of the concrete perpendicular to the
crack as zero and retaining the stiffness of concrete parallel
to the crack. Thus in this second approach cracking is not
treated as a discontinuity with accompanying separation of the
cracked surfaces, but rather, the cracked concrete is treated
as a continuous orthotropic material of widely varying stiff-
nesses in the two perpendicular directions. This latter
approach has been used in simulating cracked concrete in this

study.

It is assumed that the cracking of concrete results when the principal tensile stress exceeds the tensile strength given by the failure criteria. For the case of concrete cracked in a single direction, the constitutive matrix in the material directions takes the following form where cracking has occurred perpendicular to direction 1.

$$[c'_{ij}] = \begin{bmatrix} 0 & 0 & 0 \\ 0 & E_2 & 0 \\ 0 & 0 & \frac{E_2}{4} \end{bmatrix} \qquad (2.31)$$

It is important to note that the cracked concrete retains some shear stiffness. Taylor's extensive tests (39) indicate that an appreciable amount of shear is transferred along the cracked surfaces through aggregate interlock. It is also well known that shear is transferred across the cracked surface by dowel action of the steel reinforcement. Retention of some shear stiffness in the cracked concrete accounts approximately for the shear transfer through aggregate interlock and the dowel action of the steel reinforcement. Hand et al. (12) demonstrated in certain classes of problems (e.g., the pure torsion of a re-inforced concrete slab) that the retention of shearing stiffness in the cracked concrete is a necessity to prevent unstable crack configurations from forming well below the ultimate load. Several studies (12, 14, 30, 32) have used arbitrary shear stiffness retention factors in the constitutive matrix. In the cases of concrete cracked in two directions, crushed in

two directions, cracked in one direction and crushed in the other direction the constitutive matrix reduces to a null matrix.

When the elastic tangent modulus of cracked concrete is assumed to be zero, there is a loss of stiffness over the area of the element or a fraction of the area of the element depending upon the integration scheme used. However, cracks actually occur at finite distances and the concrete in between the cracks contributes to the stiffness of the structure. In reinforced concrete slabs, Lin (14) found that this stiffening effect (called tension stiffening effect) could be significant. The tension stiffening effect can be approximately accounted for in the analysis by adding a hypothetical unloading portion to the tensile stress-strain curve of the concrete until the value of the tensile stress is zero at a chosen value of the tensile strain. Negative stiffness modulus, however, creates numerical difficulties. Lin (14) and Salem and Mohraz (32) avoided the difficulty by using a stepwise reduction of the tensile stress over ranges of strain. In the present study, tension stiffening effects have not been incorporated.

Steel Reinforcement

In this study reinforcing bars are assumed to be perfectly elastic-plastic. Furthermore, reinforcing bars are modeled as uniaxial fibers distributed over the area of the element at the level of the centroid of the steel reinforcement. The

constitutive matrix for the steel reinforcement parallel to
the direction of the steel can be written as follows

$$[c_{ij}]_{steel} = \begin{bmatrix} E_S & 0 & 0 \\ 0 & 0 & 0 \\ 0 & 0 & 0 \end{bmatrix} \qquad (2.32)$$

where E_S is the tangent elastic modulus of steel. When the
steel has yielded E_S is assumed to be zero. In the numerical
computations the concrete at the level of the steel reinforce-
ment is treated as a composite layer. The bond-slip that
occurs between the steel reinforcement and the concrete has
not been modeled in this study.

CHAPTER 3. FINITE ELEMENT IDEALIZATION

General

The computer oriented finite element method has become one of the most powerful tools in the analysis of structures. It has unified the analysis of any arbitrary structure of any geometric form to one basic fundamental procedure. In the finite element method arbitrary geometry and support conditions, arbitrary loadings and arbitrary variation of material properties within the structure can be considered with ease. Several books (40, 41, 42, 43, 44, 45) dealing exclusively with the fundamentals of the finite element method and its application to a wide class of problems have been published. Consequently, the basic concepts of the method will only be reviewed very briefly and the formulations that are of direct relevance to the present study will be presented.

Basic Concepts of the Finite Element Method

In a very simple sense the finite element method may be considered as an extension of the displacement method of analysis of frames and trusses into a two or three dimensional continuum. The structure is idealized as an assemblage of separate elements interconnected at nodes. In trusses and frames the finite elements are one dimensional bars and/or beams. In two or three dimensional continuum the finite elements are two or three dimensional finite elements

of appropriate shapes. The type of element, the number of elements and the arrangement of the elements can be selected based on the accuracy needed and the available computer capabilities.

In a more rigorous sense the finite element method is considered to be a special case of Raleigh - Ritz method. The variational formulation of the method provides a sound mathematical foundation and extends the application of the method to all problems where an application of variational techniques is possible. This more rigorous approach gives an insight into the development of necessary convergence criteria and into the development of different possible finite element models.

Regardless of the shape or the type of the finite element the analysis is carried out using the same basic principles. In the displacement approach, the displacements within an element are assumed to be approximated by a function of the nodal displacements following simple patterns, usually polynomials. The assumed displacement functions can then be used to derive the stiffness matrices for the elements using the principle of virtual work. The element stiffnesses are then appropriately added to form the total stiffness matrix for the structure. The resulting algebraic simultaneous equations relating nodal forces to nodal displacements are then solved. From the known nodal displacements, using the assumed displacement functions, the displacements, strains, and stresses at

any point within the element can be calculated.

Causes of Geometric Nonlinearity

With increasing loads all real structures eventually behave in a nonlinear fashion. Nonlinear behavior results in total stresses, strains and displacements not being directly proportional to the applied load. The type of nonlinearity can be classified as geometric nonlinearity and/or material nonlinearity as they are due to two distinct phenomena.

Geometric nonlinearity is ascribed to large-deflection problems in which the deformed configuration must be used to write equilibrium equations, and to problems related to structural stability. Material nonlinearity is due to nonlinear stress-strain relationships of the materials that make up the structure. It is possible in an analysis to include nonlinearity due to either material or geometry alone or combined. In general it can be said that geometric nonlinear effects are important in "slender" structures and material nonlinear effects may be very dominant in "thick" structures. For example, an accurate analysis of long columns can only be obtained when geometric nonlinear effects are included in the analysis. Analysis considering material nonlinearity alone has given excellent agreement with the experimental results for the case of reinforced concrete beams.

Scope of the Geometric Nonlinear Effects Considered

Geometrically nonlinear problems can further be classi-
fied as highly nonlinear or moderately nonlinear. Some ex-
amples of the highly nonlinear problems are the inflatable
shells and the large stretching and bending of rubber-like
materials. In such cases strains are large compared to unity
and parts of the structure may undergo large rotations.
Further, the mass density and the volume of the material may
change considerably during deformation and also, the loads may
be a function of displacements. There is also another group
of problems in which the strains may still be small but
nevertheless in which large rotations could occur. For all
such problems, finite element formulations must be based on
consistent mathematical theories of finite elasticity (45, 46,
47). A careful definition of stresses and strains is required.
The strains are defined either based upon the initial unde-
formed configuration (Lagrangian Strains) or defined based
upon the current deformed configuration (Eulerian Strains).

Corresponding to the above definitions of strains,
definitions of stresses also exist. The definition of stress
as force per unit area in the deformed state is the physical
concept of stress. Such a definition of stress is called
Eulerian Stress. The Lagrangian stress tensor and the
Kirchoff's stress tensor are definitions of stresses referred
to the original undeformed configuration (48). The Lagrangian

stress tensor is generally not used in finite element formula-
tions due to its unsymmetric nature. Several investigators
have used the Kirchoff's stress tensor and the Lagrangian
strain tensor in the finite element formulation of finite
strain and finite displacement problems (47, 49, 50). The
product of the components of Lagrangian strain with components
of Kirchoff's stress results in an equation which is equivalent
to the internal work.

Attention is now directed towards the type of problems
this study is attempting to solve. In reinforced concrete
structures the concrete strains are small compared to unity.
There exists an important class of problems in which the
geometric nonlinear effects are significant even though the
displacements are small. The problems involving structural
stability need not have actual deflections which are large in
any sense. In a plate problem, the stresses due to membrane
action may cause a considerable decrease in the displacements
compared to those obtained from a linear solution even though
the displacements may still be quite small. Thus, part of
this study is directed towards problems in which the inclusion
of geometric nonlinear effect is critical even though the dis-
placements need not necessarily be large.

In the finite element formulations which follow in this
chapter, it is assumed that the displacement gradients are
small compared to unity. A simplified form of the exact
strain-displacement relationship is used. However, the

retention of certain nonlinear terms in the strain-displacement relationship is critical to the analysis when the geometric nonlinear effects are considered. As first order approximation no distinction between Kirchoff's stress and the Eulerian stress is made. Such an approximation has been used by Berg (23) and has also been suggested by Fung (48). A single nomenclature σ_i for the ith component of the stress and ϵ_i for the ith component of strain is used.

Layering Technique

In the layered approach the finite element is divided into a number of layers over the depth (Fig. 11). The number of layers used must be sufficient to follow the variation of material properties over the depth. Each concrete layer is assumed to have a single set of elastic constants determined from the magnitude of strains at the centroid of the element evaluated at the midheight of the layer. Each layer is assumed to be in a state of plane stress.

The concrete layer at the level of the steel is treated as a composite layer. Assuming the steel to be uniaxial fibers distributed over the layer, the constitutive matrix for steel parallel to the direction of reinforcement is

$$[c'_{ij}]_{steel} = \frac{A_s}{t_j} \begin{bmatrix} E_s & 0 & 0 \\ 0 & 0 & 0 \\ 0 & 0 & 0 \end{bmatrix} \tag{3.1}$$
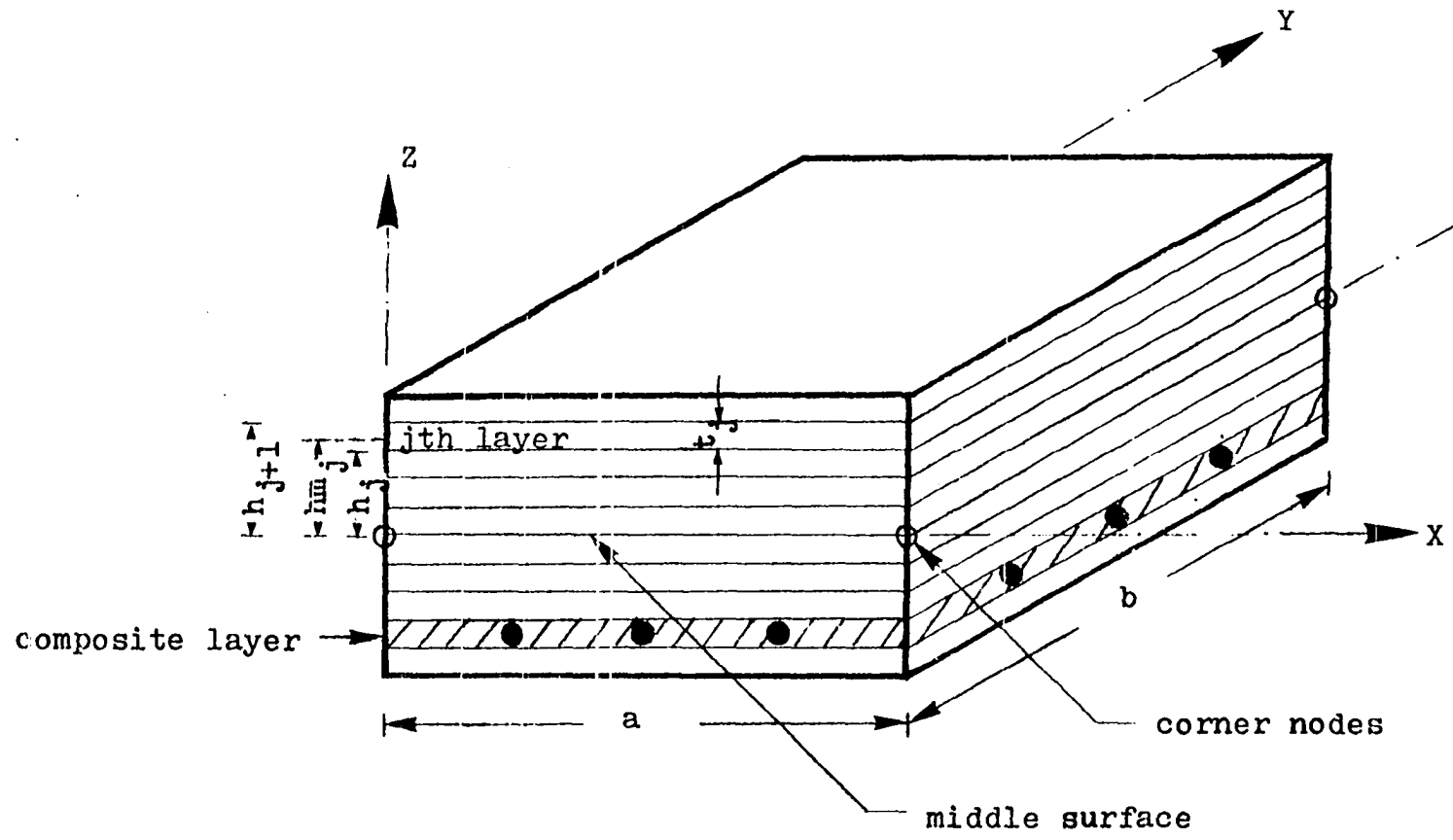
Fig. 11. A typical layering system for the rectangular element

where A_s is the area of steel reinforcement per unit width, t_j is the thickness of the composite layer j, and E_s is the tangent modulus for steel. If the direction of the steel is not along the element axes, then equation 3.1 is transformed to the element axes using the transformation matrix given in equation 2.11. The θ in equation 2.12 will be the angle between the element x-axis and the direction of the reinforcement. Thus, the constitutive matrix for the composite layer in the **element axes directions is** given by

$$[c_{ij}]_{composite} = [c_{ij}]_{concrete} + [c_{ij}]_{steel} \qquad (3.2)$$

Equation 3.2 is used when considering the contribution of the composite layer in the calculation of the stiffness matrices of the elements. It is possible to have more than one composite layer and also, the possibility exists of having steel reinforcement in more than one direction in a composite layer. Extension of the procedure described above to cover those cases is straightforward.

Rectangular Element Displacement Functions

A rectangular element having membrane and bending stiffness is used in this study (Fig. 11). With the use of Kirchoff's thin plate assumptions, the finite element model could be used to study beams, columns, thin slabs and thin shells. The rectangular element has four nodes, one in each corner. The unknown displacements in each node are the

translational displacements u, v, and w in x, y, and z
directions, respectively, and the two rotations of the node
about x and y axes. The assumed displacement functions for
the element are

$$u = \alpha_1 + \alpha_2 x + \alpha_3 y + \alpha_4 xy$$

$$v = \alpha_5 + \alpha_6 x + \alpha_7 y + \alpha_8 xy \qquad (3.3)$$

$$w = \alpha_9 + \alpha_{10} x + \alpha_{11} y + \alpha_{12} x^2 + \alpha_{13} xy + \alpha_{14} y^2 + \alpha_{15} x^3$$
$$\qquad + \alpha_{16} x^2 y + \alpha_{17} xy^2 + \alpha_{18} y^3 + \alpha_{19} x^3 y + \alpha_{20} xy^3$$

where x and y are the local coordinates of the point inside
the element and the α's are the generalized displacements
parameters. The assumed displacement function for w is non-
conforming and hence mathematical convergence proofs cannot be
given. However, for the linear elastic cases and for practical
mesh sizes used this element compares favorably with other
possible elements (42).

This rectangular finite element described above has a
total of 20 nodal displacements. The nodes are located at the
midsurface corners of the element. The list of nodal dis-
placements at any node i is

$$r_i = \begin{bmatrix} u \\ v \\ w \\ w \cdot_x \\ w \cdot_y \end{bmatrix}_{\text{node } i} \qquad (3.4)$$

where the comma denotes partial differentiation. A right
handed coordinate system is used and the positive directions

of the displacements are shown in Fig. 12.

The nodal displacement vector for the element can then be defined as

$$r = \begin{bmatrix} r_1 \\ r_2 \\ r_3 \\ r_4 \end{bmatrix} \qquad (3.5)$$

where r_1, r_2, r_3, and r_4 are the values of the nodal displacements at nodes 1, 2, 3, and 4, respectively, defined by equation 3.4. In the developments to follow, a relationship between the generalized displacement parameters α and the nodal displacements r is necessary. Using equations 3.3 and 3.4 and writing in a matrix form,

$$r = C\alpha \qquad (3.6)$$

where matrix C is obtained by the appropriate substitution of local nodal coordinates of the element. The matrix C is not to be confused with the constitutive matrix $[c_{ij}]$ or the elements of the constitutive matrix in indicial notation c_{ij}. The inverse relation of equation 3.6 is

$$\alpha = C^{-1}r \qquad (3.7)$$

where C^{-1} can be obtained using an inversion subroutine in the computer program or it can be obtained algebraically. The matrix C^{-1} is solely a function of the element's dimensions and in this study a direct algebraic inversion of matrix C was performed. (The explicit expressions for the C^{-1} matrix are given in the Appendix.)

$$r = \begin{bmatrix} u \\ v \\ w \\ w,_x \\ w,_y \end{bmatrix}$$
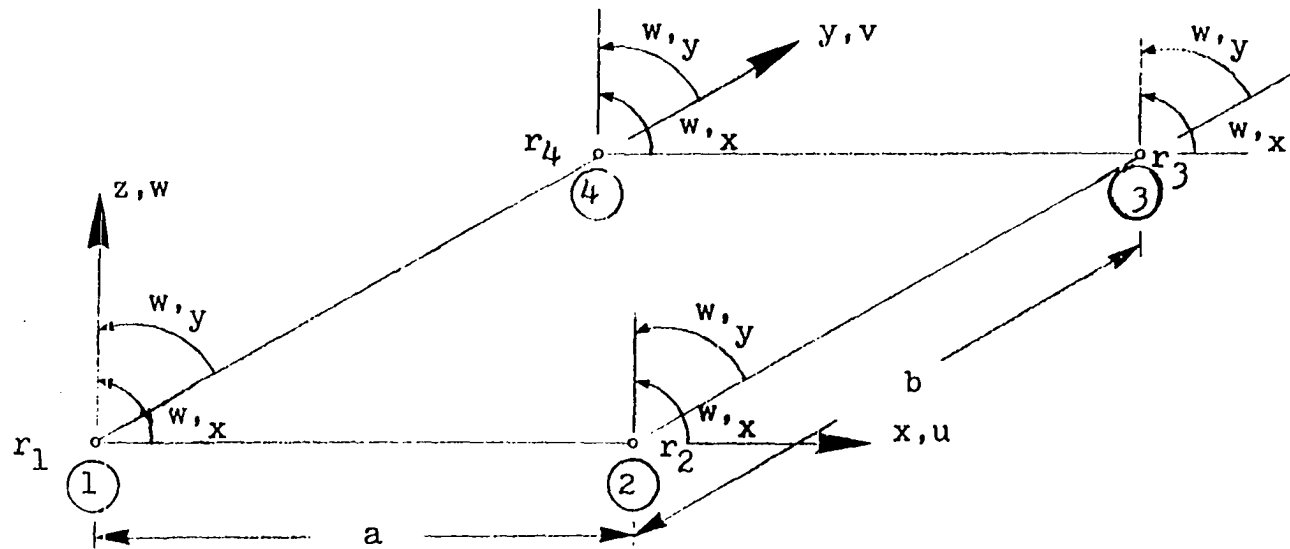
Fig. 12. Element nodal numbering system, element local coordinate system, and the positive direction of nodal displacements

Strain Displacement Relationships

Kirchoff's thin plate assumptions reduce the plate problem to a two dimensional problem and, therefore, it is necessary to consider only the strains in the plane of the plate. The components of strain in the Lagrangian form can be written as

$$\epsilon_x = u,_x + \tfrac{1}{2}[(u,_x)^2 + (v,_x)^2 + (w,_x)^2]$$

$$\epsilon_y = v,_y + \tfrac{1}{2}[(u,_y)^2 + (v,_y)^2 + (w,_y)^2] \qquad (3.8)$$

$$\epsilon_{xy} = u,_y + v,_x + [u,_x \cdot u,_y + v,_x \cdot v,_y + w,_x \cdot w,_y]$$

It can be seen that the above finite strain-displacement relationships involve linear and quadratic terms. It should also be noted that the above expressions are exact and not merely a second order approximation. As stated previously when discussing the scope of the geometric nonlinear effects accounted for in this study, considerable simplification in the details of the finite element formulation can be made by omitting certain quadratic terms from the exact expressions given in equation 3.8. In a simplified form, certain powers of $w,_x$ and $w,_y$ are only retained in the strain-displacement relationships. The simplified form is given by

$$\epsilon_x = u,_x + \tfrac{1}{2}(w,_x)^2$$

$$\epsilon_y = v,_y + \tfrac{1}{2}(w,_y)^2 \qquad (3.9)$$

$$\epsilon_{xy} = u,_y + v,_x + (w,_x \cdot w,_y)$$

The simplified strain-displacement relationships given in equation 3.9 are the same that are used in von Karman's large deflection theory of plates.

The strains at a point a distance z from the midsurface can be written as

$$\epsilon_x = u,_x - z \cdot w,_{xx} + \tfrac{1}{2}(w,_x)^2$$

$$\epsilon_y = v,_y - z \cdot w,_{yy} + \tfrac{1}{2}(w,_y)^2 \qquad (3.10)$$

$$\epsilon_{xy} = u,_y + v,_x - 2 \cdot z \cdot w,_{xy} + (w,_x \cdot w,_y)$$

where $w,_{xx} = \dfrac{\partial^2 w}{\partial x^2}$, $w,_{yy} = \dfrac{\partial^2 w}{\partial y^2}$, $w,_{xy} = \dfrac{\partial^2 w}{\partial x \partial y}$.

The above expression for strain can conveniently be expressed as a linear and a nonlinear part

$$\epsilon_i = \epsilon_i^L + \epsilon_i^{NL} \qquad (3.11)$$

where i = 1,2,3 defining ϵ_x, ϵ_y and ϵ_{xy} respectively. Expressions for strains given in equation 3.10 can be rewritten in indical notation containing linear and nonlinear parts as follows.

$$\epsilon_i = L_i^T d + \tfrac{1}{2} d^T H_i d \qquad (3.12)$$

in which L_i = a vector, H_i = a symmetric matrix, and d = a vector of displacement gradients. The matrices L_i, H_i and d are defined as follows.

$$L_1^T = \begin{bmatrix} 1 & 0 & 0 & 0 & 0 & 0 & -z & 0 & 0 \end{bmatrix}$$

$$L_2^T = \begin{bmatrix} 0 & 0 & 0 & 1 & 0 & 0 & 0 & -z & 0 \end{bmatrix} \qquad (3.13)$$

$$L_3^T = \begin{bmatrix} 0 & 1 & 1 & 0 & 0 & 0 & 0 & 0 & -2z \end{bmatrix}$$

$$d^T = \begin{bmatrix} u,_x & u,_y & v,_x & v,_y & w,_x & w,_y & w,_{xx} & w,_{yy} & w,_{xy} \end{bmatrix} \qquad (3.14)$$

H_1, H_2 and H_3 are symmetric matrices of size 9 x 9 in which all the elements are zero except those defined below which have a value of unity

$$H_1(5,5) = 1 \ , \ H_2(6,6) = 1 \ , \ H_3(5,6) = 1 \ , \ H_3(6,5) = 1$$
$$(3.15)$$

The form and the nomenclature used in equation 3.12 is the same as that introduced by Rajasekaran and Murray (51). When linear strain-displacement relationships are desired, the second term in equation 3.12 is dropped.

Incremental Tangent Stiffness Matrices

A fundamental property of the finite element models is that a typical element can be isolated from the total structure and its behavior can be studied independently. The process of connecting the elements to form the total structure is a topological one and is independent of the linearity or the nonlinearity of the problem at hand. In this chapter discussion is confined to a single element in the formulation of the tangent stiffness matrix. The tangent stiffness matrix for the total structure can be obtained by applying well documented procedures for appropriately assembling the element stiffness matrices (40).

A matrix D relating displacement gradient vector d to the generalized displacement parameters α is defined as follows

$$d = D\alpha \qquad (3.16)$$

The explicit form of the D matrix for the assumed displacement functions is given in the Appendix. Using the equation 3.7, equation 3.16 can be rewritten in terms of nodal displacements as follows

$$d = DC^{-1}r \qquad (3.17)$$

In equation 3.17 the displacement gradients at a point within the element are expressed in terms of the element nodal displacements through transformation matrices D and C^{-1}. Using the equation 3.17, the strain-displacement relationship in equation 3.12 can be rewritten as

$$\epsilon_i = L_i^T DC^{-1}r + \tfrac{1}{2}r^T C^{-1^T} D^T H_i DC^{-1}r \qquad (3.18)$$

Thus, equation 3.18 relates the strain at any point within the element at a distance z from the middle surface to the mid-surface nodal displacements.

In the formulations to follow, for an arbitrary set of small virtual nodal displacements, a corresponding virtual strain distribution inside the element is required. Using equation 3.18 we obtain,

$$\delta\epsilon_i = [L_i^T DC^{-1} + r^T C^{-1^T} D^T H_i DC^{-1}] \, \delta r \qquad (3.19)$$

where δ represents virtual quantities. In arriving at equation 3.19 the symmetric property of the second term in equation 3.18 was used. The dependence of $\delta\epsilon_i$ on the current displacement configuration r is to be noted.

In a general case the structure is subjected to inertia

forces, body forces and surface distributed forces. Since
this study deals with static loads only, the inertia forces
will not be considered in the equilibrium equations. The
body forces and the surface tractions can be converted into
equivalent nodal loads by simple statics or by procedures
consistent with the assumed displacement functions. Combining
the nodal load vector P and the principle of virtual work, the
following work equation can be written

$$\delta r^T P = \int_V \delta\epsilon_i \, \sigma_i \, dv \tag{3.20}$$

where the summation convention over the repeated index is
implied. Transposing the expression for $\delta\epsilon_i$ given in equation
3.19, equation 3.20 is rewritten as

$$\delta r^T P = \int_V \delta r^T [C^{-1^T} D^T L_i + C^{-1^T} D^T H_i DC^{-1} r] \, \sigma_i \cdot dv \tag{3.21}$$

The fact that the virtual displacement δr^T is arbitrary leads
to the equilibrium equation

$$P = \int_V [C^{-1^T} D^T L_i + C^{-1^T} D^T H_i DC^{-1} r] \, \sigma_i \cdot dv \tag{3.22}$$

With reference to the use of σ_i instead of Kirchoff's stress
in equation 3.22 attention is drawn to the earlier discussion
in this chapter regarding the scope of geometric nonlinear
effects to be considered.

The nonlinear analysis of the structure is carried out by
applying the loads in small increments. Therefore, in the
process of analysis, relationships between incremental loads

and incremental displacements, between incremental displacements and incremental strains, and between incremental strains and incremental stresses are required. Using the total strain-displacement relationships in the displacement configuration 1 and in the displacement configuration 2 as given by equation 3.12 the incremental strain quantitites are obtained as follows.

$$\Delta \epsilon_i = L_i^T \Delta d + {}^1d^T H_i \Delta d + \Delta d^T H_i \Delta d \qquad (3.23)$$

where the symbol Δ implies the incremental quantities and ${}^1d^T$ is the total displacement gradient vector at the displacement configuration 1. It should be noted that the incremental strains are related nonlinearly to the incremental displacements.

Exact expressions for the incremental strains as given by equation 3.23 when used in developing the stiffness matrices would result in a set of nonlinear equations relating the incremental loads to the incremental displacements. In this study the nonlinear problem is solved using the tangent stiffness approach. Hence, it is sufficient to form a linearized form of the equations relating the incremental loads to the incremental displacements and iterate until equilibrium is achieved. Rewriting equation 3.23 in terms of nodal displacements in a linearized form we get

$$\Delta \epsilon_i = [L_i^T D C^{-1} + {}^1r^T C^{-1^T} D^T H_i D C^{-1}] \Delta r \qquad (3.24)$$

where ${}^1r^T$ is the total nodal displacement vector at the start of the increment.

Writing the equilibrium equation in an incremental form we obtain

$$\Delta P = \int_V \Delta [C^{-1^T} D^T L_i + C^{-1^T} D^T H_i DC^{-1} r] \sigma_i \cdot dv +$$
$$\int_V [C^{-1^T} D^T L_i + C^{-1^T} D^T H_i DC^{-1} \,{}^1 r] \Delta \sigma_i \cdot dv \qquad (3.25)$$

or

$$\Delta P = \int_V C^{-1^T} D^T H_i DC^{-1} \Delta r \cdot \sigma_i \cdot dv +$$
$$\int_V [C^{-1^T} D^T L_i + C^{-1^T} D^T H_i DC^{-1} \,{}^1 r] \Delta \sigma_i \cdot dv \qquad (3.26)$$

Idealizing the material to be incrementally linearly elastic a relationship between the incremental stresses and the incremental strains is obtained.

$$\Delta \sigma_i = c_{ij} \Delta \epsilon_j \qquad (3.27)$$

where the c_{ij} are the coefficients of the constitutive matrix developed in Chapter 2. Substituting equation 3.27 into equation 3.26 we get,

$$\Delta P = \int_V C^{-1^T} D^T H_i DC^{-1} \Delta r \cdot \sigma_i \cdot dv +$$
$$\int_V [C^{-1^T} D^T L_i + C^{-1^T} D^T H_i DC^{-1} \,{}^1 r] \cdot c_{ij} \Delta \epsilon_j \cdot dv \qquad (3.28)$$

The first term under the integral sign yields the initial stress matrix and is defined by

$$K_\sigma = \int_V C^{-1^T} D^T H_i DC^{-1} \cdot \sigma_i \cdot dv \qquad (3.29)$$

Rewriting equation 3.28 with the definition of K_σ and using equation 3.24 we get

$$\triangle P = [K_\sigma + \int_V (C^{-1^T}D^TL_i + C^{-1^T}D^TH_iDC^{-1} \; {}^1r)c_{ij}$$

$$(L_j^TDC^{-1} + {}^1r^TC^{-1^T}D^TH_jDC^{-1})] \triangle r \cdot dv \qquad (3.30)$$

Expanding the terms in equation 3.30 and regrouping

$$\triangle P = [K_\sigma + \int_V C^{-1^T}D^T(c_{ij}L_iL_j^T)DC^{-1} \cdot dv$$

$$+ \int_V C^{-1^T}D^Tc_{ij}L_i \; {}^1r^T C^{-1^T}D^TH_jDC^{-1} \cdot dv \qquad (3.31)$$

$$+ \int_V C^{-1^T}D^TH_iDC^{-1} \; {}^1r \; (c_{ij}L_j)DC^{-1} \cdot dv$$

$$+ \int_V C^{-1^T}D^TH_iDC^{-1} \; {}^1r c_{ij} \; {}^1r^T C^{-1^T}D^T H_j D C^{-1} \cdot dv] \triangle r$$

Using the nomenclature commonly found in literature the
various terms under the integral signs are identified separate-
ly. The basic small displacement stiffness matrix is given by
the second term of equation 3.31 or

$$K_0 = \int_V C^{-1^T}D^T(c_{ij}L_iL_j^T)DC^{-1} \cdot dv \qquad (3.32)$$

The rest of the terms under the integral sign can be written as

$$K_D = K_1 + K_1^T + K_2 \qquad (3.33)$$

where K_D is the initial displacement matrix. The matrices
K_1 and K_2 are defined as follows

$$K_1 = \int_V C^{-1^T}D^Tc_{ij}L_i \; {}^1r^T \; C^{-1^T}D^TH_jDC^{-1} \cdot dv \qquad (3.34)$$

$$K_2 = \int_V C^{-1^T}D^TH_iDC^{-1} \; {}^1r \; c_{ij} \; {}^1r^T \; C^{-1^T}D^TH_jDC^{-1} \cdot dv \qquad (3.35)$$

In summary the relation between the incremental loads and the incremental displacements is given by

$$\triangle P = K_T \cdot \triangle r \tag{3.36}$$

where K_T is the tangent stiffness matrix. The tangent stiffness matrix can be considered to be composed of three parts as given by the following equation (3.37)

$$K_T = K_0 + K_\sigma + K_D \tag{3.37}$$

The form of the tangent stiffness matrix K_T is the same that was obtained by Felippa (52).

K_0 is the basic small displacement stiffness matrix and is a function of the material properties that exist at the start of the increment. K_σ is the initial stress matrix and is a function of the total stresses that are present at the start of the increment. K_σ in conjunction with K_0 can be used to solve linear eigenvalue buckling problems. K_D is the initial displacement matrix and is a function of the total nodal displacements and the material properties at the start of the increment. The initial displacement matrix is of the same order as the initial stress matrix and must be included in geometric nonlinear problems using a total Lagrangian formulation. For a nonlinear analysis considering material nonlinearity alone, the matrices K_σ and K_D are not formed. Finally, the summation convention in the indical notations used in the expressions for the stiffness matrix is implied.

Integration of the Stiffness Matrices

It can be seen from the expressions for the tangent stiffness matrix, that an explicit form of the stiffness matrix can only be obtained by performing the integrations over the volume. In the incremental procedure, the stiffness matrices are usually evaluated at the start of each incremental load step. In addition, the stiffness matrices may have to be updated in the midst of iterations if significant nonlinearity is encountered. Extensive cracking of concrete frequently results in slow convergence and more than one update between the increments is not unusual. The numerical evaluation of the stiffness matrices K_0, K_σ and K_D is a major time consuming operation in the numerical solution.

Refined higher order elements contain higher order displacement functions. Higher order displacement functions result in a large number of higher order terms inside the integral sign in the expressions for the stiffness matrices. Higher order stiffness matrices K_σ and K_D contain higher powers of x and y than the basic stiffness matrix K_0 and an exact albegraic integration of the expressions is exceedingly tedious if not impossible. Hence, most researchers have used some form of numerical integration to evaluate the stiffness matrices. Most of the works in published literature use Gaussian quadrature formulae. Sabir and Lock (53) used four integration points for the same rectangular finite element.

Numerical integration schemes are time consuming and require storage of a number of quantities like material constants, stress and strain quantities at every integration point. In this study, algebraic integrations are performed to obtain K_0, K_σ and K_D after making some simplifying assumptions.

An exact algebraic integration of the equation 3.32 is performed to obtain the basic stiffness matrix K_0. The initial stress matrix K_σ and the initial displacement matrix K_D are obtained using algebraic integration after certain simplifying assumptions are made. In evaluating K_σ, the stress resultants N_x, N_y and N_{xy} at the centroid of the element are first evaluated. It is then assumed that N_x, N_y and N_{xy} are constant over the entire element when integration over the area is performed. Similar approximations have previously been used by Gallagher et al. (54) for the same finite element model. A study of the initial displacement matrix expressions in equation 3.34 and 3.35 reveal that the quantities of interest in the total displacement gradient vector are the quantities $w,_x$ and $w,_y$. In the integration process used, $w,_x$ and $w,_y$ at the centroid of the element are first calculated. It is then assumed that $w,_x$ and $w,_y$ are constants while an integration over the area is performed. Such a procedure gave satisfactory results and the results are compared later in Chapter 5 with tangent stiffness matrices obtained using numerical integration. It must also be noted that if a total equilibrium check

is made at frequent intervals in the analysis, an exact evaluation of the tangent stiffness matrix is not a necessity.

The explicit forms of the stiffness matrix are lengthy and are relegated to the **Appendix**. To illustrate the integration procedure using layered discretization, the evaluation of the basic stiffness matrix K_0 is explained below in some detail. Additional details of the formulation of K_0, K_σ and K_D can be found in **the Appendix**.

The basic stiffness matrix is defined by the following equation

$$K_0 = \int_V C^{-1^T} D^T (c_{ij} L_i L_j^T) D C^{-1} \cdot dv \qquad (3.38)$$

The matrix C^{-1} is a function of element dimensions a and b only (Appendix) and can be taken out of the integral sign. The matrix D is a function of x and y only and the matrix L_i is a function of z only. Taking the matrix C^{-1} outside the integral sign and splitting the integral over the volume as an integral over the area and an integral over the depth, we get

$$K_0 = C^{-1^T} [\int_{Area} D^T (\int_z (c_{ij} L_i L_j^T) dz) D \cdot dA] C^{-1} \qquad (3.39)$$

Considering the innermost integral and defining a matrix $\hat{R}_0$,

$$\hat{R}_0 = \int_z c_{ij} L_i L_j^T \cdot dz \qquad (3.40)$$

The integration over the depth is replaced by integration over the individual layers and a discrete summation over all layers.

$$\hat{K}_0 = \sum_{\substack{All \\ layers}} \int_{h_j}^{h_{j+1}} (c_{ij} L_i L_j^T) \cdot dz \qquad (3.41)$$

where h_j and h_{j+1} are the near end and far end layer distances from the middle surface (Fig. 11). Keeping in mind the summation convention implied in the indical notation, equation 3.41 can be rewritten in an expanded form

$$\hat{K}_{09x9} = \sum_{\substack{All \\ layers}} \int_{h_j}^{h_{j+1}} (c_{11} L_1 L_1^T + c_{12} L_1 L_2^T + c_{13} L_1 L_3^T$$
$$+ c_{21} L_2 L_1^T + c_{22} L_2 L_2^T + c_{23} L_2 L_3^T \qquad (3.42)$$
$$+ c_{31} L_3 L_1^T + c_{32} L_3 L_2^T + c_{33} L_3 L_3^T) \cdot dz$$

An explicit form of the $\hat{K}_0$ matrix defined by equation 3.42 is given in Table 4 in Appendix. The material constants c_{ij} are different for each layer and the final values of each element in the $\hat{K}_0$ matrix is obtained by a summation of all layers. Some of the important characteristics of the K_0 matrix deserve attention. First, the $\hat{K}_0$ matrix is symmetric. For a nonhomogenous slab, coupling between the inplane and out of plane displacements exists at the basic linear stiffness matrix level. This can be detected by observing the terms in the upper right hand corner and lower left hand corner of the $\hat{K}_0$ matrix (Table 4, Appendix), which will only vanish if vertical symmetry exists relative to the midsurface. The matrix K_0 is then obtained by

$$K_0 = C^{-1^T} [\int_{Area} D^T \hat{R}_0 D \cdot dA] \, C^{-1} \tag{3.43}$$

The explicit form of the integral is given in Appendix. The pre and post multiplications by C^{-1^T} and C^{-1} respectively were done when the numerical calculations were performed in the computer.

Evaluation of Layer Stresses and Element Stress Resultants

In the incremental procedure, the incremental strains need to be calculated from the known incremental displacements. When geometric nonlinear effects are included the incremental strains are dependent upon the incremental displacements and the total displacements at the start of the increment (equation 3.23). Incremental strains can correctly be calculated by considering the total strains at the displacement configurations at the start and at the end of the increment. The incremental strains are given by

$$\Delta \epsilon_i = {}^2\epsilon_i - {}^1\epsilon_i \tag{3.44}$$

where ${}^2\epsilon_i$ is the total strain at the end of the increment and ${}^1\epsilon_i$ (equation 3.18) is the total strain at the start of the increment. In the numerical calculation equations 3.17 and 3.12 are used to calculate ϵ_i. When material nonlinearity alone is considered, the quadratic second term in equation 3.12 is omitted.

The incremental layer stresses are calculated from the

incremental layer strains using the constitutive matrix of the layer

$$\Delta \sigma_i = c_{ij} \cdot \Delta \epsilon_j \qquad (3.45)$$

It is important to note that the values of c_{ij} used in equation 3.45 are those that were used in the generation of the stiffness matrices of the element. When composite layers are encountered, the real incremental stresses in the concrete and steel are calculated separately using the material constants of each material separately. The total stresses in the layers are obtained by direct addition of the incremental quantities to the previous totals.

Total element stress resultants are calculated from the known total layer stresses. The stress resultants N_x, N_y and N_{xy} and M_x, M_y and M_{xy} are given by

$$N_x = \sum_{Layers} \sigma_x \cdot t_j \qquad\qquad M_x = \sum \sigma_x \cdot t_j \cdot hm_j$$

$$N_y = \sum \sigma_y \cdot t_j \qquad\qquad M_y = \sum \sigma_y \cdot t_j \cdot hm_j$$
$$\qquad\qquad\qquad\qquad\qquad\qquad\qquad\qquad (3.46)$$
$$N_{xy} = \sum \sigma_{xy} \cdot t_j \qquad\qquad M_{xy} = \sum \sigma_{xy} \cdot t_j \cdot hm_j$$

where t_j is the thickness of the layer j and hm_j is the distance from the middle surface to the midpoint of layer j (Fig. 11). It is assumed in the expressions that the stresses are constant over the thickness of a layer. When composite layers are encountered equivalent steel stresses distributed over the thickness of the composite layer and the real concrete

stresses in the composite layer are used in evaluating the stress resultants. In the numerical procedure used, stresses and stress resultants at the centroids were calculated for each element.

CHAPTER 4. NUMERICAL SOLUTION OF THE NONLINEAR PROBLEM

General

Linear structural analysis assumes linear strain-displacement relationships and linear stress-strain laws. In linear structural analysis with any arbitrary loading, the displacements and stresses are unique and can be found in a single operation. However, the use of nonlinear relationships lead to a set of nonlinear equations. Exact solutions to a set of general nonlinear equations are difficult to obtain. Thus, quantitative solutions to the nonlinear problems are obtained by using numerical techniques and by using the computing power of modern high speed digital computers. In addition, incremental procedures have to be used in many practical cases, due to the fact that the final solution may be path dependent. As an example, the sequence of cracking of elements may have a significant effect on the internal redistribution of stresses. Due to the path dependent nature of the problems encountered in this study, only procedures using incremental techniques will be reviewed.

Available Solution Techniques

An explanation of the various solution schemes employed to solve nonlinear structural problems incrementally will point out parallels with the various numerical procedures used for the solution of differential equations. Incremental nonlinear

analysis procedures can be explained as a series of linear solutions with corrections to these linear solutions determined from the inclusion of the nonlinear effects.

For the purpose of explanation, consider simple one degree of freedom load-deflection and stress-strain diagrams as shown in Fig. 13. It must be emphasized that Fig. 13 represents a highly simplified form of what actually happens in a multidimensional space. Let the curved lines in Fig. 13 represent the true response of the structure and the material.

The simplest approach to the solution of a nonlinear problem is the use of a pure incremental approach with no corrections (Fig. 13a). Loads are applied in small increments and the structure is assumed to behave linearly within each increment based on their initial values at the start of the increment. For an increment of load, the corresponding linear increase in the stresses and the strains are represented in the stress-strain diagram. It is obvious that the linearization errors accumulate as the analysis proceeds. Hence, the size of the increment must necessarily be small. If the non-linearities are small, the above procedure would give very satisfactory results with the least number of required numerical calculations. However, it must be noted that at no point does the calculated load-deflection diagram and the stress-strain diagram lie on the true curve. Various improvements to the solution procedure can be made by considering the state of the structure both at the start and at the end of the
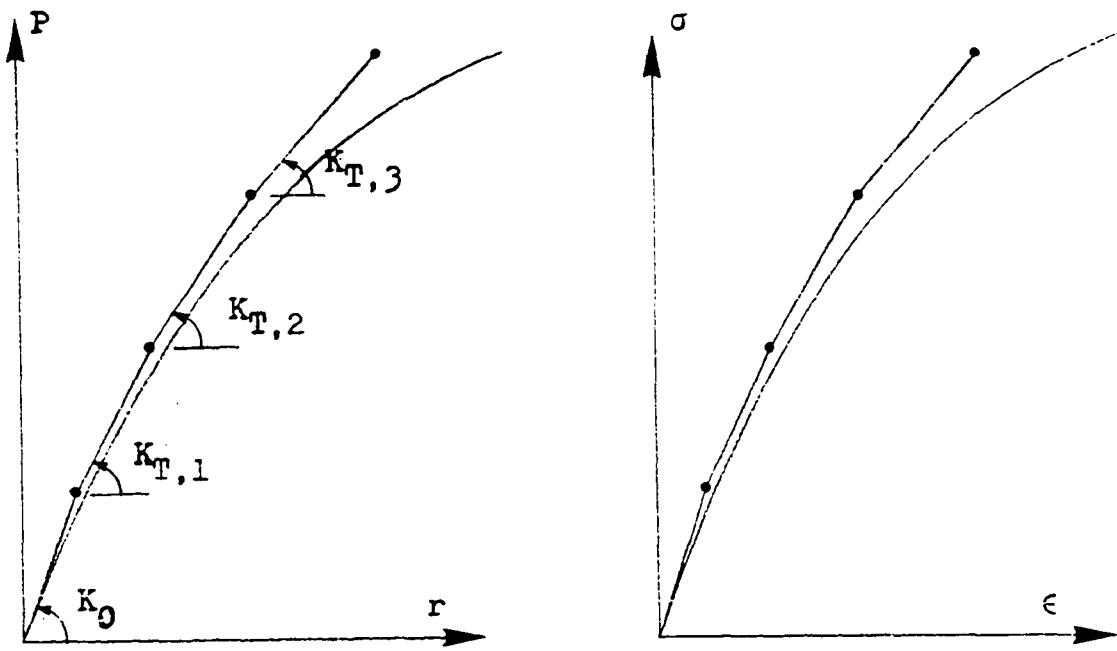
a. Purely increment approach
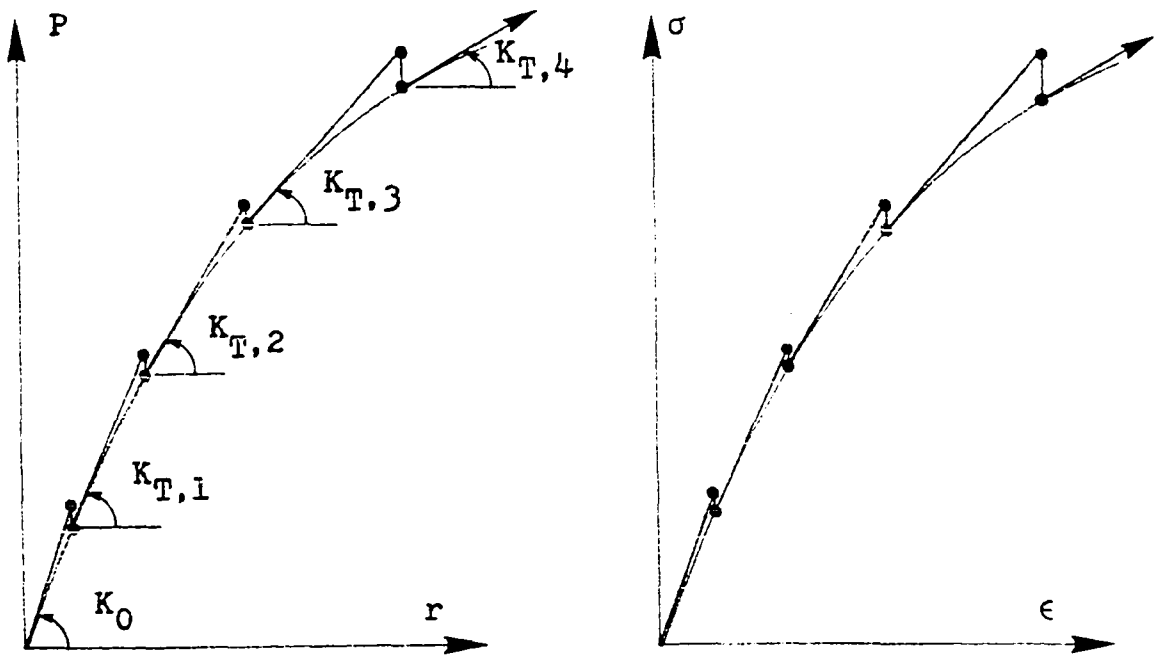
b. Incremental approach with one step correction

Fig. 13. Numerical techniques for the solution of nonlinear problems
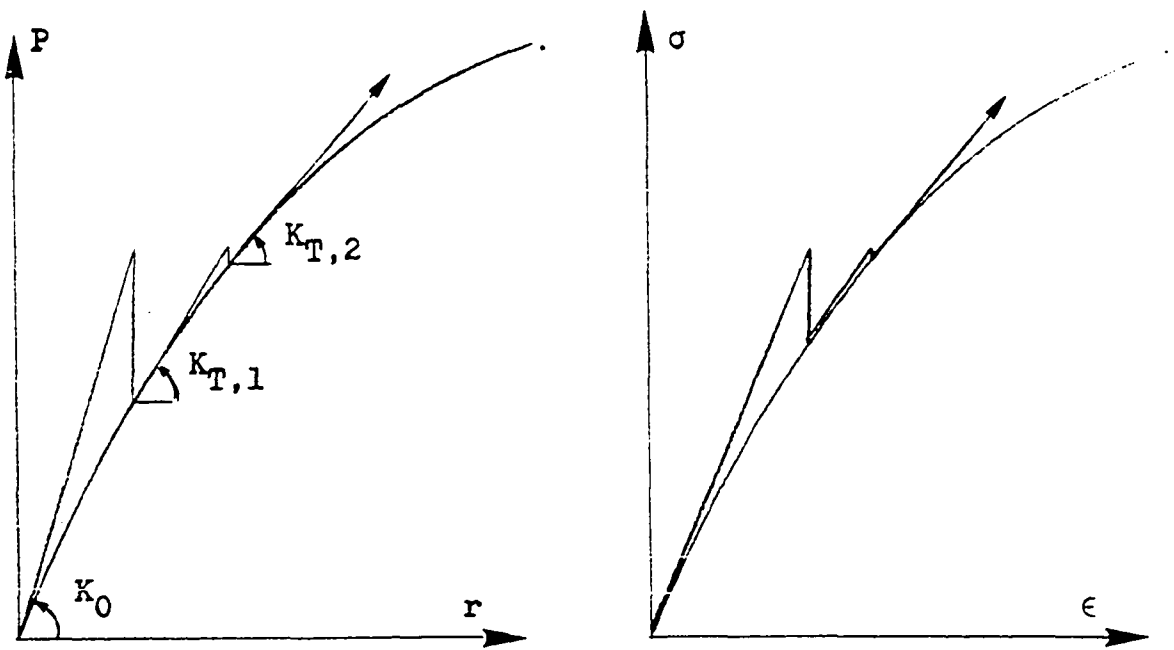
c. Basic Newton-Raphson procedure
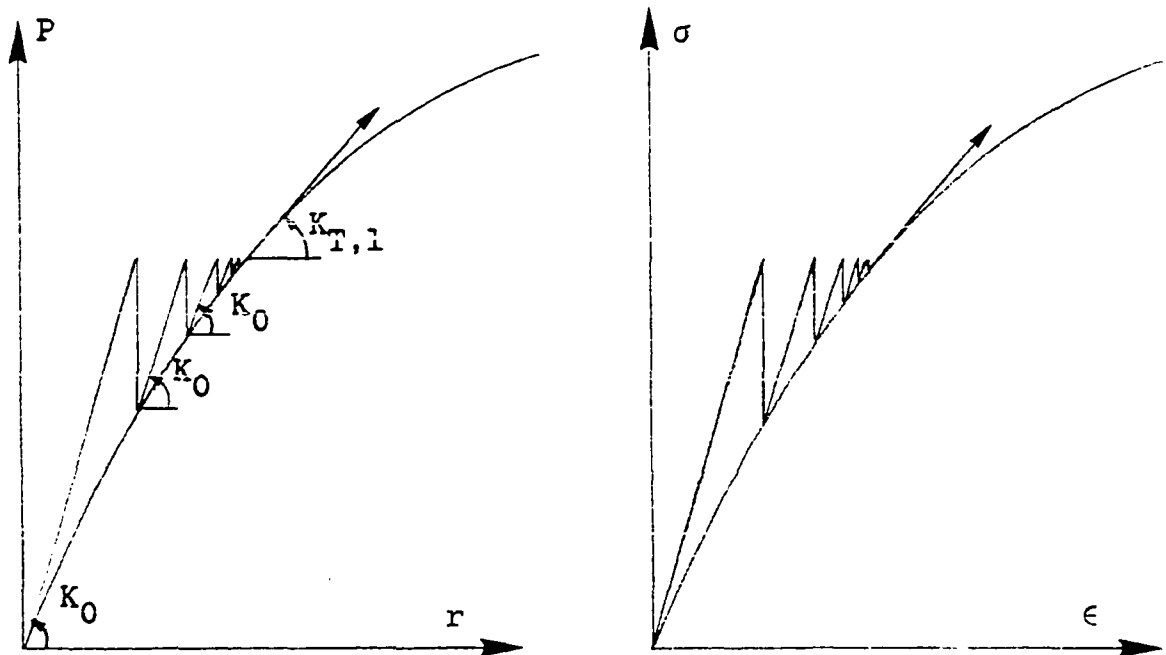
d. Modified Newton-Raphson procedure

Fig. 13. (Continued)

increment. In one such method, instead of using the values at the start of the increment, material stiffness and tangent stiffness matrices at the middle of the increment can be used to give a better estimate of deflections and stresses for the current increment. Such improvements give answers closer to the true curve at the expense of more numerical calculations.

The next group of numerical techniques can conveniently be classified as residual load correction methods. In all these methods, loads are increased in small increments and iterations within each increment are performed until equilibrium and material properties are simultaneously satisfied. In its simplest form, the method employs at least one correction for each increment. In the numerical procedure the loads are applied in increments and the corresponding incremental and total quantities of stress and strain are then calculated. Due to linearization errors material properties will not be satisfied exactly and when geometric nonlinearities are included in the analysis, equilibrium based on the current deformed configuration will also not be satisfied exactly. Corrective steps are then taken in the form of so-called iterations. For the computed total strain, the actual stress level that the material can sustain in conformity with the true stress-strain diagram is calculated. Using the corrected stress level and the equilibrium equations based on the current deformed geometry, the equivalent equilibrating nodal

loads are then calculated. The residual load vector is then defined as the difference between the total applied load vector and the equilibrating nodal load vector. In the one step correction procedure (Fig. 13b) the residual load vector is added to the next incremental load vector and the analysis proceeds in a similar manner. The disadvantage of this particular method is the lack of close control over the incremental quantities, due to the presence of residual loads from the previous increment which regardless of their magnitude are added to the current incremental load vector.

An improved version of this method is to do several corrective iterations within each increment and reduce the residuals to as small a value as possible before a new increment of load is applied on the structure. Two versions of the numerical procedure, the basic Newton-Raphson method and the modified Newton Raphson method are widely used. The two methods are figuratively explained in Fig. 13c and Fig. 13d where the slope of the incremental stiffness values should be carefully noted. The choice of any one of these methods depends upon its computational efficiency when applied to the particular nonlinear problem under consideration.

In the basic Newton-Raphson procedure the most current information available concerning the structure is used to calculate the incremental quantities at any step. In other words, the material stiffness and tangent stiffness matrices at the start of each iteration are used to estimate the next

incremental quantities. It means the generation of element

stiffness matrices, assembly of element stiffness matrices

and decomposition of the global stiffness matrix at the start

of each iteration. When the number of elements and the number

of unknown displacements are large in the structure, the above

step could lead to significant amounts of computer time re-

quired for a solution.

An analysis of the numerical procedure would indicate

that it is not absolutely necessary to use the exact tangent

stiffness matrix to estimate the incremental quantities as long

as a correct residual load vector is calculated based on the

true curve. The modified Newton-Raphson method is based on

this concept (Fig. 13d). Incremental quantities during the

iterations are estimated by using the same stiffness matrix

developed at the start of the increment. Thus, this method

has the obvious advantage of reducing the number of times the

formation, assembly and decomposition operations that are re-

quired on the stiffness matrix. The modified Newton-Raphson

method, in general, takes more iterations to converge than the

basic Newton-Raphson method. However, in many practical prob-

lems, the modified Newton-Raphson method takes less total

computer time for execution because the same reduced stiffness

matrix is used again and again in the iterations within an

increment. When the degree of nonlinearity is large at a

particular increment, as in the case of extensive cracking of

the concrete, it is advantageous to update the stiffness matrix

after several iterations in order to accelerate the conver-
gence. The number of iterations after which the stiffness
matrix must be updated will depend upon the degree of non-
linearity present, the path dependent nature of the problem
and the relative time expended in the stress calculation and
back substitution routines as compared to the time expended
for the stiffness generation, assembly and decomposition
routines. In this study depending upon the numerical example
considered, the stiffness matrix was updated after five to
ten iterations.

Discussion of the Calculation of Residual Loads

The calculation of the residual loads is an important
step in the iterative solution of a nonlinear problem and
hence it will be discussed in detail in this section. Since
an exact integration of the expression for the residual load
vector is difficult to perform, several approximate procedures
have been used in the past. Attention is directed in this
section on a single element.

A consistent numerical algorithm based on Lagrangian
formulation would involve the following steps in calculating
the residual load vector.

1. The residual load vector from the previous increment
   ΔR_0 is added to the current increment of load and
   the net incremental load vector ΔP is obtained. Let
   the current total load vector be P.

2. Incremental displacements are calculated using the incremental relation

$$\Delta r = K_T^{-1} \cdot \Delta P \qquad (4.1)$$

where Δr is a vector of incremental displacements and K_T is the tangent stiffness matrix of the structure at the start of the increment. The notation K_T^{-1} is used only symbolically and in practice only a triangularization of the stiffness matrix with back-substitution is used instead of a full inversion.

3. Current total displacements are obtained by adding the incremental displacements to the previous total displacements.

4. Incremental strains are calculated from the incremental strain-displacement relationships (equation 3.44) and the incremental stresses are calculated from the incremental stress-strain relations.

5. The current total stress and strain quantities are calculated by adding the incremental quantities to the total quantities.

6. Based on the current total strains, the true total stress σ_i is calculated from the stress-strain curves. The estimated total stress quantities are replaced by the corrected total stress quantities.

7. Using the corrected stress components σ_i and the current total displacement vector r, the corresponding equilibrating nodal loads are calculated by the relation

$$R = \int_V [\, C^{-1^T} D^T L_i + C^{-1^T} D^T H_i D C^{-1} r \,] \, \sigma_i \cdot dv \qquad (4.2)$$

When geometric nonlinear effects are to be omitted, the second term in equation 4.2 containing the

current total displacement vector is omitted. Thus, for the case of material nonlinearity alone, equation 4.2 reduces to the following equation

$$R = \int_V C^{-1^T} D^T L_i \sigma_i \cdot dv \qquad (4.3)$$

8. The residual load vector $\triangle R$, is then given by the relation

$$\triangle R = P - R \qquad (4.4)$$

9. If $\triangle r$ and $\triangle R$ satisfy convergence criteria, the next increment of load is applied and the analysis proceeds from step 1.

10. If the convergence criteria is not met, iteration will continue and the next incremental displacements are calculated by

$$\triangle r = K_T^{-1} \triangle R \qquad (4.5)$$

11. Using the incremental displacements from step 10 the analysis proceeds again from step 3 until convergence criteria are met.

If the above discussed algorithm is used to calculate the residual loads, it can be seen that the critical step is the evaluation of equation 4.2 (or equation 4.3). An exact integration of equation 4.2 (or 4.3) is difficult when the stress components σ_i are functions of local coordinates of the element. In practice an exact evaluation of those equations is seldom carried out except possibly in the case of constant stress elements. The most commonly used approach is the numerical integration of equation 4.2 (or equation 4.3) to obtain the value of the equilibrating nodal loads. Berg

(23) used such an approach in the nonlinear analysis of reinforced concrete plates. The number of integration points over the area and the depth must be sufficient to represent the stress distribution adequately but at the same time does not require the expending of excessive computational time. For a rectangular element using a layered approach an approximate numerical integration can be performed by using a four point or nine point Gaussian quadrature integration over the area. However, its numerical integration would require additional storage and computer time.

Considering material nonlinearity alone, Lin (14) and Hand et al. (12) used a simplified procedure to calculate the residual loads. Rewriting equation 4.3 for the layered analysis we get

$$R = C^{-1^T} \int_{Area} D^T \left(\sum_{\substack{All \\ layers}} \int_{h_j}^{h_{j+1}} L_i \, \sigma_i \, dz \right) \cdot dA \qquad (4.6)$$

Lin (14) calculated the estimated total stress and the corrected total stresses at the centroid of the layers and defined the difference between them as excess stresses for the layer. The excess stresses are assumed to be constant over the entire layer while integrations are performed to obtain the excess residual load vector. The residual load vector (an approximation of equation 4.4) is defined by

$$\triangle R = C^{-1^T} \int_{Area} D^T \left(\sum_{\substack{All \\ layers}} \int_{h_j}^{h_{j+1}} L_i \, \sigma_i^{ex} \, dz \right) dA \qquad (4.7)$$

where σ_i^{ex} are the excess stress components in layer j. Rewriting equation 4.7 in an expanded form for the range of index i and using the definition of L_i given in equation 3.13 we get,

$$\triangle R = C^{-1^T} \int_{\substack{\text{Area}}} D^T \sum_{\substack{\text{All} \\ \text{layers}}} \begin{bmatrix} \sigma_i^{ex} \ t_j \\ \sigma_{12}^{ex} \ t_j \\ \sigma_{12}^{ex} \ t_j \\ \sigma_2^{ex} \ t_j \\ \cdot \\ \cdot \\ \cdot \\ -\sigma_1^{ex} \ \dfrac{h_{j+1}^2 - h_j^2}{2} \\ -\sigma_2^{ex} \ \dfrac{h_{j+1}^2 - h_j^2}{2} \\ -\sigma_{12}^{ex} \ h_{j+1}^2 - h_j^2 \end{bmatrix} dA \qquad (4.8)$$

where σ_1^{ex}, σ_2^{ex}, σ_{12}^{ex} are the excess stress components. Hand et al. (12) preferred to calculate the integrated average strains for each layer instead of calculating the strains at the centroid of the layers. The exact location of the strains and stresses thus calculated are unknown but they give a representative set of average strains and stresses for each layer.

The simplifying assumptions of Lin (14) and Hand et al. (12) make the numerical calculations comparatively easy and there are fewer quantities to be stored in the computer memory. Lin and Hand obtained very satisfactory results using this

simplified procedure. However, it must be noted that the use of simplified procedure affects the manner in which the excess stresses are distributed in the structure.

Procedure Used for the Calculation of Residual Loads

When combined material and geometric nonlinearity is considered two distinct contributions to the magnitude of residual loads occur. The first is due to the loss of material stiffness and the second is due to change in structure geometry. As already explained a consistent procedure for calculating the residual loads must use the corrected stress components σ_i and the current total displacement vector r (steps 7 and 8 of the previous section).

This study uses a simplified procedure for the calculation of residual loads. In the procedure used the estimated stresses and the actual stresses at the centroid of the layers are calculated first. The excess stresses are defined by

$$\sigma_1^{ex} = \sigma_i^{est} - \sigma_i \qquad (4.9)$$

where σ_i^{ex} are the excess stresses, σ_i^{est} are the stresses calculated using the current constitutive relationships for the increment used in the generation of the stiffness matrices and σ_i are the actual stresses. When the material nonlinearity alone is considered the residual loads are given by

$$\Delta R = C^{-1^T} \int_{Area} D^T \left(\sum_{\substack{All \\ layers}} \int_{h_j}^{h_{j+1}} L_i \sigma_i^{ex} dz \right) \cdot dA \qquad (4.10)$$

When combined material and geometric nonlinearity is considered the residual loads are given by

$$\triangle R = C^{-1^T} \int_{Area} D^T \left(\sum_{\substack{All \\ layers}} \int_{h_j}^{h_{j+1}} L_i \, \sigma_i^{ex} \, dz \right) \cdot dA$$

$$\text{(4.11)}$$

$$+ \, C^{-1^T} \int_{Area} D^T \left(\sum_{\substack{All \\ layers}} \int_{h_j}^{h_{j+1}} H_i \, \sigma_i^{ex} \, dz \right) D \cdot dA \cdot C^{-1} r$$

where r is the total displacement vector at the end of each iteration. Thus, for the case of combined material and geometric nonlinearity the residual loads calculated are not exact and equilibrium in the deformed state is not exactly satisfied. The geometric nonlinear effects are considered by using the tangent stiffness matrix containing K_0, K_σ, and K_D and then converting the excess stresses due to material softening into equivalent nodal loads using the current geometry. This approximate procedure has the advantage of only one stress calculation per layer and also that the number of quantities to be stored in computer memory is reduced. This simplified procedure gave very satisfactory results for the beam-column examples considered in this study.

Assembly and Solution of Linear Simultaneous Equations

In the solution process, stiffness matrices for each element are first generated. When material nonlinearity alone is considered, only the basic stiffness matrix K_0 using the current material properties is generated. When geometric

nonlinearity is included, the basic stiffness matrix K_0, the initial stress matrix K_σ, and the initial displacement matrix K_D for each element are generated and added at element level. The element tangent stiffness matrices which are symmetric in nature are assembled to form the global stiffness matrix. Boundary conditions are introduced in the global stiffness matrix by altering the elements in the rows and columns corresponding to the restrained degrees of freedom. The diagonal elements are made equal to unity and the other elements in the particular rows and columns are made equal to zero. The corresponding elements in the particular rows of the load vector are also made equal to zero. The symmetric and the banded nature of the global stiffness matrix is used during assemblage. The assembled global stiffness matrix is of rectangular form in which the diagonal elements and the other off diagonal elements within the lower semi-bandwidth alone are stored.

The solution for the incremental displacements is achieved by solving equations of the form

$$\triangle P = K_T \cdot \triangle r \qquad (4.12)$$

where $\triangle P$ is the vector of incremental loads or a vector of residual loads as the case may be. The solution is obtained using Gaussian elimination procedure. The double precision version of the IMSL routines (55) LUDAPB and LUELPB available at the Iowa State University Computation Center were used for

the decomposition of the stiffness matrix and for the back-substitution step respectively. For the size and type of numerical examples considered in this study round-off error difficulties were not encountered.

Convergence Criteria

In the adaptation of the modified Newton-Raphson method, specification of certain convergence criteria is necessary for the termination of iterations for an increment of load. The two quantities that can be checked for the convergence of the solution are the residual loads and the incremental displacements. During the course of this study it was found desirable to satisfy both the residual load convergence criteria and the incremental displacement convergence criteria before the iterations were terminated.

For the case of displacements, the ratios of incremental displacements to total displacements are calculated for all the nodal displacements. When the maximum value of the calculated ratios is less than a specified amount (usually 1%) the solution is assumed to satisfy the convergence criteria for displacements. The convergence criteria for displacements can be written as

$$\left|\frac{\Delta r_i}{r_i}\right|_{i=1,N} \leq \text{ a specified amount} \qquad (4.13)$$

where N is the total number of unknown displacements.

The convergence criteria for residual loads is satisfied when the absolute magnitude of all of the residual loads is less than a specified amount, the specific value depending upon the numerical example under consideration. The convergence criteria for the residual loads can be written as

$$\left|\triangle R_i\right|_{i=1,N} \leq \text{a specified amount} \qquad (4.14)$$

where N is the order of the residual load vector.

Step by Step Outline of the Computations Procedure

This section outlines the principal computational steps in the numerical solution. The following steps are done for a typical increment.

1. At the start of an increment add the residual load vector from the previous increment to the applied incremental load vector.

2. Generate the tangent stiffness matrices for each element and assemble the global tangent stiffness matrix for the structure.

3. Introduce the boundary conditions and decompose the global stiffness matrix.

4. Calculate the incremental displacements and update the total displacement vector.

5. Separate element incremental and total displacement vectors from global displacement vectors. Calculate the incremental and total displacement gradient vectors d for the centroid of the element.

Do steps 6 through 11 for all layers.

6. Calculate the incremental layer strains from the known displacement gradient vectors.

7. Using the constitutive matrix of the layer used in the generation of systems equations, calculate the increments in stresses corresponding to the incremental strains.

8. Update the total stress and strain quantities. Calculate the direction and magnitude of the principal stresses. If the material axes are fixed due to the presence of cracking in a previous step, calculate the components of stress in the fixed material axes direction.

9. Using the total stress at the start of the current step use an applicable material routine tension-tension, tension-compression or compression-compression. A typical material routine will contain the following steps:
   a. Using the ratio of the total stresses in direction 1 and 2 of the material axes, calculate the failure stresses using failure criteria and the failure equivalent uniaxial strains.
   b. Calculate the current incremental uniaxial strains and update total equivalent uniaxial strains.
   c. Using the total equivalent uniaxial strains calculate the correct stresses in the material. Calculate the new material stiffness values. This step requires the construction of the equivalent uniaxial curve for compressive stresses. If the material is cracked or crushed, flag it for output.

10. Calculate the excess concrete stress in the layer.

11. If the layer is a composite layer, calculate the stress in steel, check for yielding, correct the total stresses in the steel, compute the equivalent excess layer stresses due to the steel and add to the concrete excess layer stresses.

12. Convert excess layer stresses into residual nodal loads using proper integration and store in global residual load vector.

13. Obtain element stress resultants using corrected total stresses.

14. Check the incremental displacements and the residual loads for convergence. If converged output results and go to step 1.

15. If iteration has not converged and the maximum allowable number of iterations have not been exceeded go to step 4 and continue to iterate. If the maximum specified iterations have been exceeded and the solution has not converged output results and store all the necessary values on a disc or tape for a possible restart.

Computer Program

The numerical algorithm is implemented in a computer program written in Fortran IV language. The program is not completely a general purpose program but a simple specialized program written for beams, beam-columns and slabs using rectangular finite element idealization. In any nonlinear finite element analysis, implementation of the finite element formulation into a computer program requires significant programming

effort. In addition, storage requirements and solution time are also large compared to the requirements of a single linear solution due to the fact that the nonlinear solution is a superposition of a large number of independent incrementally linear solutions.

The program is in a modular form and the main program can be considered as a driver routine which calls a series of sub-routines to perform the different steps in the numerical solution. The general organization of the program is along the lines given by Zienkiewicz (40). The input for the program contains the following details:

1. Control data, such as the number of elements, number of nodes, number of increments, maximum number of iterations, etc.

2. Coordinates of nodal points and element nodal connectivity.

3. Fundamental material properties of steel and concrete.

4. Details of concrete and steel layers.

5. Details of boundary support conditions.

6. Details of incremental loads.

A typical output contains:

1. Printout of input values for checking.

2. Incremental and total loads.

3. Residual loads and convergence factors.

4. Concrete layer stresses and strains for the elements including the magnitude and direction of principal stresses and the curvature values for each element. Information regarding the cracking of concrete, angle between the cracking direction and the x-axis and cracking of concrete for each concrete layer.

5. Stresses and strains in the reinforcement steel and their yield status.

6. Element stress resultants.

The numerical calculations were done on an IBM 360/65 using double precision arithmetic for all the calculations. Depending upon the type and size of the numerical example considered, execution times ranged from $1\frac{1}{2}$ to 8 minutes.

CHAPTER 5. NUMERICAL EXAMPLES

General

Several numerical examples are presented in this section to show the applicability and the accuracy of the numerical method previously developed. The theoretical investigation is approximate in nature due to the approximations inherent in the finite element modeling technique, approximations in the concrete material modeling, approximate integrations of functions in the numerical solution and the approximations introduced due to the type of procedure used in solving the nonlinear equations. Therefore, the theoretical results are compared with the results from actual experiments to check the accuracy and to suggest improvements for a better correlation with the experimental results.

Several numerical examples considering material nonlinearity alone are first presented. The numerical examples include:

1. An under-reinforced simply supported beam.

2. Two slabs subjected to uniaxial bending with steel reinforcement parallel and at angle to the applied moment axis.

3. A corner supported slab subjected to central concentrated load.

4. A simply supported slab subjected to a series of concentrated loads resembling a uniformly distributed loading condition.

A numerical example considering geometric nonlinearity
alone is presented next.

5. Large deflection analysis of a clamped elastic plate
   subjected to central concentrated load.

Several numerical examples of beam-columns considering
material and geometric nonlinear effects are then considered.
The numerical examples include:

6. A long slender column bent in double curvature.

7. Three long cantilever columns subjected to lateral
   forces.

The theoretical investigation considers the biaxial
stress field in each layer of the element to determine its
stress-strain behavior. To implement the material model in
the numerical procedure, the following experimentally deter-
mined material properties must be known.

1. The cylinder strength of the concrete, f'_c.

2. The initial tangent modulus of the concrete, E_o.

3. Failure uniaxial strain of concrete (corresponding
   to the peak stress), ϵ_{cu}.

4. Modulus of rupture of the concrete, f_t.

5. The failure strain of the concrete in the biaxial
   stress state of $\sigma_1/\sigma_2 = 1$ (ϵ_{ic} at $\alpha_c = 1$).

Frequently except for the cylinder strength none of the
other concrete properties are documented in the experimental
investigations. When not available, the values of E_o and f_t
were determined using the values recommended by the ACI code
(38). Unfortunately, the assumed value of the modulus of

rupture is a source of uncertainty in the theoretical calculations. It was observed in some examples (e.g., the case of slabs) that the assumed value of f_t could significantly affect the load-deflection response of the structure in the intermediate range of loading. When the information was not available, the uniaxial failure strain of the concrete was also assumed.

In all of the numerical examples, the finite element is divided into ten layers not necessarily of equal thickness. Care was taken to make certain that the centroid of the composite layer coincided with the effective depth of the actual reinforced concrete section. It is also advantageous to have thinner layers near the edge such that the moment and extreme fiber stress values can be more accurately calculated.

Examples Considering Material Nonlinearity

Simply supported beam

Ultimate strength and flexural behavior of an under-reinforced concrete beam are studied theoretically and compared with experimental results obtained by Janney, Hognestad, and McHenry (56). The beam was tested with a third point loading and was designed to assure flexural failure. The finite element discretization, layering system and the assumed material properties are shown in Fig. 14. The double symmetry of the element could be used to advantage such that only one quarter of the beam need to be analyzed.

a. Test beam geometry

Elevation

Plan (quarter of the beam)
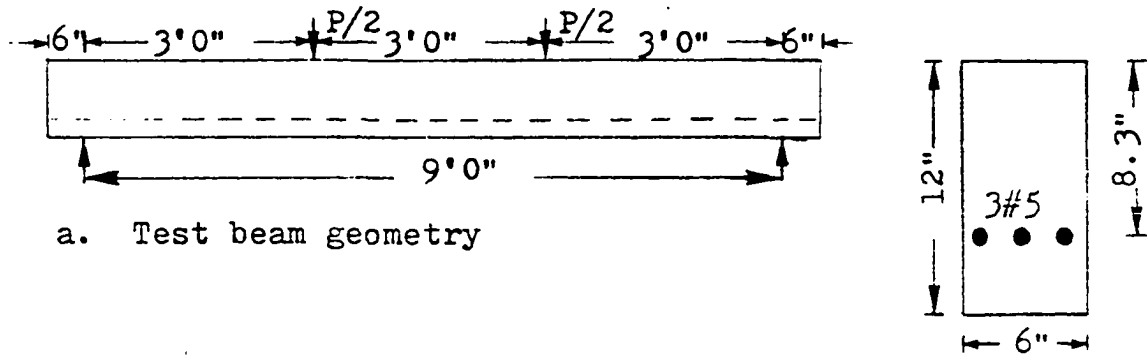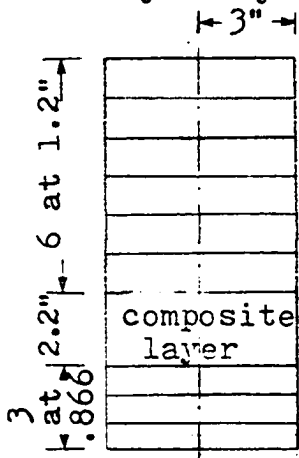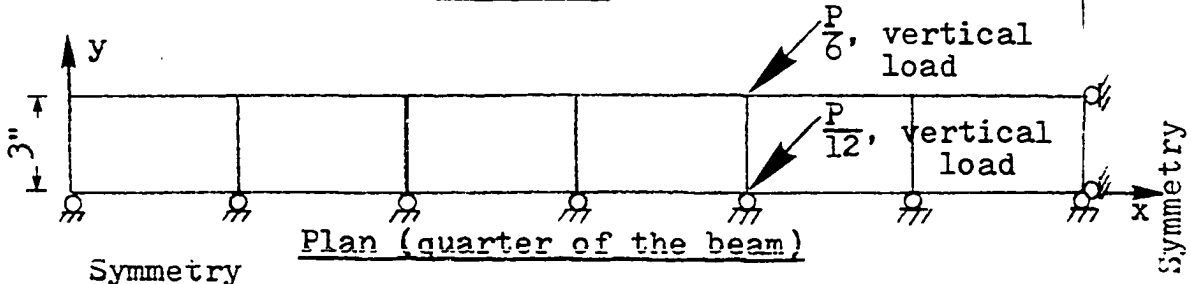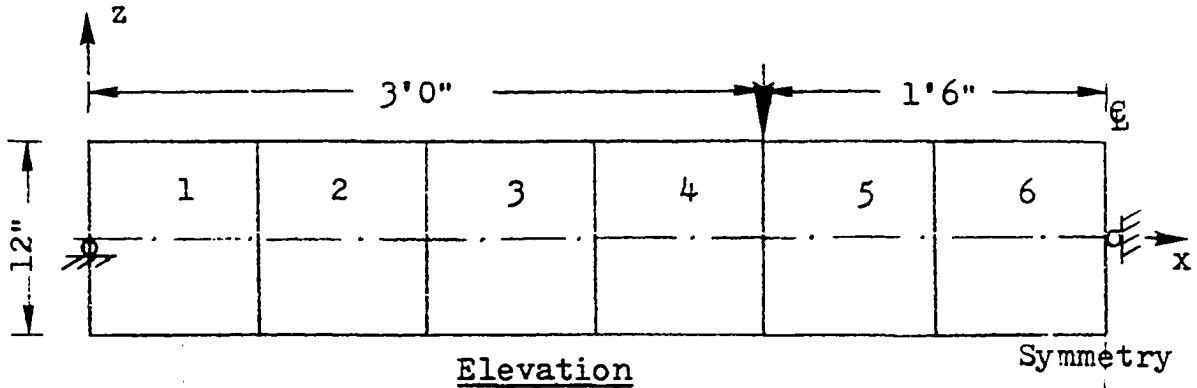
Symmetry

Material properties

E_0 = 4130 ksi

$|f'_c|$ = 5.25 ksi

f_t = 0.55 ksi

ϵ_{cu} = 0.003

E_s = 29,000 ksi

f_y = 48.3 ksi

Slope boundary conditions

Along x axis : $w,_y = 0$

Along the center line axis of symmetry :
$w,_x = 0$

composite layer

b. Finite element idealization details

Fig. 14. Details of the simply supported test beam (56)

The load-deflection response of the beam is shown in Fig. 15. The horizontal plateau in the theoretical curve is due to the iterations required for the same load until material properties and equilibrium are simultaneously satisfied. Cracking of layers results in large number of iterations before convergence can be obtained. As an example, using the modified Newton-Raphson procedure, at the initiation of the first crack, 16 iterations were required with one additional updating at the end of tenth iteration before convergence could be achieved.

The cracking of the concrete and yielding of the steel at 93% of the theoretical ultimate load is shown in Fig. 16. It must be noted that the theoretical model does not predict the number of cracks or the crack width but only the cracked zones and the depth of the cracked zones. It must be noted that the plate bending model, as used in this investigation, is inadequate to model beams that fail by diagonal tension. In such cases plane stress elements could be used as was done by Scordelis, Ngo, and Franklin (57) and Houde and Mirza (58).

Slabs subjected to uniaxial bending

Several isotropically and nonisotropically reinforced concrete slabs subjected to combination of flexural and torsional moments were studied by Cardenas and Sozen (59). The experimental results of two slabs subjected to uniaxial moment are compared with the theoretical results. The
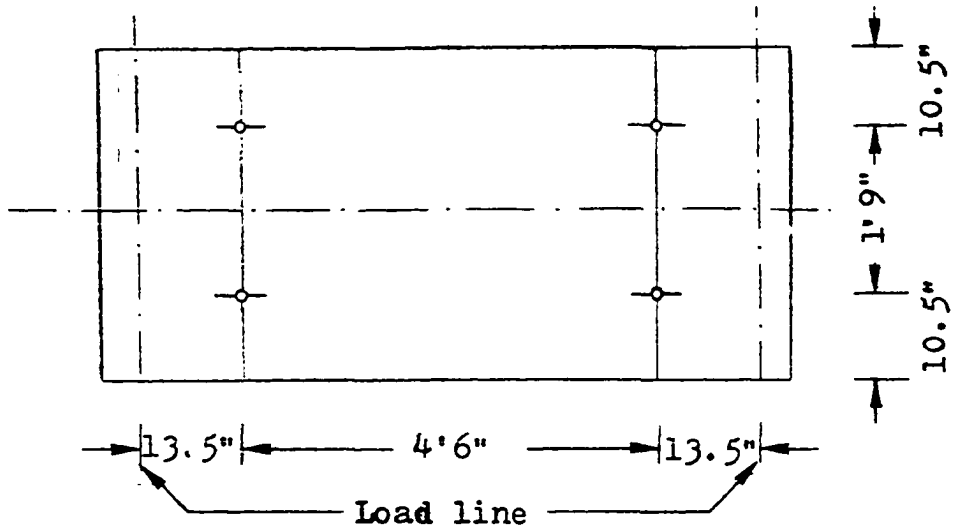
experimental set up, the finite element idealization and the layering system is shown in Fig. 17. The assumed material properties are given in Fig. 18.

Slab B-10 contains reinforcement parallel to x and y axis. Slab B-7 contains reinforcement at angles +45° and at -45° to the x-axis. Steel reinforcement at any arbitrary angle to the element axes presents no serious difficulty in the numerical calculations. Due to the double symmetry of the problem it is sufficient to consider one quarter of the slab. Due to the nature of applied loading it can be assumed that a single finite element idealizing the quarter of the slab should give sufficiently accurate results. The moment-curvature, moment-steel strain and moment-concrete strain plots for slabs B-7 and B-10 are shown in Fig. 19 through Fig. 23.

The theoretical results correctly model the general trend and give acceptable results but indicate a slightly stiffer slab than that which the experimental results indicate. The theoretical results of Hand et al. (12) and Lin (14) also show such a tendency. The difference between the theoretical and experimental results may be due to the following reasons.

1. The material properties which are based on the stresses at the centroid of the element may not be the true average for the region. Further, the stresses in the extreme fiber are checked at the midheight of the layer. These may have the effect of delaying the nonlinear process.

2. Some of the concrete material properties needed for the theoretical analysis were assumed. The actual initial tangent modulus of the concrete, the modulus of rupture of the concrete and the failure strain

Fig. 15. Load-deflection curve for the simply supported beam

Fig. 16. Concrete cracking and steel yielding for the simply
supported beam at 93% ultimate

Plan
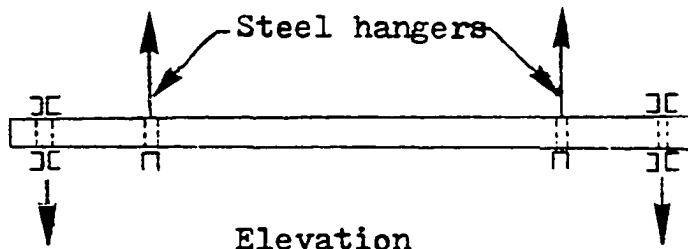
Elevation

a. Slabs B-7 and B-10 test details
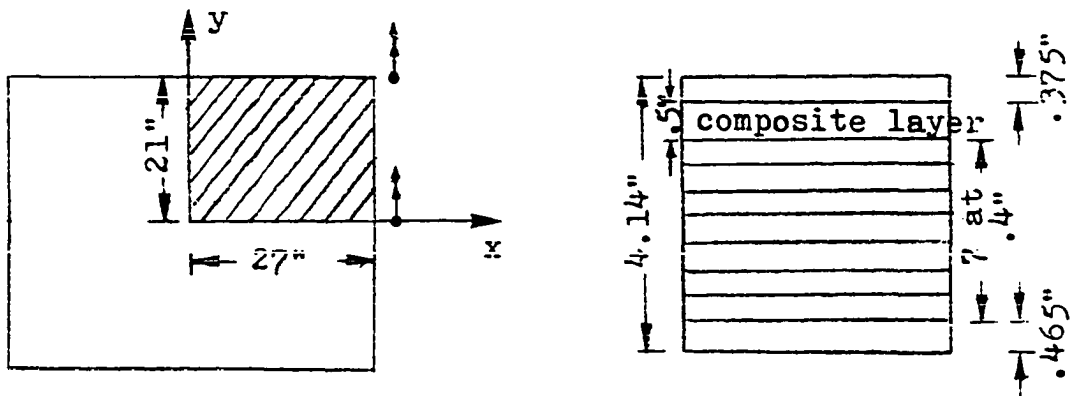
b. Single element quarter slab idealization

Fig. 17. Details of the Cardenas slab (59)

Slab B-7

E_0 = 4090 ksi

$|f'_c|$ = 5.15 ksi

f_t = 0.54 ksi

ϵ_{cu} = 0.003

E_s = 29,000 ksi

F_y = 50.0 ksi

A_s = 0.04 sq inches/inch
width at +45° and -45°
to the x-axis

Slab B-10

E_0 = 4000 ksi

$|f'_c|$ = 4.92 ksi

f_t = 0.525 ksi

ϵ_{cu} = 0.003

E_s = 29,000 ksi

F_y = 50.0 ksi

A_s = 0.04 sq inches/inch
width at 0° and 90°
to the x-axis

Fig. 18.   Assumed material properties for slab B-7 and B-10
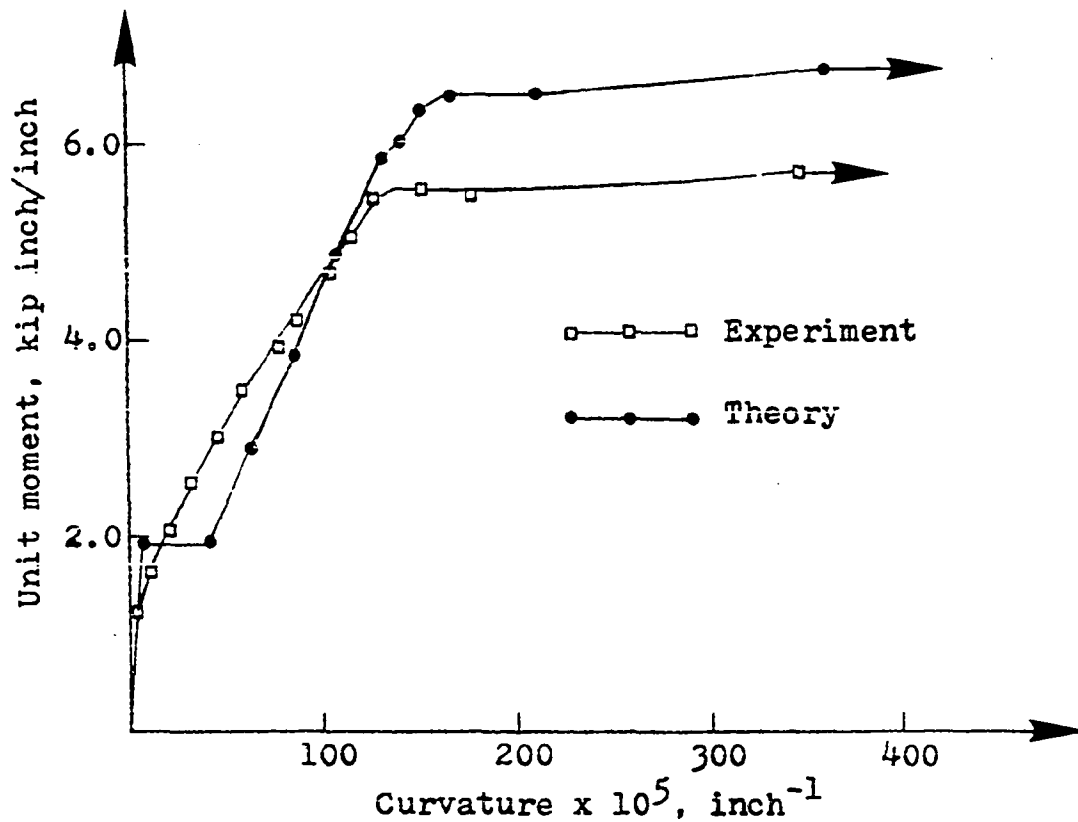
Fig. 19.   Moment-curvature diagram for slab B-7
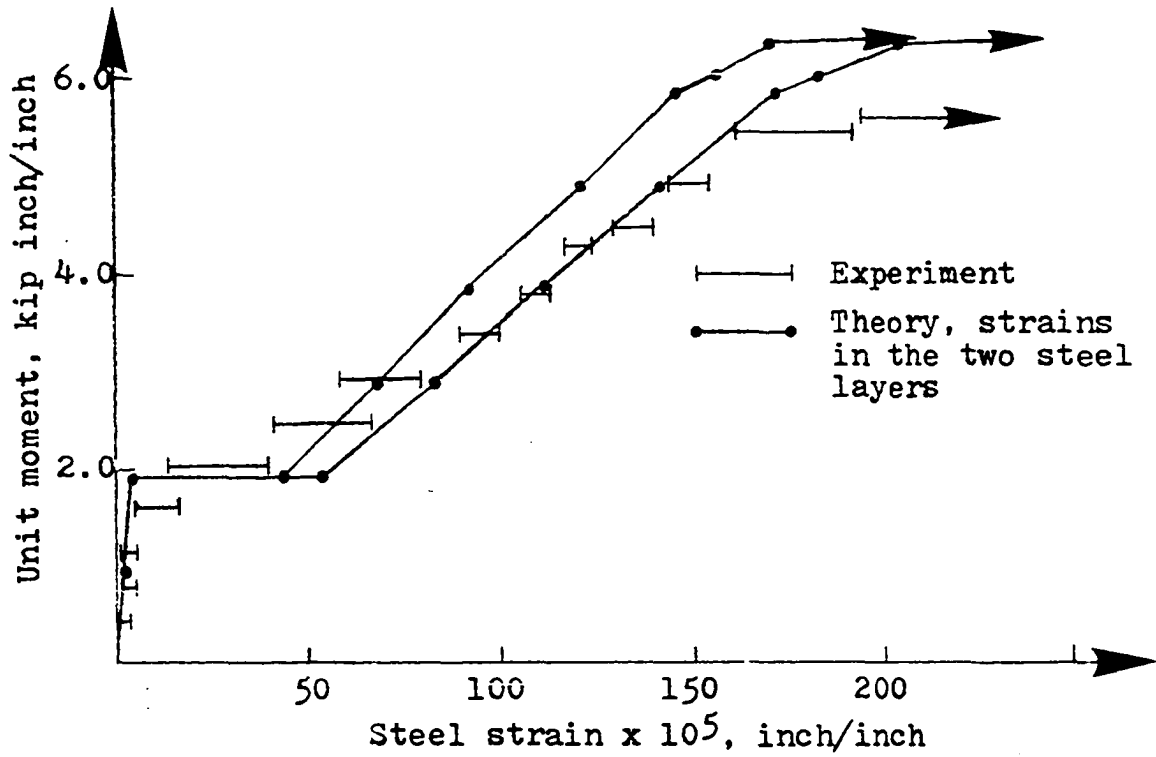
Fig. 20. Moment-steel strain diagram for slab B-7
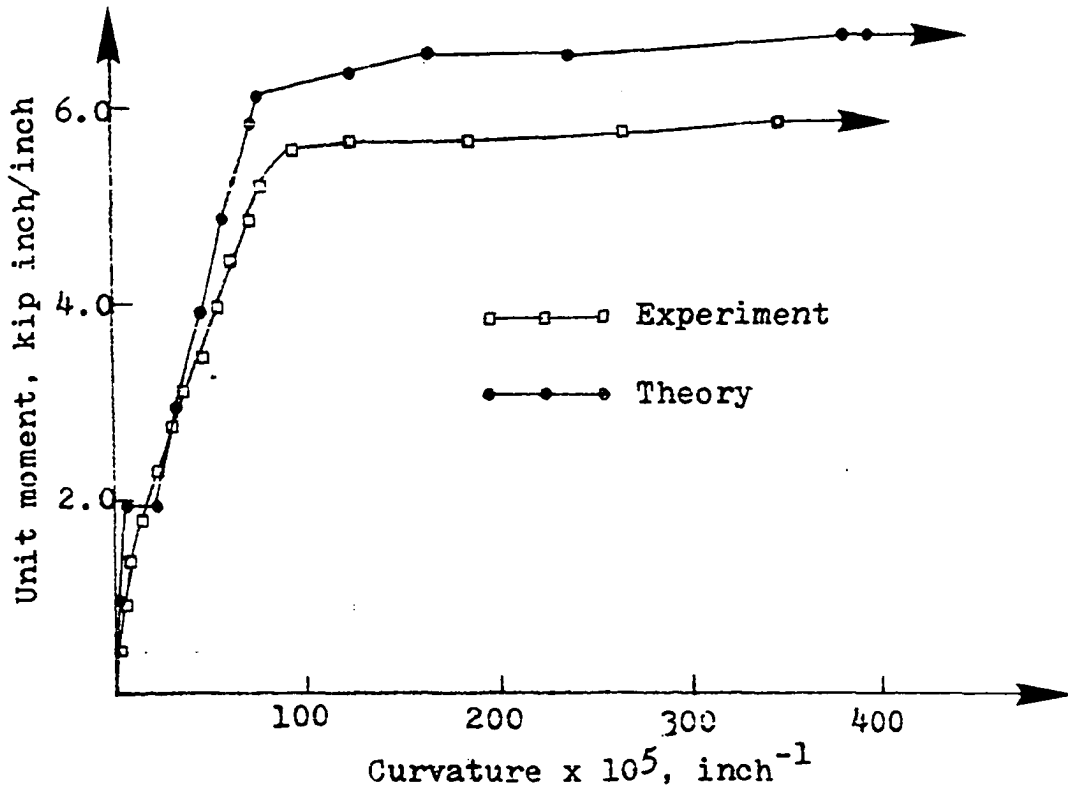
Fig. 21. Moment-curvature diagram for slab B-10
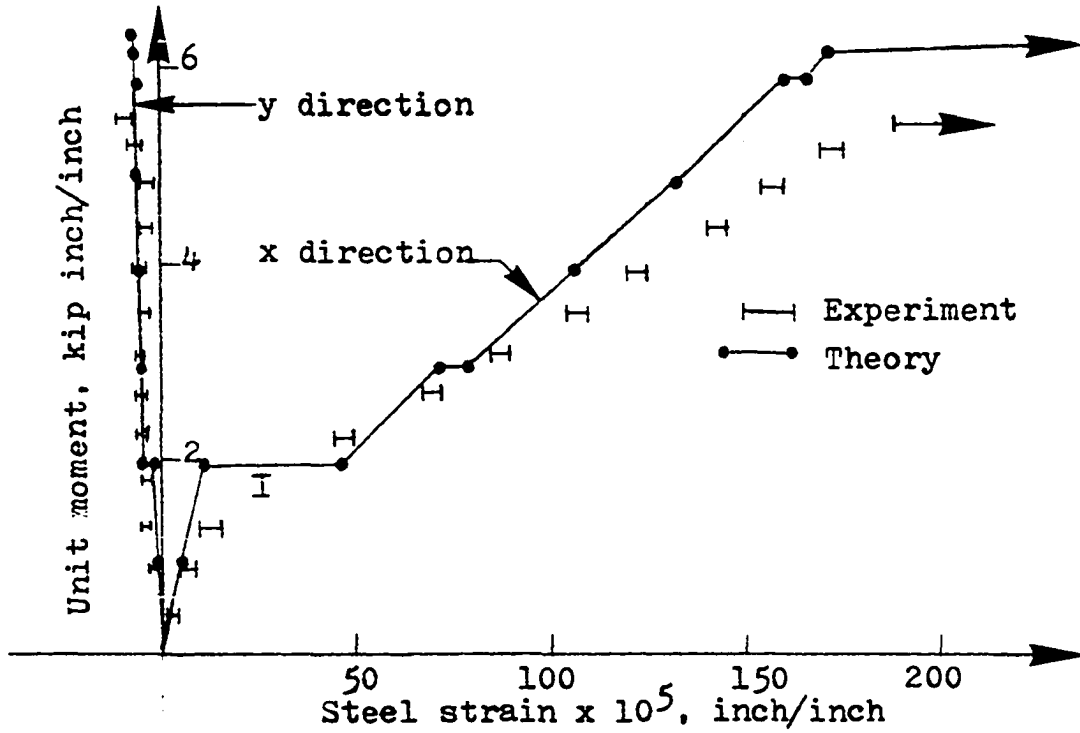
Fig. 22. Moment-steel strain diagram in x and y directions
for slab B-10
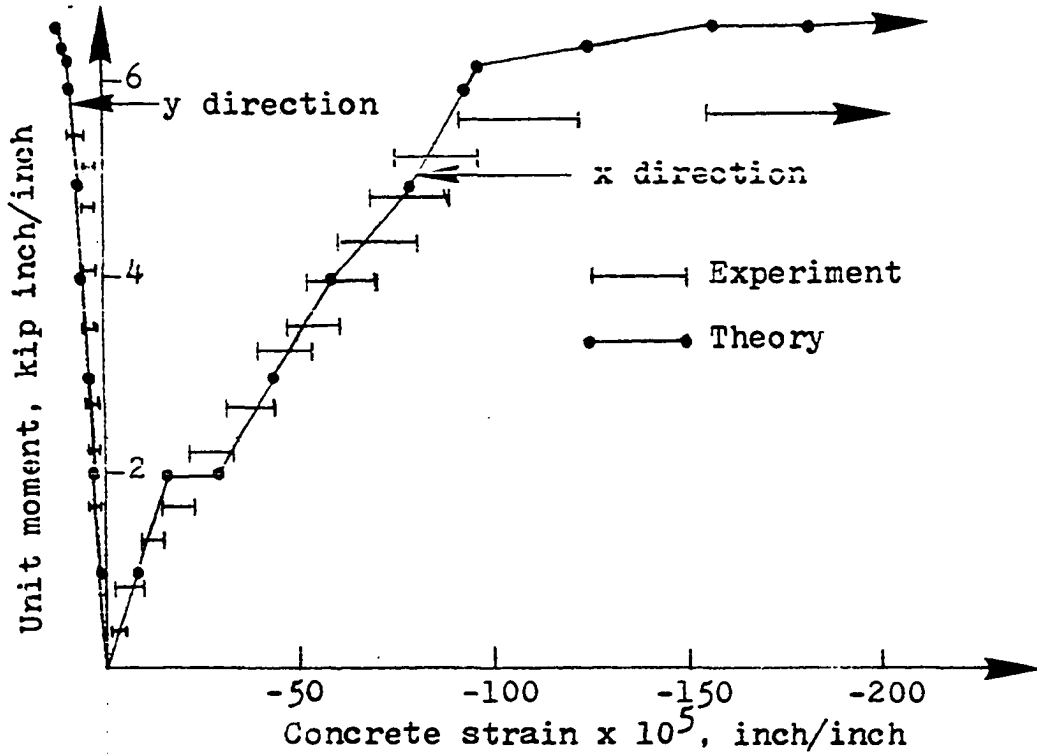
Fig. 23. Moment-concrete strain plot on the compression face
in x and y directions for slab B-10

of the concrete for the uniaxial case may be different from the assumed values.

Numerical results from these slabs indicate that treating reinforcement steel as uniaxial fibers is a good approximation. The agreement of the results when the steel reinforcement is inclined to the moment axis (Slab B-7, Fig. 20) is noteworthy. The theoretical results also agree well with the extreme concrete strains (Fig. 23).

Corner supported reinforced concrete slab

The behavior of the corner supported reinforced concrete slab reported by Jofriet and McNeice (60) is considered in this section. Hand et al. (12) and Lin (14) have also analyzed the same problem considering different material modeling and finite element idealization. The geometric details of the corner supported slab, layering system and the assumed material properties are shown in Fig. 24.

The load-deflection response of point A and point B (Fig. 24a) is shown in Fig. 25 and Fig. 27, respectively. Since point A is not a nodal point, the theoretical deflections of point A were obtained by cubic interpolation. It should also be mentioned that the cubic function is consistent with the assumed displacement function of the finite element model (equation 3.3). The slab was analyzed with two values of the modulus of rupture, $f_t = 0.556$ ksi ($7.5 \sqrt{f_c'}$) and $f_t = 0.77$ ksi ($10.38 \sqrt{f_c'}$). The solution with $f_t = 0.77$ ksi was obtained to form at least a partial common basis to compare the
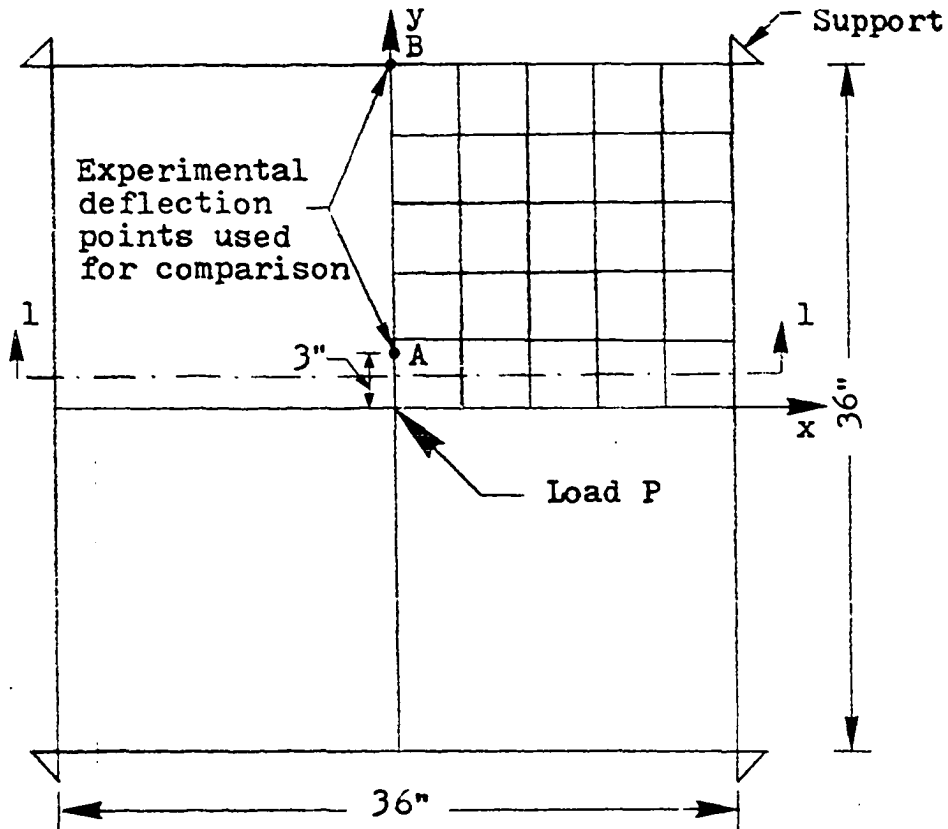
a. Finite element idealization for quarter of the slab

E_0 = 4150 ksi

$|f_c'|$ = 5.5 ksi

f_t = 0.556 and 0.77 ksi

ϵ_{cu} = 0.003

E_s = 29,000 ksi

F_y = 50 ksi

A_s = 0.014875 sq inch/ inch width in the x and y directions
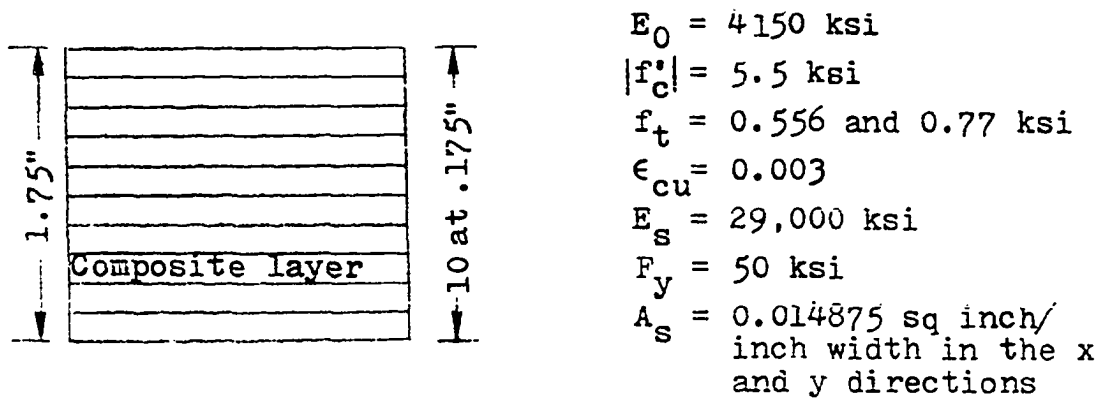
b. Layering system and the assumed material properties

Fig. 24. Details of the corner supported McNeice slab (60)
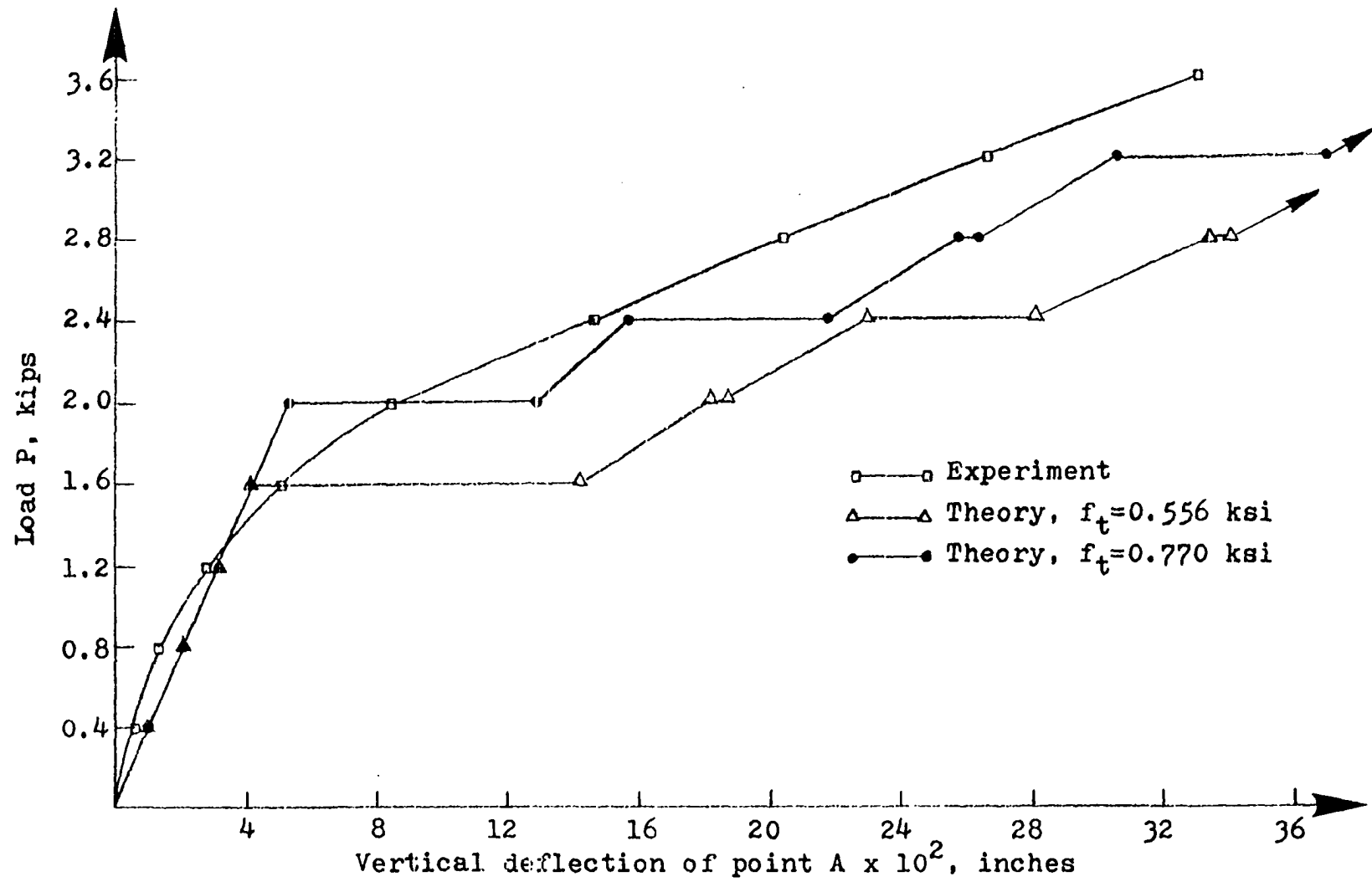
Fig. 25. Load-deflection diagram for point A of the McNeice slab (varying f_t)
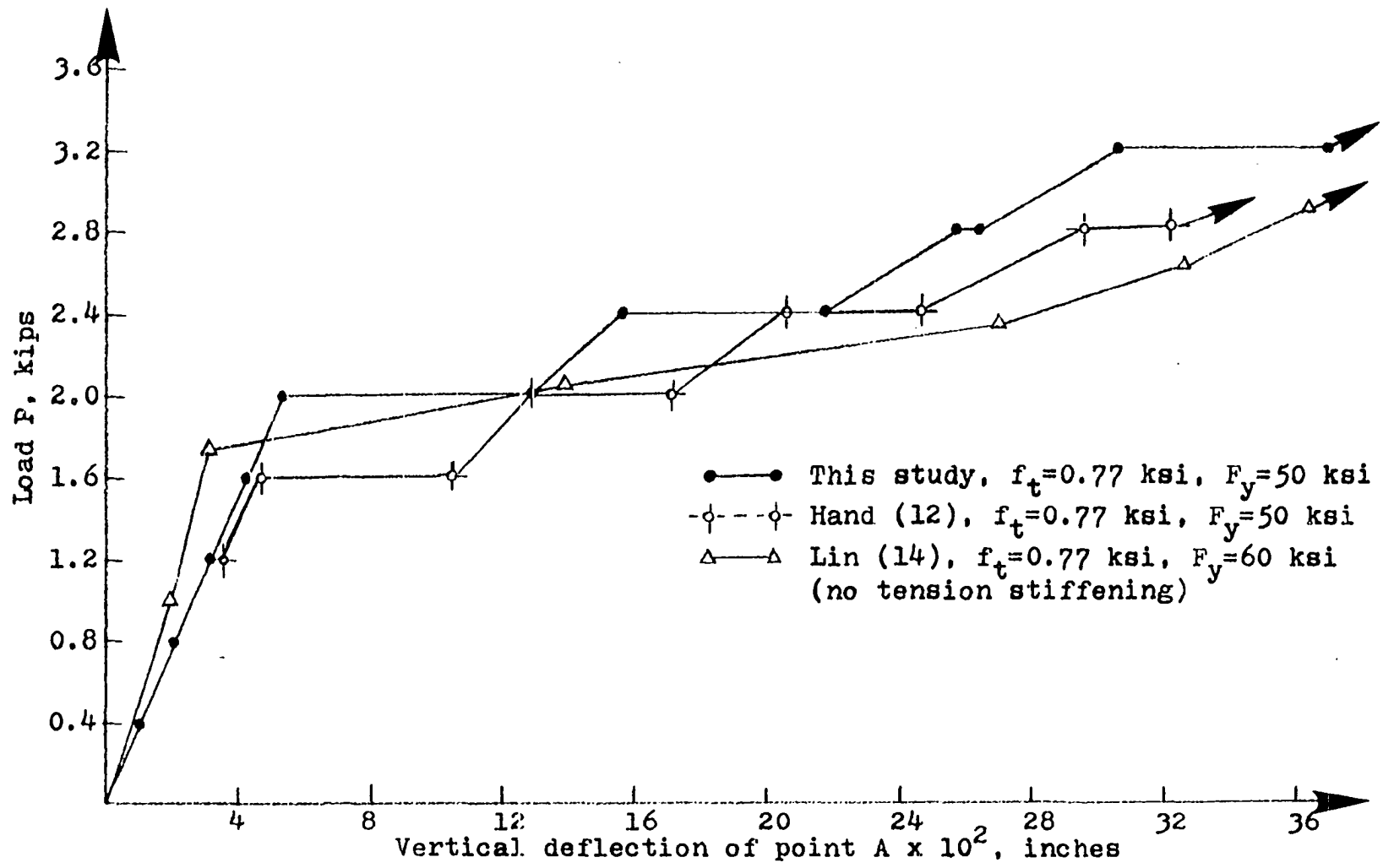
Fig. 26. Load-deflection diagrams for the McNeice slab (compared with other authors)
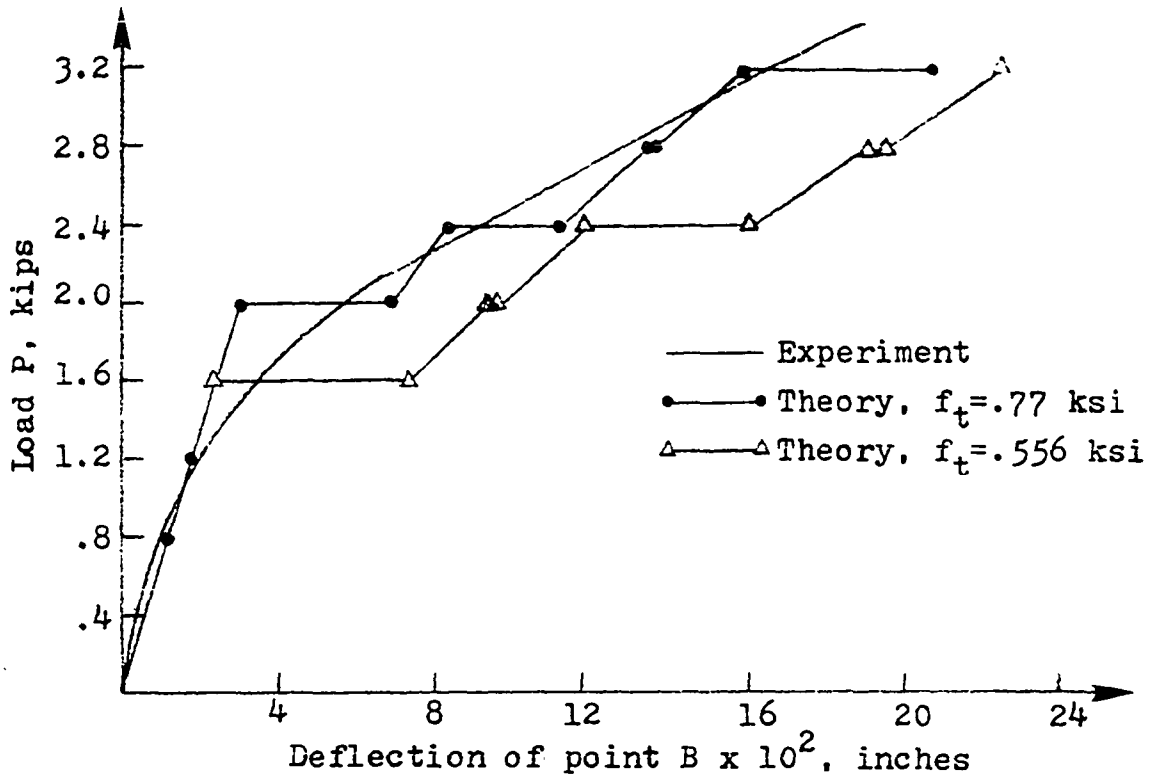
Fig. 27. Load-deflection diagram for point B of the McNeice
slab
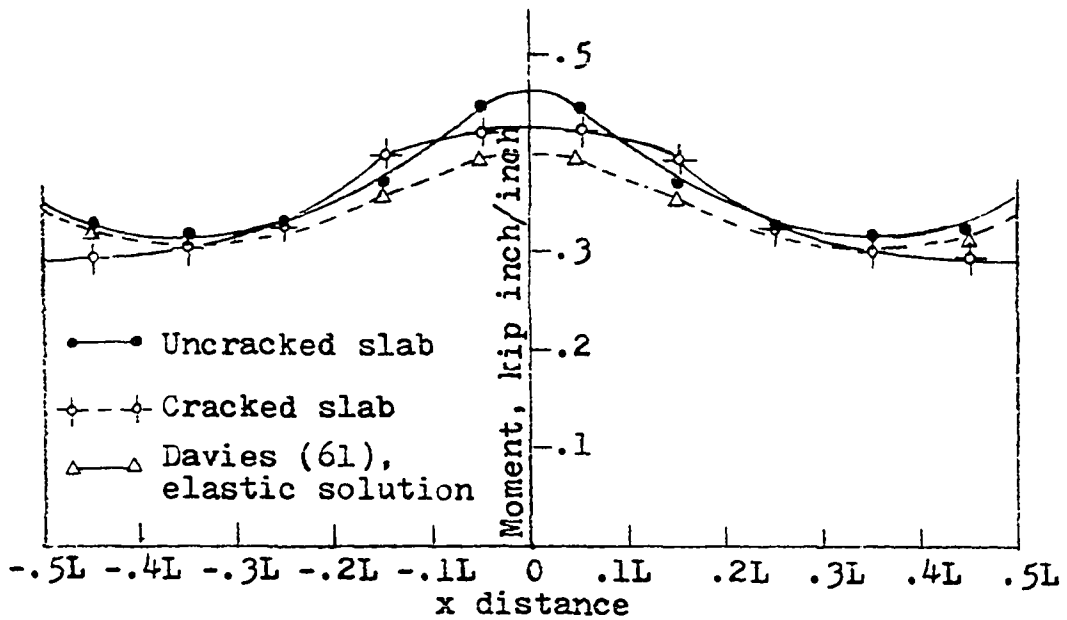
Fig. 28. Distribution of moment M_y along section 1-1 (Fig.
24) for the uncracked and cracked slab for P =
4 kips

results with that of Hand et al. (12) and Lin (14) and also to study the sensitivity of the solution to the assumed values of the modulus of rupture. The theoretical results are compared with that of Hand et al. (12) and Lin (14) in Fig. 26.

For the load levels considered, the theoretical investigation overestimates the slab deflections (Fig. 25). The sensitivity of the solution to the modulus of rupture is rather disappointing as a correct estimation of the modulus of rupture is not easy. The modulus of rupture can vary from 7.5 $\sqrt{f_c'}$ to 12 $\sqrt{f_c'}$. The actual modulus of rupture of the microconcrete used in the model is unknown.

In the numerical solution, after the first cracking of the maximum stressed layer further extensive cracking of the concrete took place before equilibrium was achieved. At the increment when the first crack developed, an increase in deflection values of about 250% over the values at the start of the increment was observed before convergence could be achieved. The overestimation of deflections of slabs in the intermediate ranges of loading appears to be a major problem in the application of the finite element technique to the nonlinear analysis of slabs. This can be observed from the results of Hand et al. (12), Lin (14), Berg (23) and this study.

One source of the error could be the large area associated with each set of material properties. This could be a significant factor when cracking of the concrete takes place. An improvement in the accuracy can be obtained by increasing

the number of elements but at the same time this results in increased computational effort. Lin (14) achieved some success by adding a hypothetical unloading portion to the tensile stress-strain curve of the concrete until the value of tensile stress is zero at a chosen value of strain. Berg (23) reduced the elastic modulus perpendicular to the crack in a parabolic manner after the initiation of the crack. A tension stiffening procedure incorporating parameters of crack spacing is yet to be developed.

Corner supported reinforced concrete slabs are usually designed using moment values based on elastic assumptions. However, the concrete is usually cracked in the tension zone under service loads and therefore the stiffness properties of the cracked slab are different. A comparison of the distribution of the longitudinal moment M_y near the middle of the slab for the cracked and uncracked slab is shown in Fig. 28. Cracking of the concrete results in reduction of peak moment near the center and at the ends and an increase in moments in the intermediate points.

The finite element elastic solution obtained by Davies (61) is also plotted in Fig. 28 using some interpolation. The elastic solution of the corner supported slab is known to be sensitive to Poisson's ratio. The discrepancy between the two elastic solutions may be due to the Poisson's ratio used. Davies used a value of $\nu = 0.15$ and in this study a value of $\nu = 0.2$ was used.

The cracking pattern, the reinforcement steel yielding pattern and the deflection along the centerline axis of symmetry are shown in Fig. 29. The slab is extensively cracked at the bottom layers. The deflection curve and yielding of the steel along the x and y axis (Fig. 29) confirm with the yield line pattern of the limit analysis. The theoretical results (Fig. 29) are in general agreement with the finite element elastic-plastic analysis of corner supported reinforced concrete slabs reported by McNeice and Kemp (62).

Simply supported reinforced concrete slab

Taylor, Maher, and Hayes (63) tested several simply supported reinforced concrete slabs in order to determine the effect of the arrangement of the reinforcement on the behavior of slabs. Test results of an isotropically reinforced slab S-1 is chosen here for comparison purposes. The same slab was also analyzed theoretically by Wanchoo and May (33) and Berg (23). The geometry of the slab, the finite element idealization, layering system and the assumed material properties are shown in Fig. 30. The cube strength of concrete was converted into an equivalent cylinder strength using a factor of 0.81. In the experimental set up loads were applied to the slab through two-inch square plates at 16 uniformly spaced positions. In the theoretical investigation a concentrated load was applied at all the interior nodes as shown in Fig. 30.

The load-deflection curve for the midpoint of the slab is
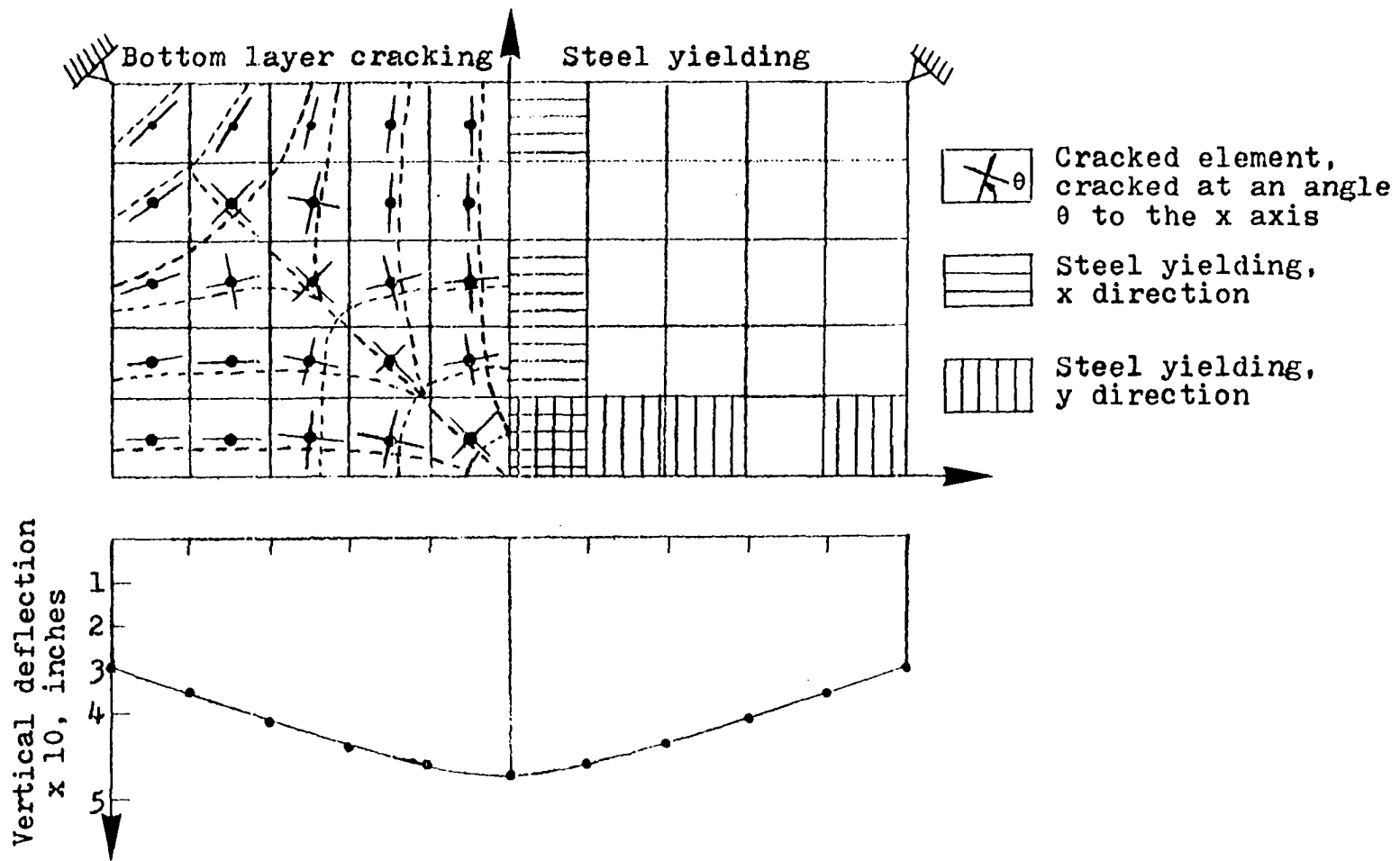
Fig. 29. Cracking pattern, steel yielding pattern, and the deflection along the center line for the McNeice slab for P = 4 kips and f_t = 0.55 ksi

Concentrated
loads act on
all interior
nodes

Deflection
point used
for compari-
son purposes

Simply sup-
ported on
all edges

6'0"

6'0"
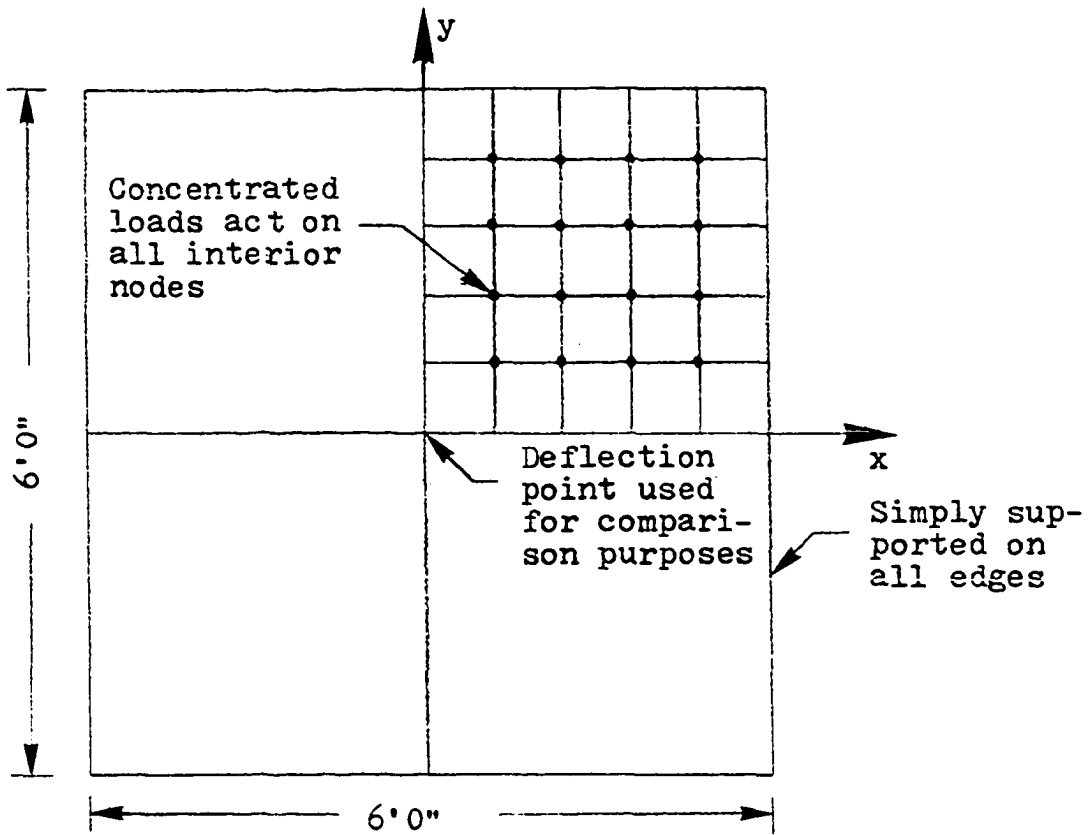
a. Finite element idealization for the quarter of the slab

composite layer

5 at .1675"

2" at

3 at

.375"

.1875

E_0 = 3656 ksi

$|f'_c|$ = 4.115 ksi

f_t = 0.480 ksi

ϵ_{cu} = 0.003

E_s = 29,000 ski

F_y = 54.5 ksi

A_s = 0.01 sq inch/inch
       width in x and y
       direction
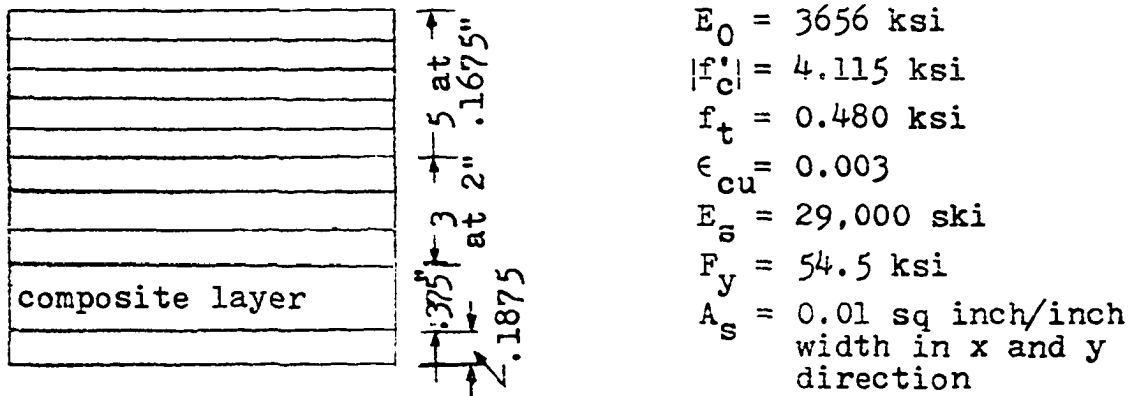
b. Layering system and assumed material properties

Fig. 30. Details of the simply supported Taylor (63) slab S1

plotted in Fig. 31. As in the case of corner supported slabs, the finite element solution overestimates the deflections. One reason for the overestimation, as explained earlier, could be the nature of the modeling of the cracks in concrete. Theoretical results of this study are also compared with the material nonlinear analysis results of Berg (23) in Fig. 31. Berg used a more refined quadrilateral element than the simple rectangular element used in this study. Berg calculated stresses and material properties at 48 points per layer per quarter of the slab as against 25 points per layer per quarter of the slab used in this study. Thus the simple rectangular element and simplified procedure of calculating residual loads has given results comparable to the solutions obtained by Berg (23). Thus it appears from a practical standpoint significant improvement in the finite element solutions for slabs cannot be achieved by increasing the number of elements but rather by improving the crack modeling of the concrete and calculating the stiffness of the cracked slab more accurately.

The collapse load obtained by considering material nonlinear analysis alone is less than the experimental collapse load. This is because geometrical nonlinear effects gain importance near ultimate loads and the slab will take considerable more load by membrane action. This can be observed by the material and geometrical nonlinear solution of Berg (23).

The cracking pattern, steel yielding pattern, and the center line deflection pattern are shown in Fig. 32. The
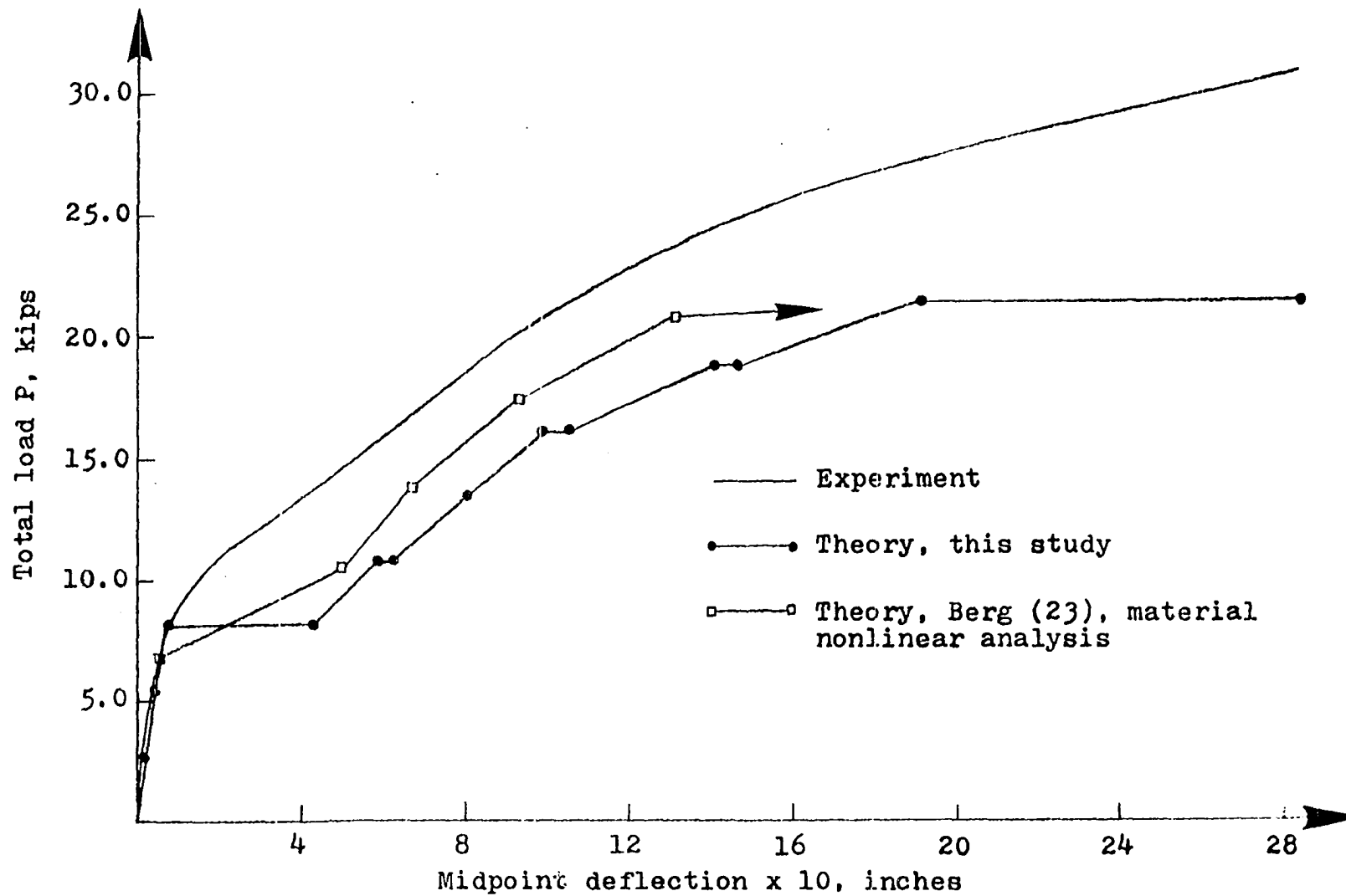
Fig. 31. Load-deflection diagram for the Taylor slab S1

Top layer cracking   Bottom layer cracking

Cracked element,
crack at one angle θ

Steel yielding in
x and y direction

Deflection x 10, inches

8

16

24

32

Deflection along
x axis
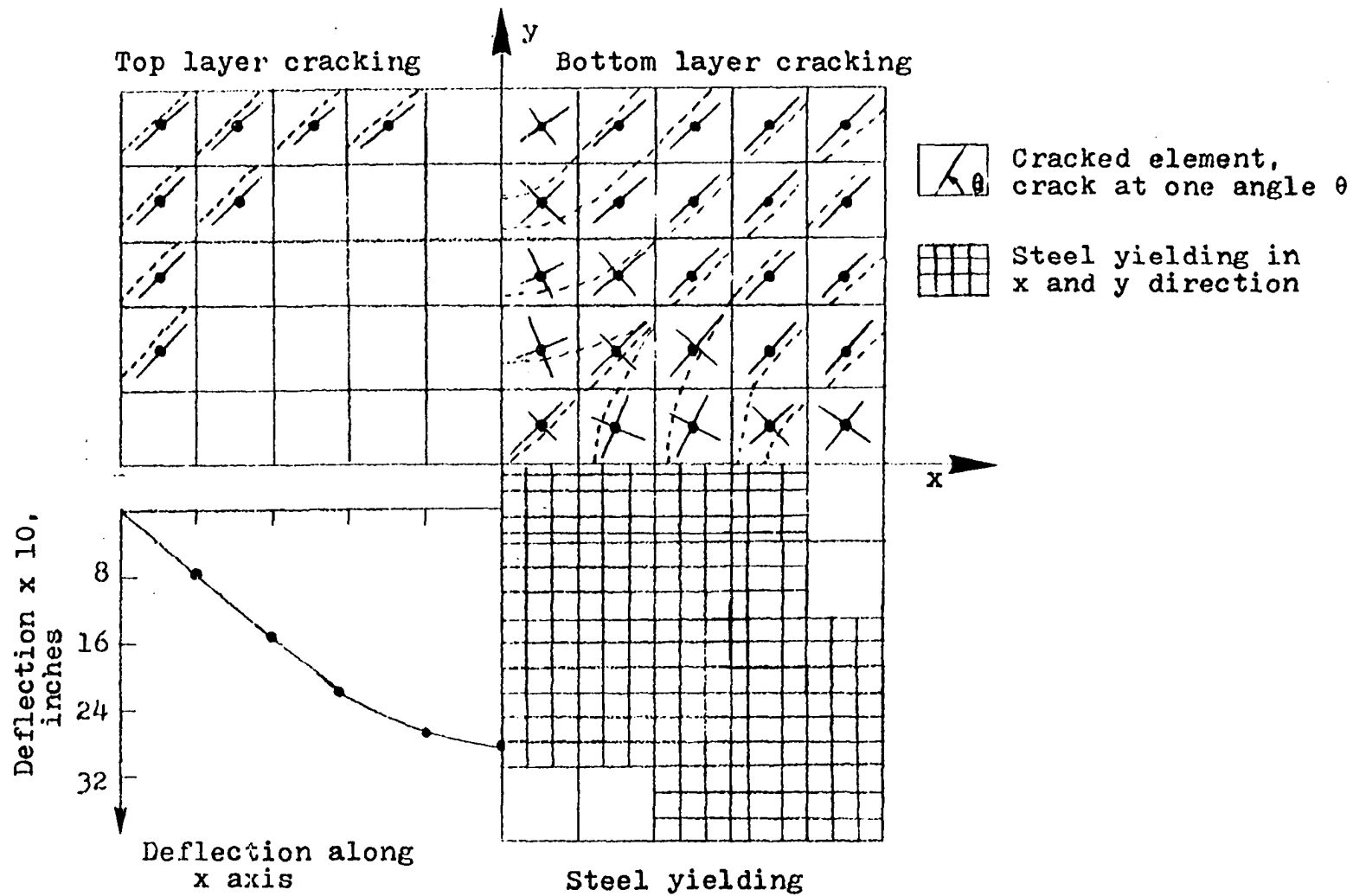
Steel yielding

Fig. 32. Cracked concrete, steel yielding, and deflection along center line for the
Taylor slab Sl at ultimate load

cracking of top layers near the corners due to corner uplift must be noted. The cracking pattern and the steel yielding pattern along the diagonals agree with the diagonal yield line pattern developed during the actual slab experiment.

In the theoretical analysis at the initiation of the first crack considerable redistribution of stresses took place. At the increment when the first crack developed (approximately 38% of the theoretical ultimate load) an increase in midpoint deflection value of about 600% over the value at the start of the increment took place. The principal moments $\bar{M}_1$ and $\bar{M}_2$ along the diagonal for the cracked slab computed by the finite element method are compared with the elastic solution given by Timoshenko and Woinowsky-Krieger (64) in Fig. 33. The considerable deviation in the computed moment values M_1 between the two methods due to cracking of the concrete is noteworthy.

Geometric Nonlinear Analysis of a Clamped Elastic Plate

In the geometric nonlinear analysis, the tangent stiffness matrix is composed of the basic element stiffness matrix K_0, the initial stress matrix K_σ, and the initial displacement K_D. Exact integration of higher order stiffness matrices are difficult to perform and simplified procedures are widely used in generating higher order stiffness matrices. In the generation of the initial stress matrix it is assumed that N_x, N_y and N_{xy} are constants when an integration over the area is performed
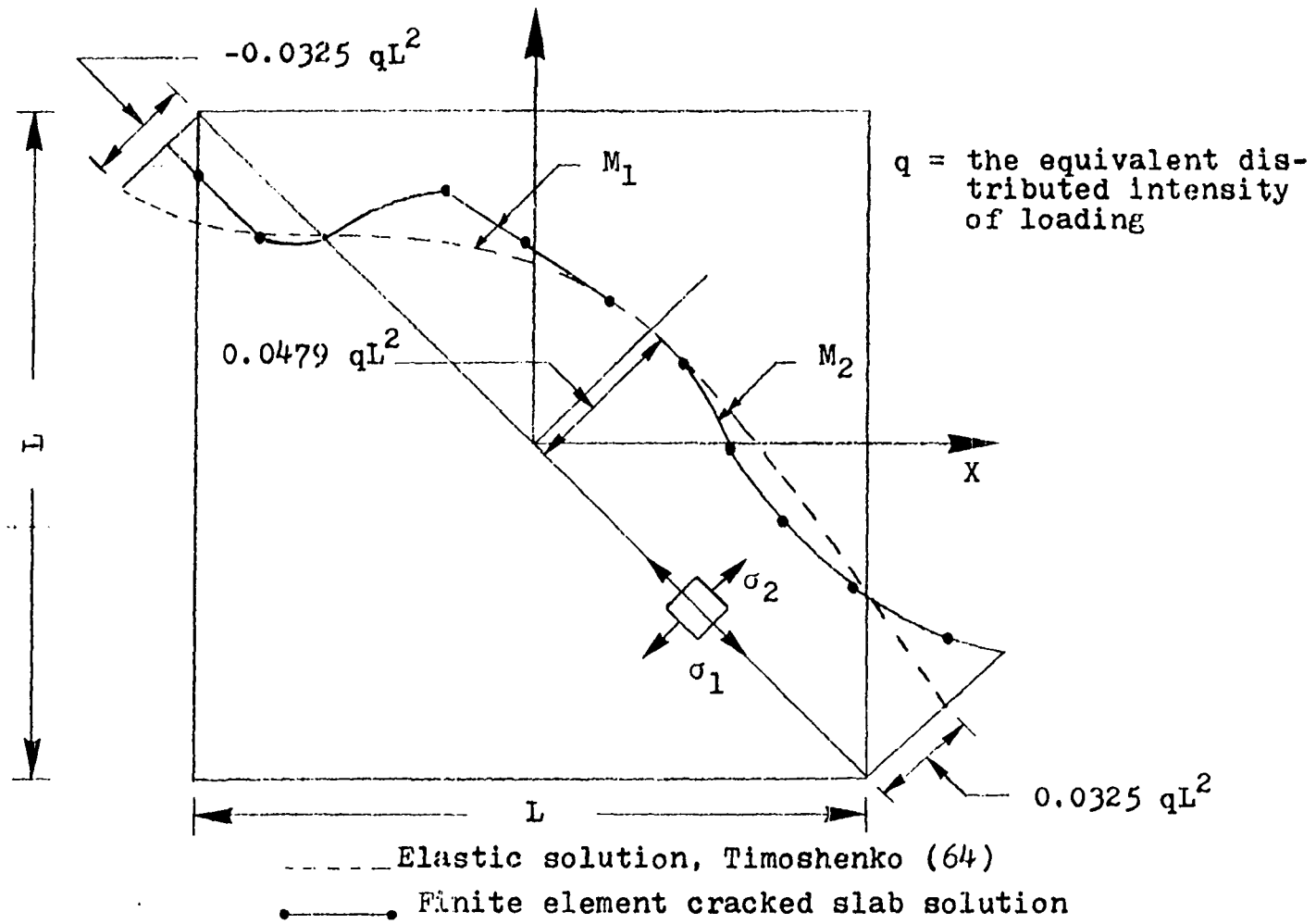
Fig. 33. Distribution of the principal moments at 38% of the theoretical ultimate load along the diagonal for Taylor slab S1

(Appendix). The initial displacement matrix is developed
by considering the total displacement gradients $w,_x$ and $w,_y$ to
be constants evaluated at the centroid of the element while an
integration is performed over the area. Brebbia and Connor
(65) used the same rectangular element in making a geometric
nonlinear analysis of a clamped square plate subjected to
central concentrated load and used a numerical integration pro-
cedure to develop higher order stiffness matrices. Adotte
(66) solved the same plate problem by directly solving the
basic differential equations using finite difference and
series solution procedures. The dimensions of the plate and
the layering system used is shown in Fig. 34. The deflection
results are compared in Fig. 35. As the purpose of this
example was to check the tangent stiffness matrices generated,
no iterations were performed at any increment. It can be seen
in Fig. 35 that for a given deflection the stiffness (slope
of the tangent) calculated by the three methods agree closely.

Material and Geometric Nonlinear Analysis

General

It is well known that the strength of slender columns is
reduced by second order deformations. Serious limitations in
the treatment of slender columns in ACI Code 318-63 led to re-
vised recommendations in ACI Code 318-71. A good background to
the current ACI Code procedure is given in the paper by
McGregor, Breen, and Pfrang (67). The revised code encourages
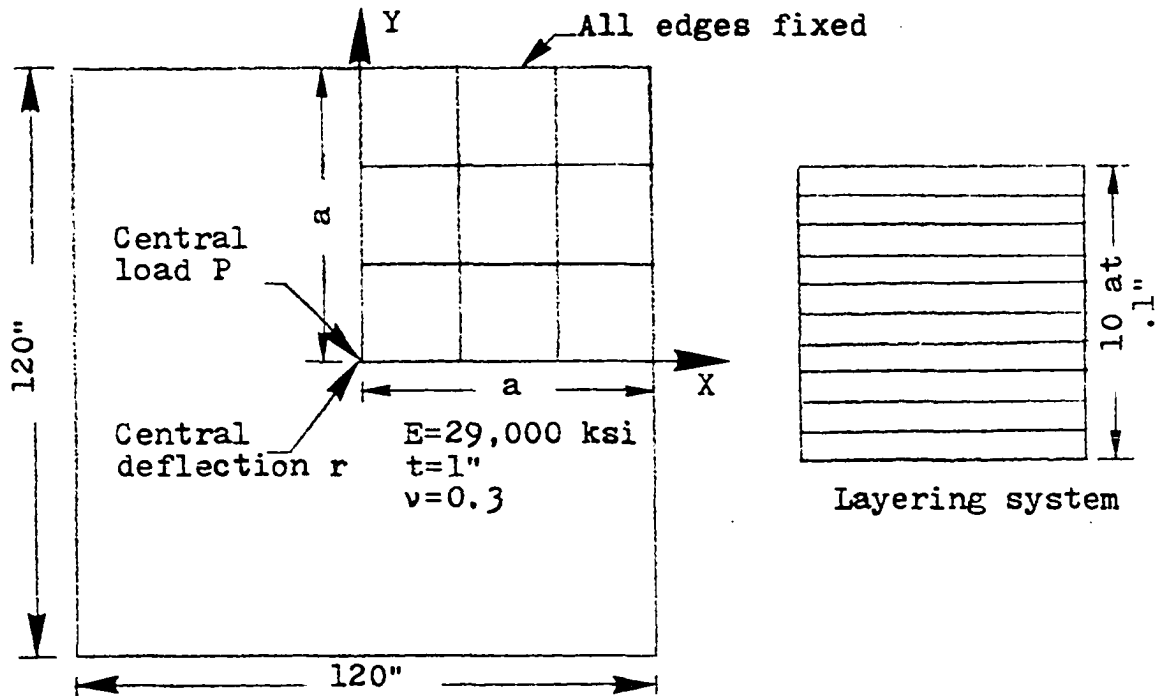
Fig. 34. Finite element idealization for one quarter of a homogenous elastic clamped square plate

$t=thickness; \quad \beta=\dfrac{Pa^2}{Dt}; \quad D=\dfrac{Et^3}{12(1-\nu^2)}; \quad \nu=0.3$
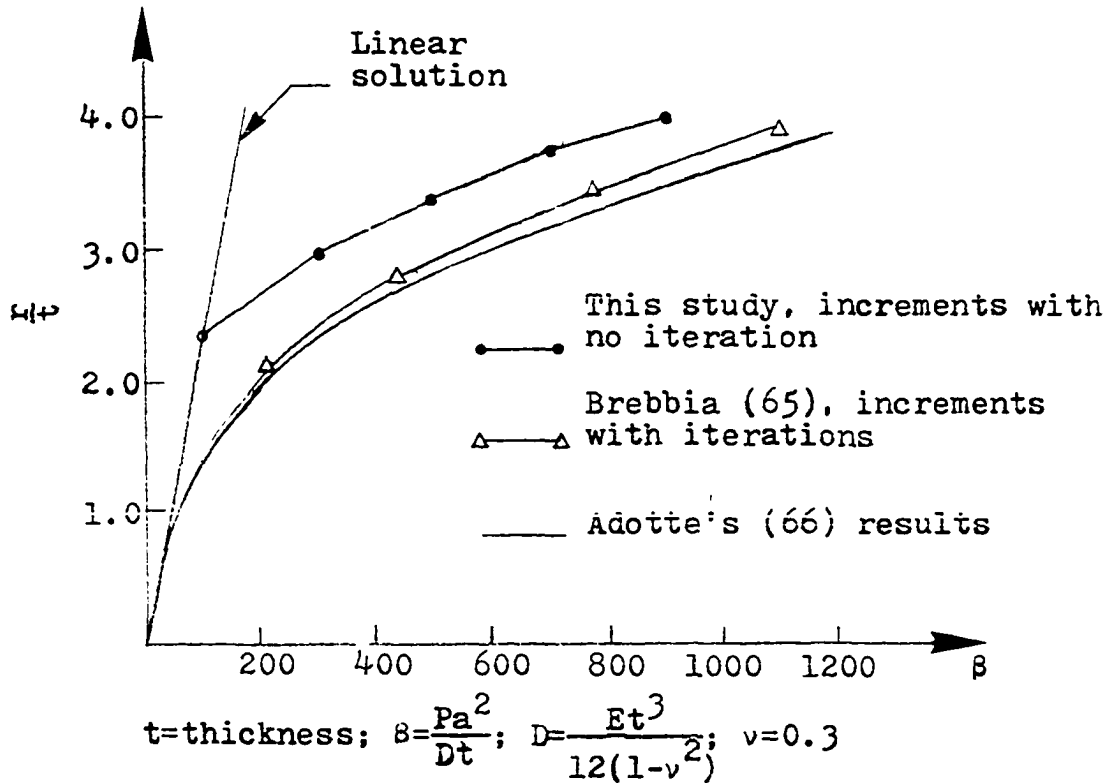
Fig. 35. Load-deflection diagram for a clamped elastic plate considering geometric nonlinearity

a rational second order analysis of slender reinforced concrete columns whenever possible and in lieu of that recommends approximate design procedures. In this section several long slender columns are analyzed and the applicability and the performance of the finite element procedure used is studied. The ease of combining second order deformations, complex loading and boundary conditions, varying material properties along the length and depth of the column, and the time dependent deformations in the finite element procedure make it very attractive to the solution of this class of problem. In this section a concrete column bent in double curvature, columns that had high compressive stresses and extensive cracking near failure and columns that failed by instability are theoretically analyzed.

Column bent in double curvature

Martin and Olivieri (68) tested eight reinforced concrete columns to study the column behavior under opposite eccentric loading. They tested the columns with ratio of end eccentricities $\frac{e_1}{e_2}$ = -0.5 to reproduce the condition of the most loaded column in a building which has one end fixed at the foundation. The columns were loaded to cause bending about the weak axis. The behavior of the column 422-2 with the ratio of $\frac{e_2}{t}$ = 0.388 where e_2 is the larger of the two end eccentricities is chosen here for comparison.

The details of the geometry, layering system and the

material properties are shown in Fig. 36. The load-maximum lateral deflection diagram is plotted in Fig. 37. The theoretical collapse load obtained was 17.5 kips as compared to 16.5 kips observed experimentally. The load deflection diagram for the entire column length is shown in Fig. 38. The theoretical deflections are less than the experimentally observed deflections. The tendency of the column to deform without any increase in load (time dependent deformation) observed during the experiment could be one reason for the discrepancy. Short term or long term creep of concrete is not considered in this study. Smaller increments of loads will also reduce the difference between the theoretical and the experimental results.

The moment diagram and the cracking pattern of the column just before collapse is shown in Fig. 39. The shifting of the maximum moment value from the end towards the center of the column is due to the secondary effects. In the experiment, a tendency to displace the point of contraflexure and increase the length of the main wave of the deflected column was observed. A similar behavior can also be observed in the theoretical results (Fig. 39).

Theoretical results also indicated longitudinal splitting cracks at many locations at the outer surface and inside of the column. This behavior is directly related to the tension-compression failure criterion used in this study. It is noteworthy that the experimental failure section was located at 47.5" from the left end (Fig. 39) and the theoretical results

Z

P

M

1   2   15   16

X

P

M/2

3.543"

141.72"

Elevation

Y

M/2

M/2

1   2   15   16

5"

141.72"

Plan

N/4

P/2

X

P/2

M/4

119

5"

composite layer

composite layer

3.543"

.375"

.375"

.375"

2 at .2607"

4 at .43755"

2 at .2607"

Layering system
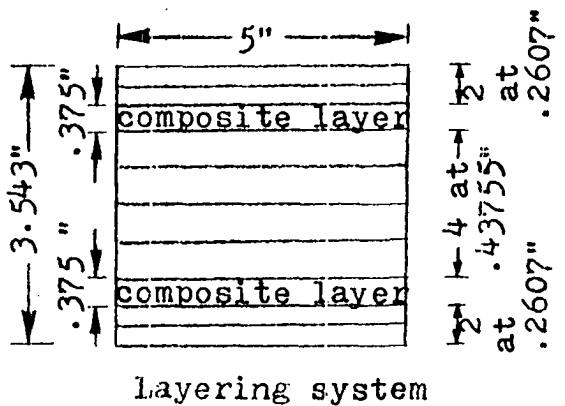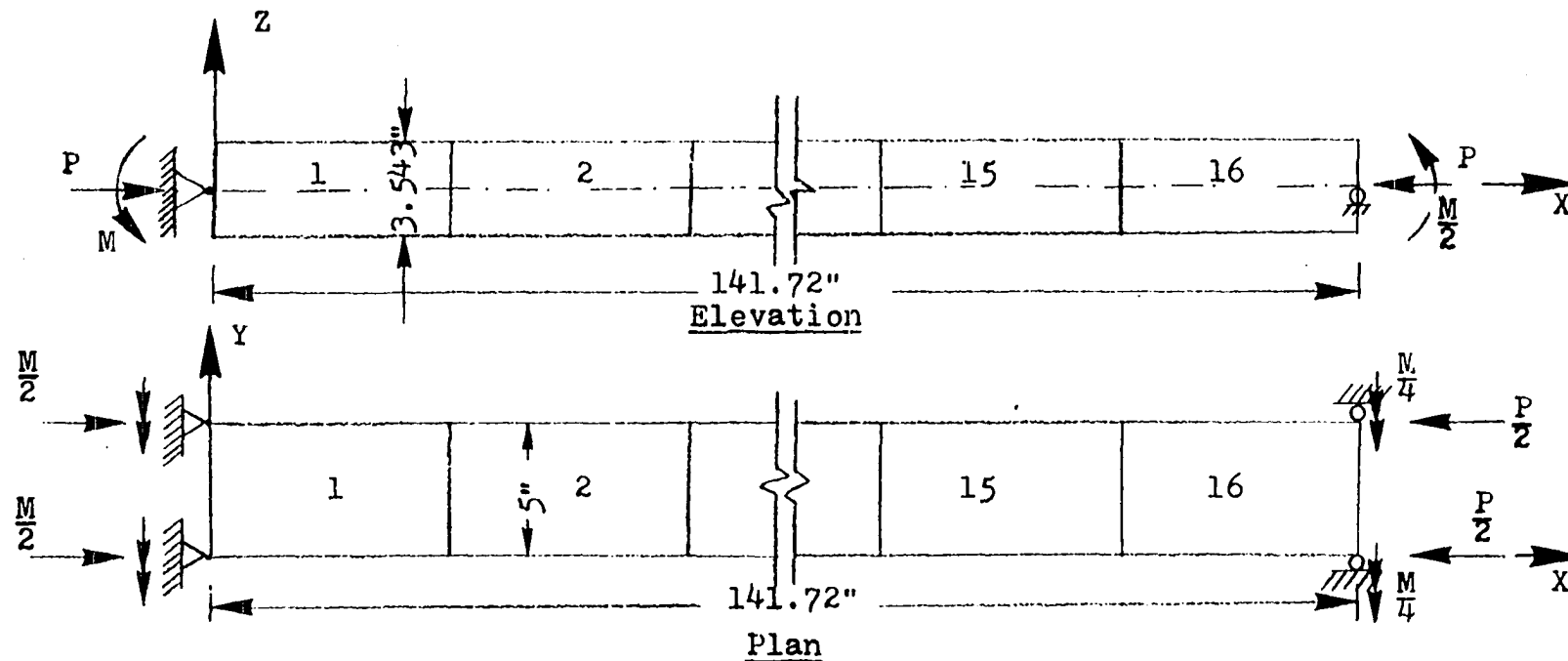
Material properties

$E_0 = 3481$ ksi

$|f'_c| = 3.73$ ksi

$f_t = 0.458$ ksi

$\epsilon_{cu} = 0.003$

$E_s = 29,000$ ksi

$F_y = 40$ ksi

$A_s = 0.044$ sq inches/inch width in each composite layer along x direction

Fig. 36.   Details of Martin's column (68) 422-2 bent in double curvature
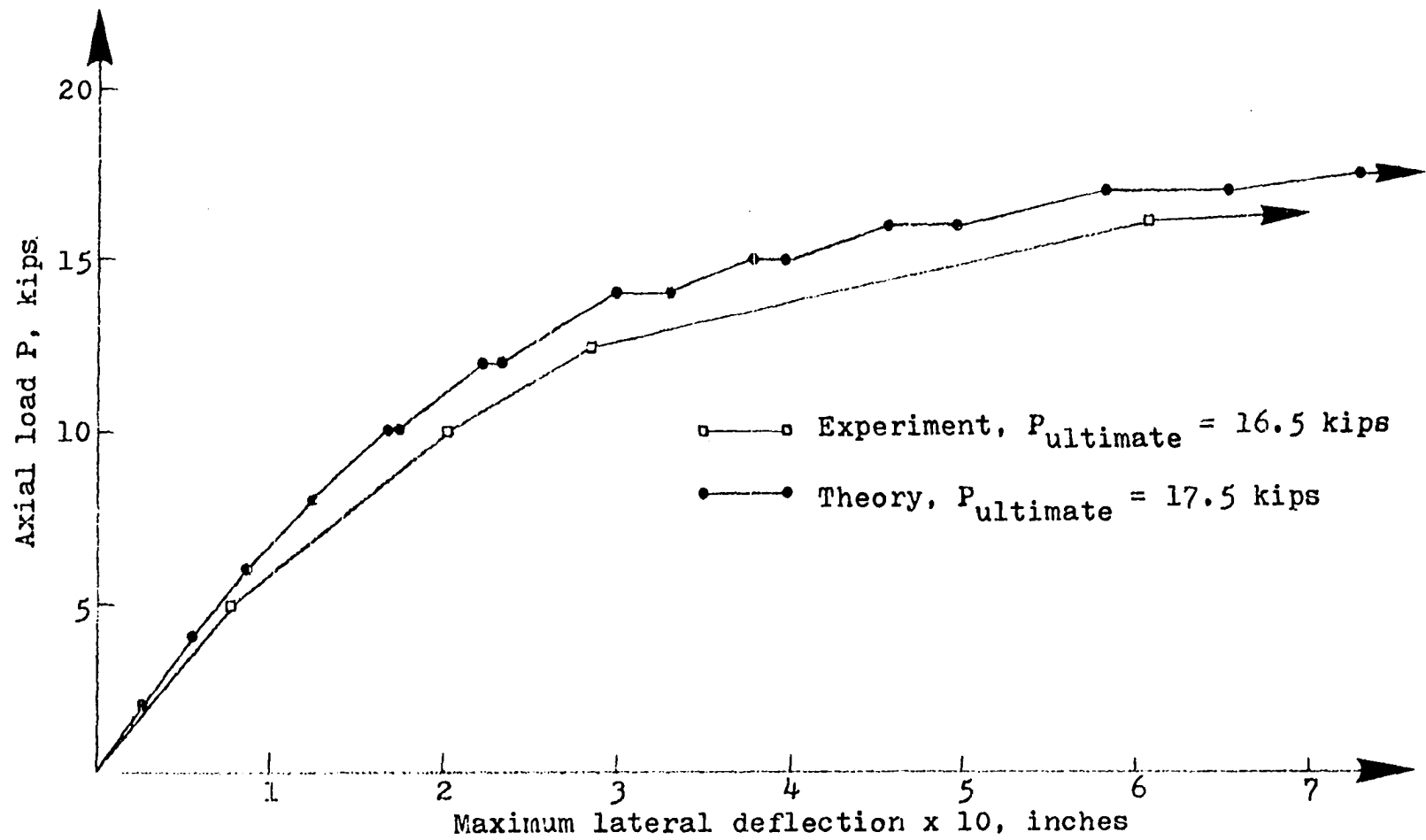
Fig. 37. Load-maximum lateral deflection diagram for column 422-2
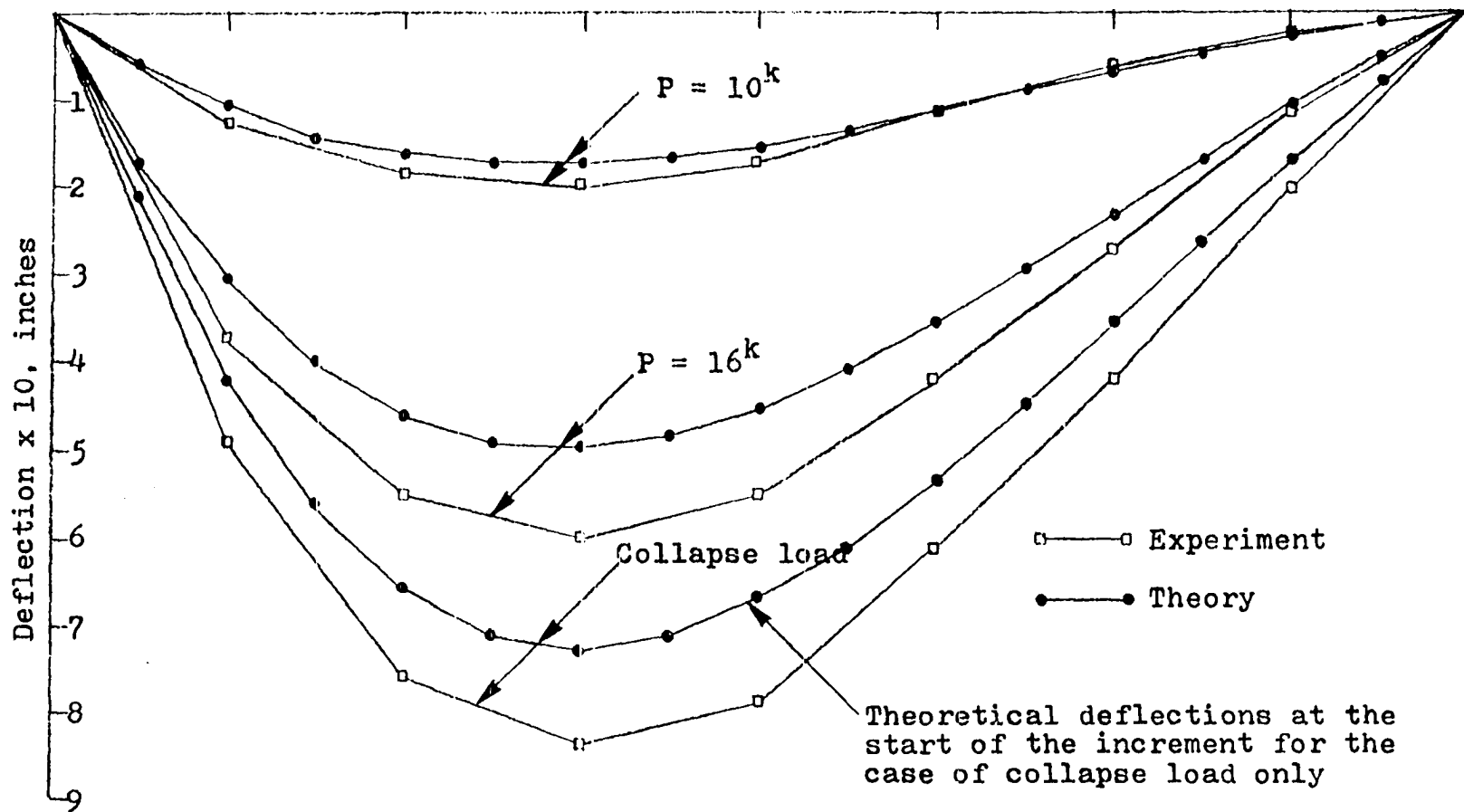
Fig. 38. Load-lateral deflection diagram for column 422-2

Moment, kip inch/inch

Movement of
point of inflection

Linear Solution

Lateral flexure cracks

Longitudinal splitting cracks
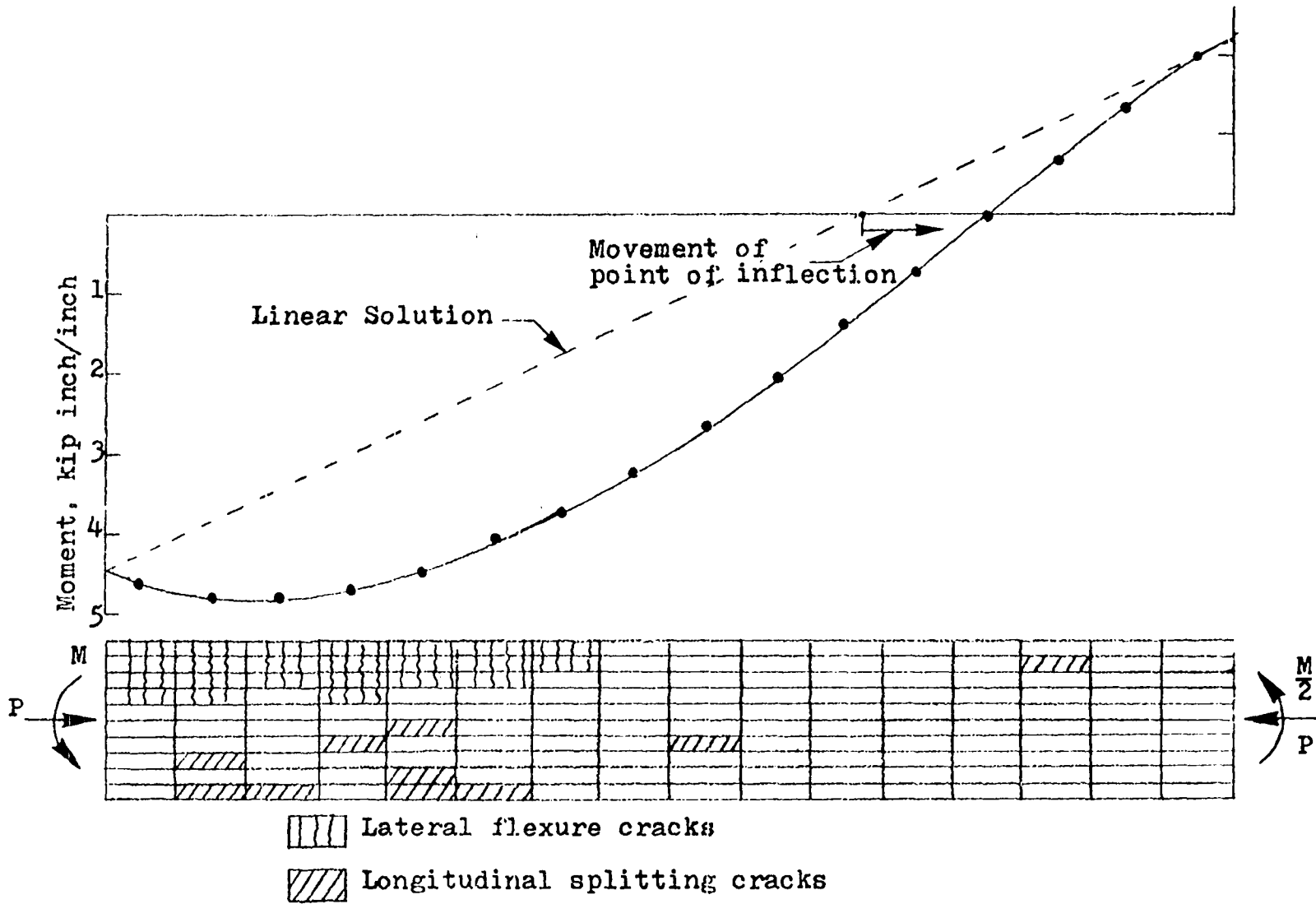
Fig. 39. Moment diagram and cracking pattern for column 422-2 just before collapse

correctly indicated the maximum stressed element at the same
location (sixth element, Fig. 39). Maximum theoretical stress
in the reinforcement steel just before collapse was 38.48 ksi
$(0.81 \ F_y)$.

Long cantilever columns subjected to lateral forces

Long cantilever flagpole type columns subjected lateral
forces is frequently encountered in civil engineering. A tall
pier subjected to longitudinal bridge forces due to braking or
wind or earthquake etc. is a typical example. Breen and
Ferguson (69) tested ten model cantilever columns subjected to
lateral forces. They studied the behavior of the columns for
different height to thickness and lateral force to axial force
ratios. Three columns G1, G2, and G4 which showed different
failure patterns are chosen here for comparison with theory.

The geometry, layering system and the assumed material
properties for the columns are shown in Fig. 40 and Fig. 41.
The load-end deflection diagram for column G1 is shown in
Fig. 42. The theoretical collapse load was 39.375 kips while
the experimental collapse load was observed to be 34 kips. The
column sustained high compressive stresses and strains at the
maximum stressed point before failure occurred. The theoreti-
cal load prediction, which did not include creep effect, is
roughly 16% too high. Thus for short columns, rapid creep
under high compressive stresses observed in the experiments
could be the source of problem for the large deviation in
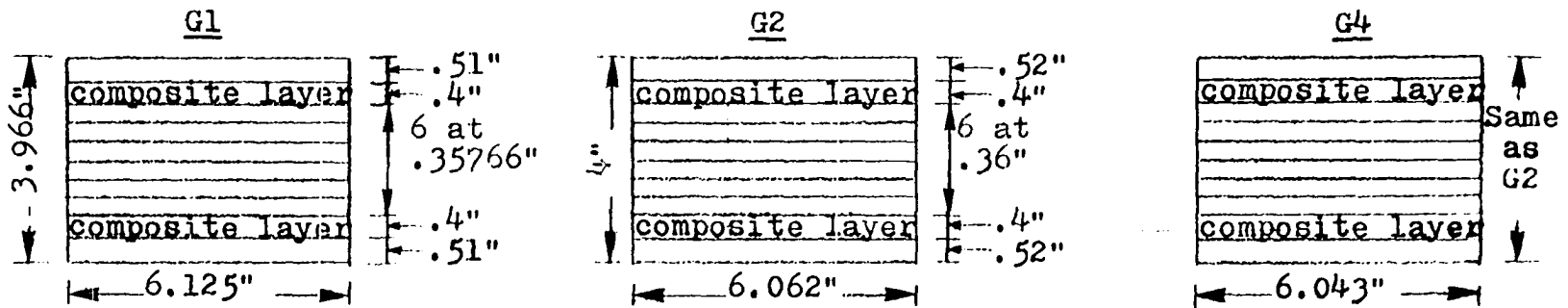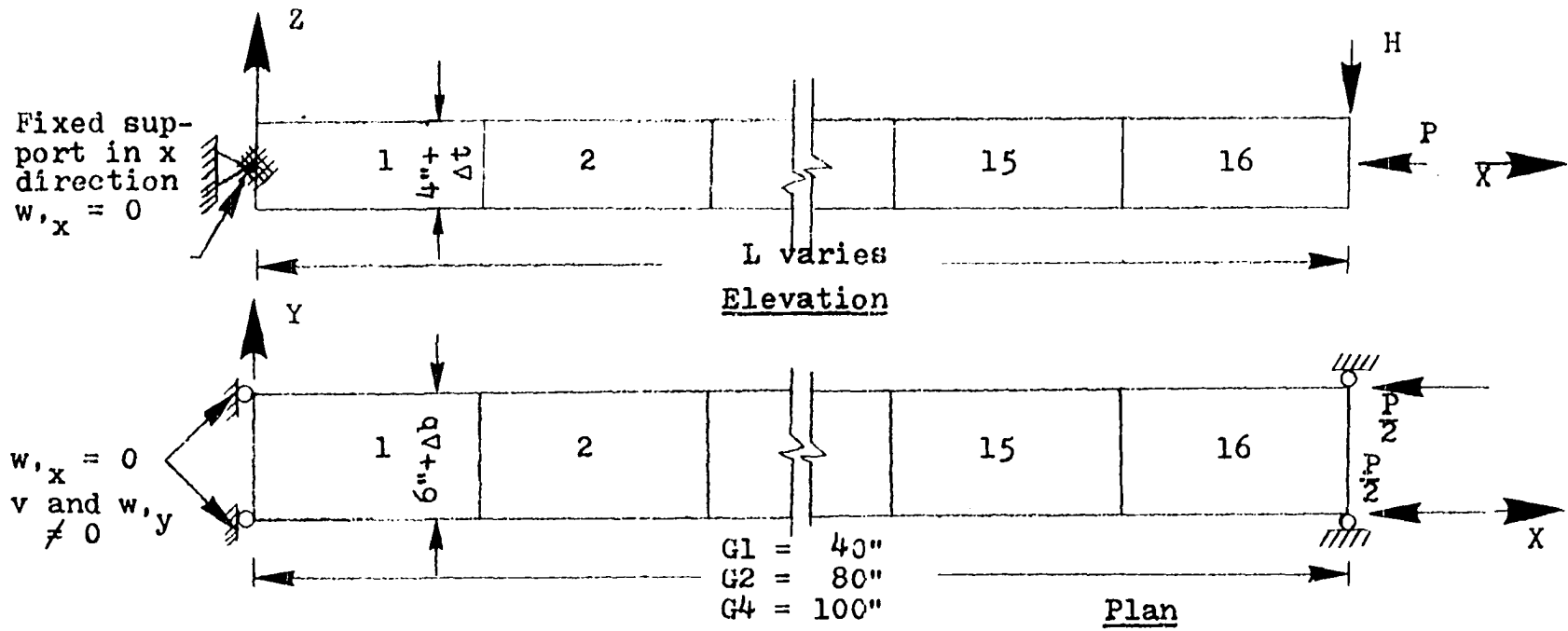
Fig. 40. Geometry and the layering system for Breen's columns (69) G1, G2, and G4

G1	G2	G4
E_0=3476 ksi	E_0=3448 ksi	E_0=3467 ksi
$|f_c'|$=3.72 ksi	$|f_c'|$=3.66 ksi	$|f_c'|$=3.7 ksi
f_t=.457 ksi	f_t=.453 ksi	f_t=.456 ksi
E_s=29,000 ksi	E_s=29,000 ksi	E_s=29,000 ksi
F_y=59.4 ksi	F_y=58.8 ksi	F_y=58.4 ksi
A_s=.03592 sq inch/ inch width in each composite layer	A_s=0.03629 sq inch/ inch width in each composite layer	A_s=0.03637 sq inch/ inch width in each composite layer
$\frac{H}{P}$ =0.03	$\frac{H}{P}$ =0.03	$\frac{H}{P}$ =0.012

Fig. 41. Material properties and load ratios for Breen's columns
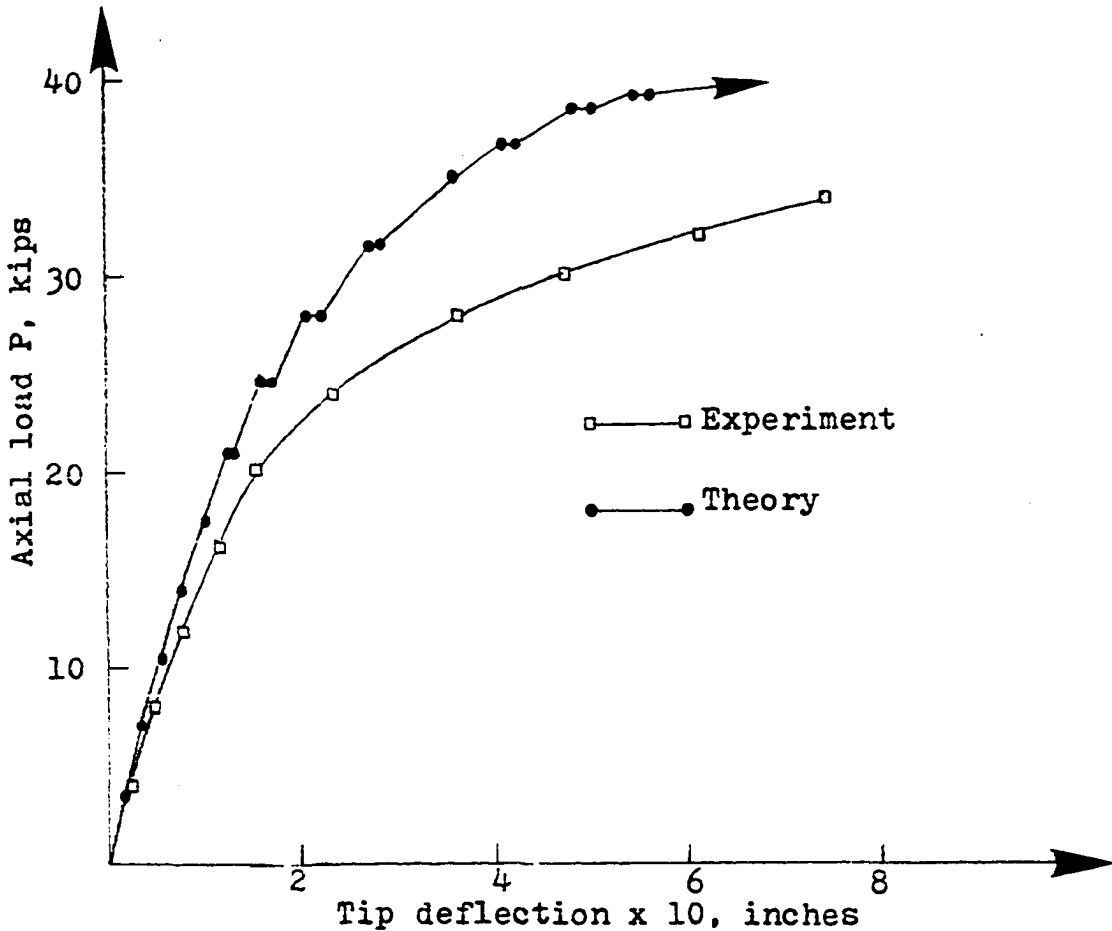
Fig. 42. Load-deflection curve for column G1

deflection values between theory and experiment (Fig. 42).
Further, in theory the stresses are checked at the centroid
of the element whereas the maximum stress in the cantilever
occurs at the end closest to the support. This has the effect
of delaying the nonlinear behavior. Also the biaxial stress
state and the failure stresses in the critical end element are
affected by the lateral boundary conditions used for the ele-
ment nodes at the support. An improvement in the results can
be obtained when time dependent deformations are included in
the analysis.

The moment diagram, crack patterns, and deflected shape
of column G1 is shown in Fig. 43. The theoretical results
indicate a large number of flexure cracks and longitudinal
splitting cracks in the column G1 just before failure (Fig. 43).
The moment diagram clearly indicates the moment magnification
along the length of the column due to secondary effects. The
maximum moment in the critical end element 1 relative to the
interaction diagram is shown in Fig. 44 in which the theo-
retical values are compared with the experimental values. The
reduction in the strength of the column due to the long column
effect is easily seen.

Length of column G2 was twice that of column G1 and hence
column G2 was subjected to a greater moment than column G1 for
the same lateral force. Column G1 had greater lateral deflec-
tions for the same axial load and the concrete section had a
greater number of flexure cracks. The theoretical results for
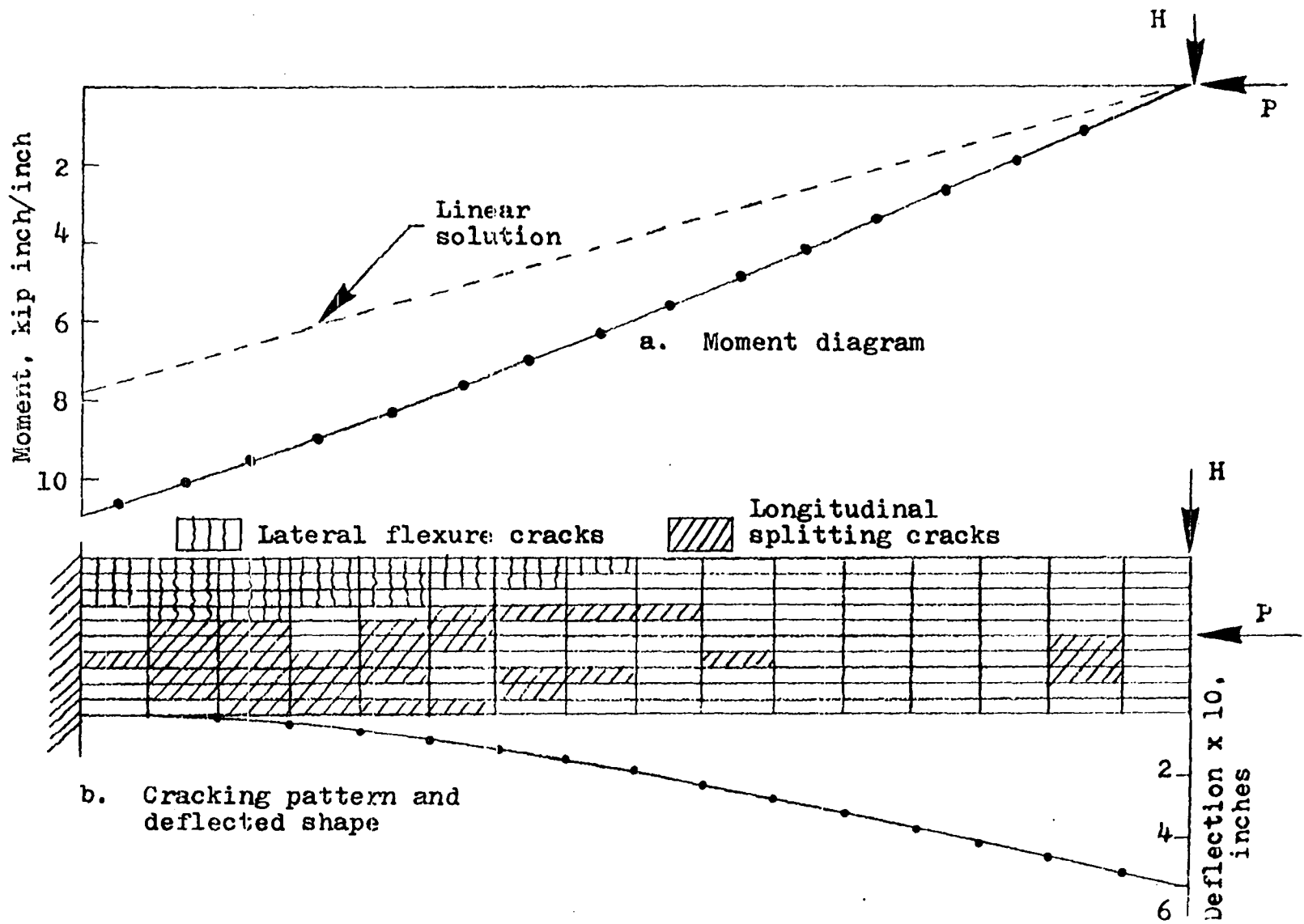
Fig. 43. Cracking pattern, deflection diagram and moment diagram for column G1 just before collapse

Fig. 44. Maximum bending moment relative to interaction diagram for column G1
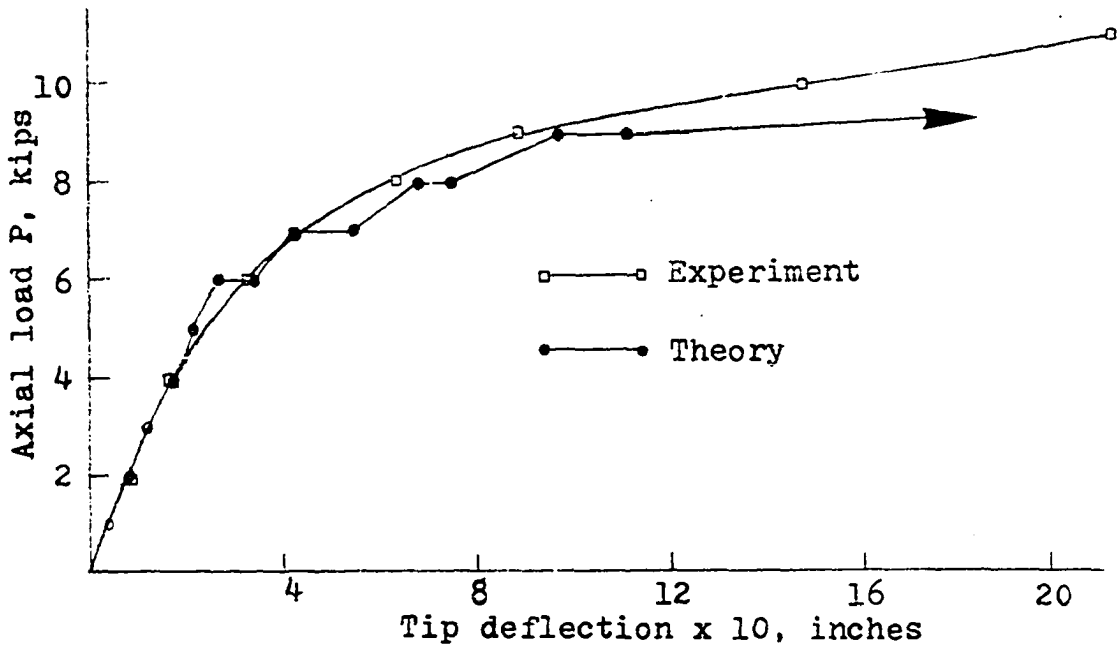
Fig. 45. Load-deflection diagram for column G2

column G2 are shown in Fig. 45 through **Fig. 47**. The theo-
retical ultimate load for column G2 was 10 kips as compared
with the experimental ultimate load of 10.75 kips. The over-
estimation of deflections at higher load levels may be due to
the nature of the concrete crack modeling. The concrete be-
tween the cracks might have contributed additional stiffness
to the experimental column. The maximum moment in the critical
end element 1 for column G2 relative to the interaction diagram
is shown in Fig. 47. The theoretical results model very satis-
factorily the moment magnification due to the second order
effects (Fig. 47).

Column G4 has the highest height to thickness ratios of
the three columns G1, G2, and G4 (Fig. 40). Column G4 failed
by instability in the experiment. The theoretical load-deflec-
tion response for G4 is shown in Fig. 48. The experimental
load-deflection curve for column G4 is not available. The
theoretical load-deflection diagram (Fig. 48) correctly models
the sudden nature of the instability failure. The theoretical
collapse load was 11.5 kips as compared with the experimental
collapse load of 12 kips. The maximum moment in the end criti-
cal element 1 relative to the interaction diagram is plotted in
Fig. 49. The characteristics of the instability failure can
clearly be seen in Fig. 49. The concrete strains and stresses
were also small just before the instability failure occurred.

a. Moment diagram

Lateral flexure cracks   Longitudinal splitting cracks

b. Cracking pattern and deflection diagram

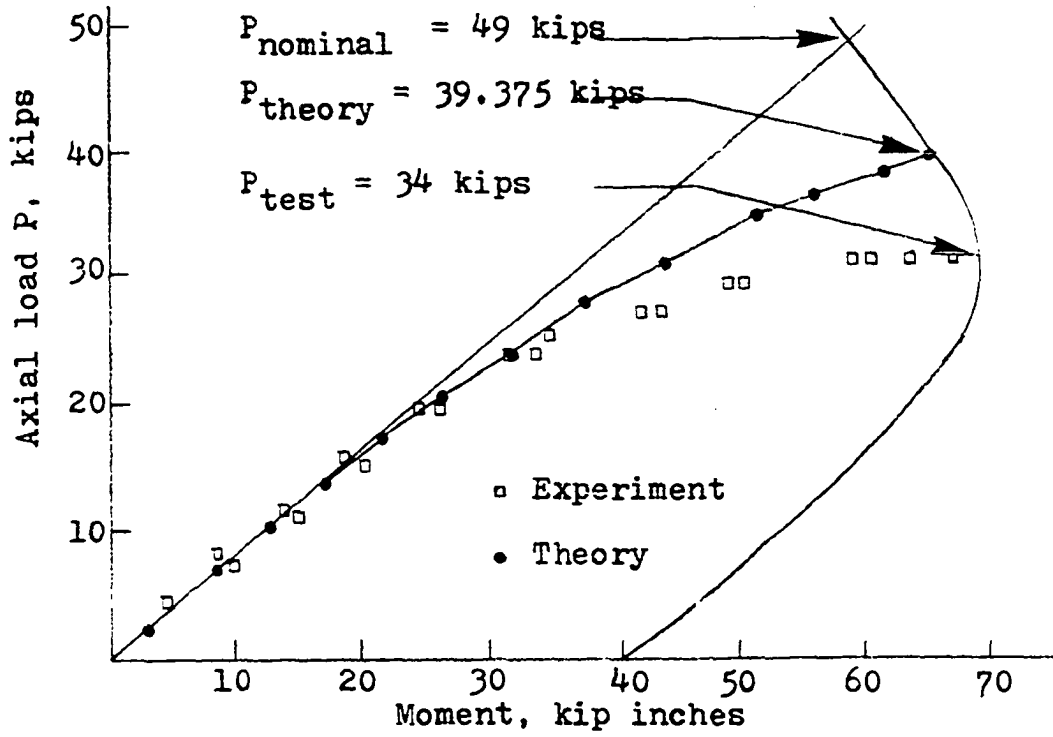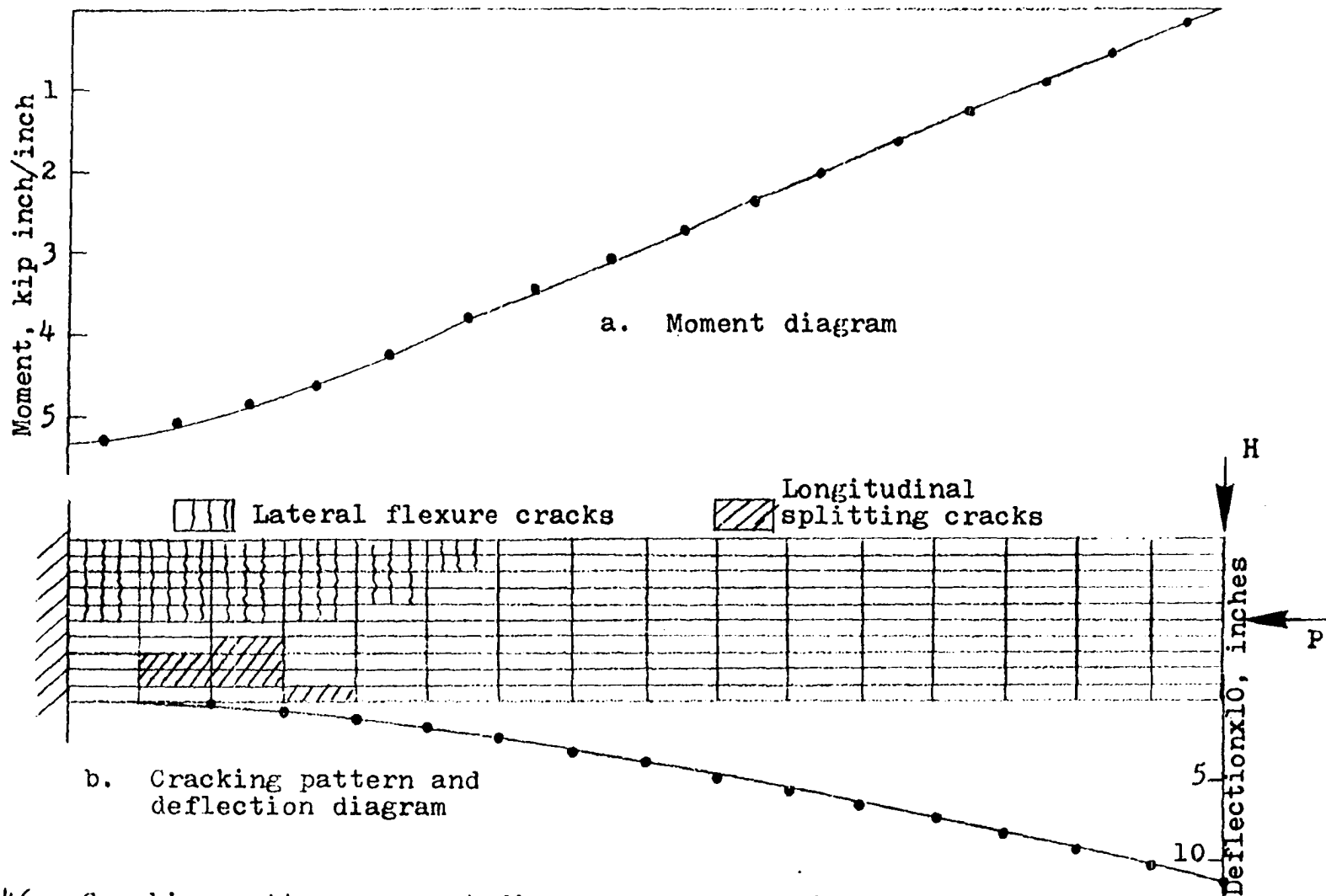Fig. 46. Cracking pattern, moment diagram and deflection diagram for column G2 at load P = 9 kips
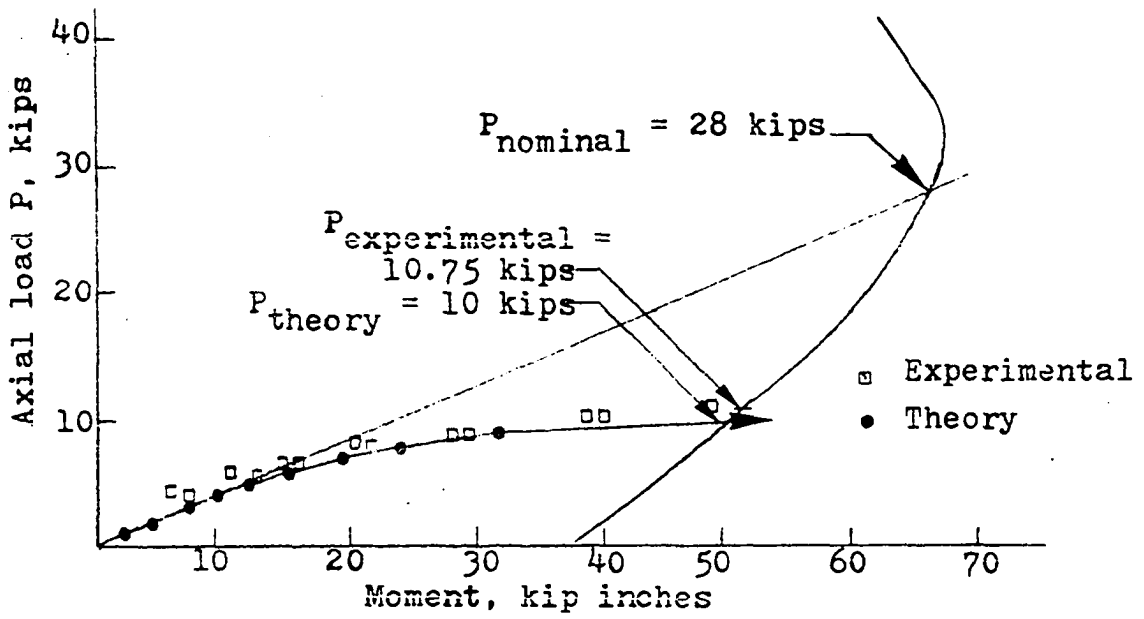
Fig. 47. Maximum bending moment relative to interaction diagram for column G2
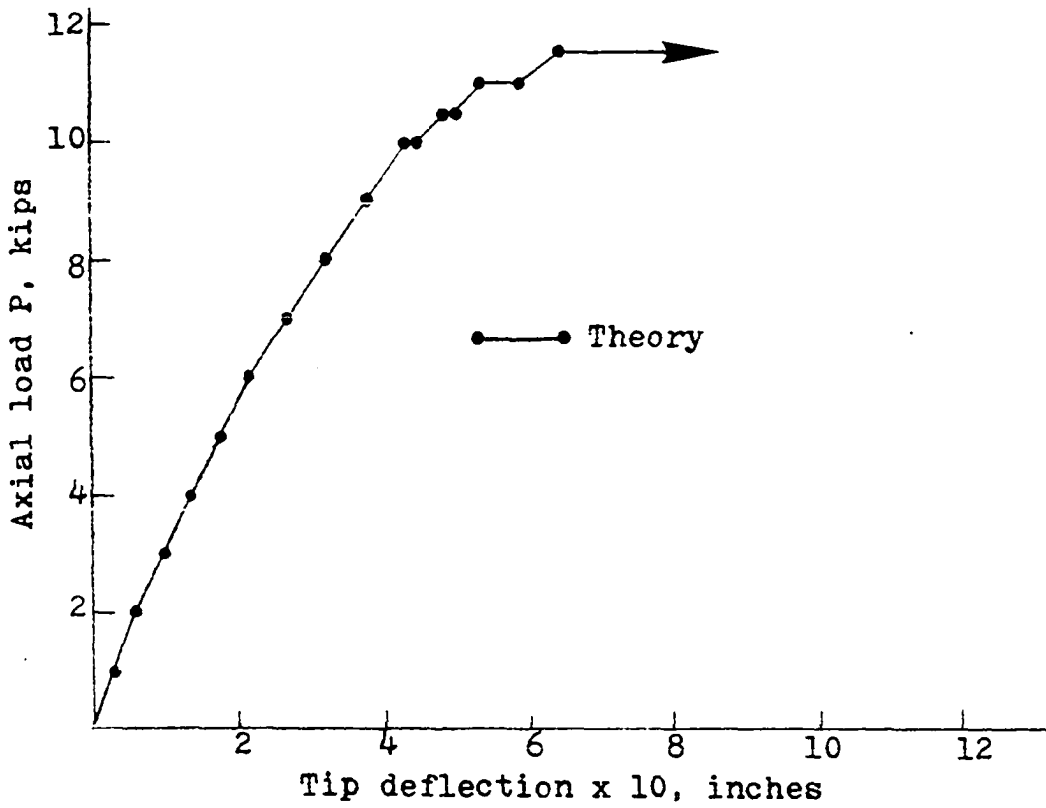
Fig. 48. Load-deflection diagram for column G4
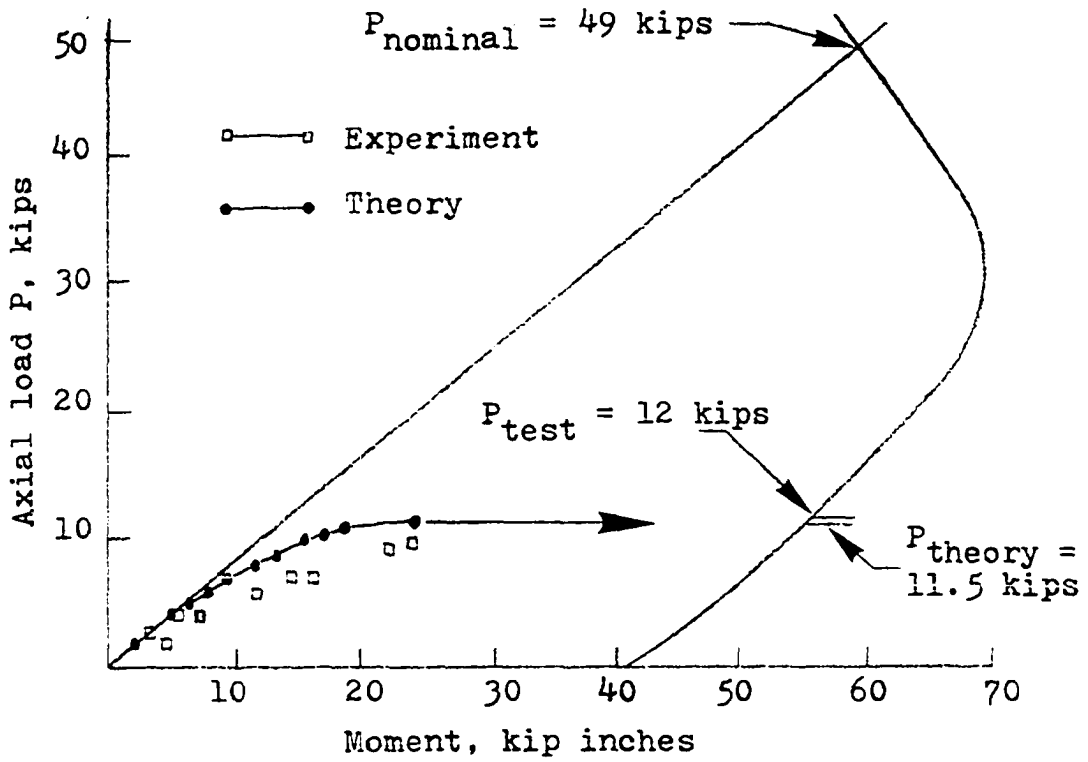
Fig. 49. Maximum bending moment relative to interaction
diagram for column G4

CHAPTER 6. SUMMARY AND CONCLUSIONS

Summary

A nonlinear analysis of reinforced concrete beams, beam-columns and slabs by finite elements has been presented. Failure stresses for concrete are obtained by considering the biaxial stress state. Empirical equations that closely fit the experimental failure points are used to define the failure envelope in the tension-tension, tension-compression and compression-compression regions. The concrete is treated as an orthotropic material. The concept of the equivalent uniaxial strain is used to calculate the material tangent moduli in the two principal directions. Constitutive equations in an incremental form are used to define biaxial stress-strain relationship. Cracking of the concrete is modeled by assuming the elastic modulus of the concrete perpendicular to the crack as zero. Different methods of obtaining an approximate value of the shear modulus of concrete is discussed. The expression used for the shear modulus results in retaining some shear stiffness for the concrete material cracked in a single direction.

A rectangular element having membrane and bending stiffness is used in the finite element analysis. Varying material properties over the depth is modeled by using a layered discretization of the element. All of the concrete layers are assumed to be in a state of plane stress. The steel

reinforcement is modeled as uniaxial fibers and the layer at
the level of the steel is treated as a composite layer. Any
number of steel layers and steel reinforcement in any arbitrary
direction in a layer can be conveniently handled. Steel re-
inforcement is considered to be elastic-perfectly plastic.

Incremental finite element Lagrangian formulation con-
sidering material and geometric nonlinearity is used. The
scope of the geometric nonlinear effects considered is dis-
cussed. Explicit forms of the basic element stiffness matrix,
initial stress matrix and the initial displacement matrix are
presented. Simplified procedures used in the evaluation of
higher order stiffness matrices are discussed. Several
numerical techniques available for the solution of the non-
linear equations are reviewed and the incremental and itera-
tive techniques used in this study are discussed in detail.
The procedure used in the calculation of residual loads is
also discussed. A computer code has been written based on the
finite element procedure described.

Finally several numerical examples are presented. Theo-
retical results obtained by considering material nonlinearity
alone are compared with the experimental results for a rein-
forced concrete beam and a number of reinforced concrete slabs.
Geometrical nonlinearity is included in the analysis of beam-
columns. Several columns which failed by instability and by
material failure due to moment magnification are studied. The
theoretical results are compared with the experimental results.

Conclusions

1. The orthotropic material model for concrete essen-
tially duplicates the experimental biaxial stress-strain curves
in the tension-compression and compression-compression region.

2. The simple concrete cracking model used in this in-
vestigation gave very good results for the under reinforced
concrete beam analyzed ($p \approx 0.5\ p_b$, where p is the percentage
of reinforcement and p_b is the balanced percentage steel). The
results were also satisfactory in the case of columns. Hence
it can be expected in a nonlinear analysis of reinforced con-
crete frames, the simple cracking model for concrete adopted in
this study should give very satisfactory results.

3. The results of this study for the case of McNeice slab
gave better results than that obtained by Hand et al. (12) (bi-
linear elastic-plastic concrete material) and Lin (14) (elas-
tic-plastic concrete material) as can be seen from Fig. 26.

4. A more realistic estimate of the distribution of
moments under service loads can be obtained by considering the
cracking of the concrete and using the finite element procedure.
This has been illustrated for the case of corner supported slab
in Fig. 28 and for the case of simply supported slab in Fig. 33.

5. In the case of simply supported slab, the results ob-
tained from this investigation for a material nonlinear analy-
sis using a simple rectangular finite element model and the
simplified residual load calculation procedures gave comparable

results to the material nonlinear analysis results obtained by Berg (23) which used a more refined finite element model.

6. Overestimation of slab deflections in the intermediate range of loading is a common feature of all the theoretical investigations using finite element technique. Use of a very refined biaxial model for concrete in tension-compression and compression-compression regions (as used in this study), or including the effect of geometric nonlinearity (Berg, 23), or increasing the number of points at which material properties are evaluated within practical limits (Berg, 23), do not significantly reduce the problem of overestimation of deflections in the intermediate range of loading.

7. The theoretical investigation of slabs has indicated that the next important step in the finite element analysis of reinforced concrete slabs is the development of satisfactory tension stiffening procedure which will be a function of the parameters which affect the crack spacing like the bond-slip characteristics, reinforcement spacing, percentage reinforcement, etc.

8. The finite element method predicts the behavior of reinforced concrete slender columns very satisfactorily.

9. In the case of columns with low slenderness ratios it is necessary to include the time dependent deformations to predict accurate collapse loads and the load-deflection response.

10. When combined material and geometric nonlinearity is considered, numerical instabilities can occur. The simplified

procedure for calculating the residual loads as explained in Chapter 4 and used successfully for columns did not work well for the case of simply supported slabs. However, in such cases solutions can be obtained by changing the solution technique as was done by Berg (23).

LITERATURE CITED

1. Oden, J. T., Clough, R. W., and Yamamoto, Y., Eds.
    Advances in Computational Methods in Structural Mechanics.
    Huntsville, Alabama: University of Alabama in Huntsville
    Press, 1972.

2. Ngo, D., and Scordelis, A. C. "Finite Element Analysis of
    Reinforced Concrete Beams." American Concrete Institute
    Journal, Proceedings, 64, No. 3 (March 1967), 152-163.

3. Nilson, A. H. "Nonlinear Analysis of Reinforced Concrete
    by Finite Element Method." American Concrete Institute
    Journal, Proceedings, 65, No. 9 (September 1968), 757-766.

4. Franklin, A. H. "Nonlinear Analysis of Reinforced Con-
    crete Frames and Panels." Division of Structural Engineer-
    ing and Structural Mechanics, Department of Civil Engineer-
    ing, University of California, Berkeley, California, SESM
    Report No. 70-5, 1970.

5. Rashid, Y. R. "Ultimate Strength Analysis of Prestressed
    Concrete Pressure Vessels." Nuclear Engineering and De-
    sign, 7, No. 4 (1968), 334-344.

6. Cervenka, V., and Gerstle, K. H. "Inelastic Analysis of
    Reinforced Concrete Panels, Part I: Theory." Inter-
    national Association for Bridge and Structural Engineer-
    ing, Publications, 31-II (1971), 31-45.

7. Yuzugullu, O., and Schnobrich, W. C. "Finite Element
    Approach for the Prediction of Shear Wall-Frame Systems."
    Department of Civil Engineering, University of Illinois,
    Urbana, Illinois, Structural Research Series No. 386, 1972.

8. Jofriet, J. C., and McNeice, G. M. "Finite Element An-
    alysis of Reinforced Concrete Slabs." Journal of the
    Structural Division, American Society of Civil Engineers,
    Proceedings, 97, No. ST3 (March 1971), 785-806.

9. Bell, J. C., and Elms, D. G. "Nonlinear Analysis of Re-
    inforced Concrete Slabs." Magazine of Concrete Research,
    24, No. 79 (June 1972), 63-70.

10. Scanlon, A., and Murray, D. W. "Time Dependent Reinforced
    Concrete Slab Deflections." Journal of the Structural
    Division, American Society of Civil Engineers, Proceedings,
    100, No. ST9 (September 1974), 1911-1924.

11. Dotreppe, J. C., Schnobrich, W. C., and Pecknold, D. A. "Layered Finite Element Procedure for Inelastic Analysis of Reinforced Concrete Slabs." _International Association for Bridge and Structural Engineering, Publications_, 33-II (1973), 53-68.

12. Hand, F. R., Pecknold, D. A., and Schnobrich, W. C. "A Layered Finite Element Nonlinear Analysis of Reinforced Concrete Plates and Shells." Department of Civil Engineering, University of Illinois, Urbana, Illinois, Structural Research Series No. 389, 1972.

13. Hand, F. R., Pecknold, D. A., and Schnobrich, W. C. "Nonlinear Layered Analysis of RC Plates and Shells." Journal of the Structural Division, _American Society of Civil Engineers, Proceedings_, 99, No. ST7 (July 1973), 1491-1505.

14. Lin, C. S. "Nonlinear Analysis of Reinforced Concrete Slabs and Shells." Division of Structural Engineering and Structural Mechanics, Department of Civil Engineering, University of California, Berkeley, California, SESM Report No. 73-7, 1973.

15. Lin, C. S., and Scordelis, A. C. "Nonlinear Analysis of RC Shells of General Form." Journal of the Structural Division, _American Society of Civil Engineers, Proceedings_, 101, No. ST3 (March 1975), 523-538.

16. Bell, J. C., and Elms, D. G. "A Finite Element Post-elastic Analysis of Reinforced Concrete Shells." _International Association for Shell and Spatial Structures, Bulletin_, No. 54 (April 1974), 43-52.

17. Kupfer, H. B., Hilsdrof, H. K., and Rusch, H. "Behavior of Concrete under Biaxial Stresses." _American Concrete Institute Journal, Proceedings_, 66, No. 8 (August 1969), 656-666.

18. Liu, T. C. Y. "Stress-Strain Response and Fracture of Concrete in Biaxial Compression." Ph.D. Thesis, Cornell University, Ithaca, New York, 1971.

19. Liu, T. C. Y., Nilson, A. H., and Slate, F. O. "Stress-Strain Response and Fracture of Concrete in Biaxial Compression." _American Concrete Institute Journal, Proceedings_, 69, No. 5 (May 1972), 291-295.

20. Liu, T. C. Y., Nilson, A. H., and Slate, F. O. "Biaxial Stress-Strain Relations for Concrete." Journal of the Structural Division, _American Society of Civil Engineers, Proceedings_, 98, No. ST5 (May 1972), 1025-1034.

21. Kupfer, H. B., and Gerstle, K. H. "Behavior of Concrete under Biaxial Stresses." Journal of the Engineering Mechanics Division, American Society of Civil Engineers, Proceedings, 99, No. EM4 (August 1973), 852-866.

22. Darwin, D., and Pecknold, D. A. "Inelastic Model for Cyclic Biaxial Loading of Reinforced Concrete." Department of Civil Engineering, University of Illinois, Urbana, Illinois, Structural Research Series No. 409, 1974.

23. Berg, S. "Nonlinear Finite Element Analysis of Reinforced Concrete Plates." Division of Structural Mechanics, The Norwegian Institute of Technology, Trondhein, Norway, Report No. 73-1, 1973.

24. Berg, S., Bergan, P. G., and Holland, I. "Nonlinear Finite Element Analysis of Reinforced Concrete Plates." Proceedings, Second International Conference on Structural Mechanics in Reactor Technology, Vol. M., Berlin, Germany, September 10-14, 1973.

25. Aldstedt, E. "Nonlinear Analysis of Reinforced Concrete Frames." Division of Structural Mechanics, The Norwegian Institute of Technology, Trondheim, Norway, Report No. 75-1, 1975.

26. Argyris, J. H., Faust, G., Szimmat, J., Waranke, E. P., and William, K. J. "Recent Developments in the Finite Element Analysis of Prestressed Concrete Reactor Vessels." Nuclear Engineering and Design, 28, No. 1 (1974), 41-75.

27. Zienkiewicz, O. C., Owen, D. R. J., Phillips, D. V., and Nayak, G. C. "Finite Element Methods in the Analysis of Reactor Vessels." Nuclear Engineering and Design, 20, No. 2 (1972), 507-541.

28. Valliappan, S., and Nath, P. "Tensile Crack Propagation in Reinforced Concrete Beams--Finite Element Technique." Proceedings, International Conference on Shear, Torsion and Bond in Reinforced Concrete and Prestressed Concrete, Coimbatore: India, January 1969.

29. Valliappan, S., and Doolan, T. F. "Nonlinear Stress Analysis of Reinforced Concrete." Journal of the Structural Division, American Society of Civil Engineers, Proceedings, 98, ST4 (April 1972), 885-897.

30. Suidan, M., and Schnobrich, W. C. "Finite Element Analysis of Reinforced Concrete." Journal of the Structural Division, American Society of Civil Engineers, Proceedings, 99, ST10 (October 1973), 2109-2122.

31. Colville, J., and Abassi, J. "Plane Stress Reinforced Concrete Finite Elements." Journal of the Structural Division, American Society of Civil Engineers, Proceedings, 100, ST5 (May 1974), 1067-1083.

32. Salem, M. H., Mohraz, B. "Nonlinear Analysis of Planar Reinforced Concrete Structures." Department of Civil Engineering, University of Illinois, Urbana, Illinois, Structural Research Series No. 410, 1974.

33. Wanchoo, W. K., and May, G. W. "Cracking Analysis of Reinforced Concrete Plates," Journal of the Structural Division, American Society of Civil Engineers, Proceedings, 101, ST1 (January 1975), 201-215.

34. Scordelis, A. C. "Finite Element Analysis of Reinforced Concrete Structures." Proceedings, Specialty Conference on the Finite Element Method in Civil Engineering, McGill University, Montreal: Canada, June 1-2, 1972.

35. Popovics, S. "A Review of Stress-Strain Relationships for Concrete." American Concrete Institute Journal, Proceedings, 67, No. 3 (March 1970), 243-248.

36. Malvern, L. E. Introduction to the Mechanics of Continuous Medium. Englewood, N.J.: Prentice-Hall Inc., 1969.

37. Calcote, L. R. The Analysis of Laminated Composite Structures. New York: Van Nostrand Reinhold Company, 1969.

38. American Concrete Institute. Building Code Requirements for Reinforced Concrete (ACI 318-71). Detroit, Michigan: American Concrete Institute, 1971.

39. Taylor, H. P. J. "Investigation of Forces Carried Across Cracks in Reinforced Concrete Beams in Shear by Interlock of Aggregate." London, England: Cement and Concrete Association, Technical Report 42.447, 1970.

40. Zienkiewicz, O. C. The Finite Element Method in Engineering Science. 2nd Edition. London, England: McGraw-Hill Publishing Company, 1971.

41. Holland, I., and Bell, D. Eds. Finite Element Methods in Stress Analysis. Trondheim, Norway: Tapir Forlag, 1970.

42. Tottenham, H., and Brebbia, C. Eds. Finite Element Techniques in Structural Mechanics. Southampton, England: Southampton University Press, 1970.

43. Gallagher, R. H. Finite Element Analysis Fundamentals. Englewood Cliffs, N.J.: Prentice-Hall Inc., 1975.

44. Martin, H. C., and Carey, G. F. Introduction to Finite Element Analysis: Theory and Application. New York: McGraw-Hill Book Company, Inc., 1973.

45. Oden, J. T. Finite Elements of Nonlinear Continua. New York: McGraw-Hill Book Company, 1972.

46. Bathe, K. J., and Ramn, E., and Wilson, E. L. "Finite Element Formulations for Large Strain and Large Displacement Analysis." Division of Structural Engineering and Structural Mechanics, Department of Civil Engineering, University of California, Berkeley, California, SESM Report No. 73-14, 1973.

47. Hibbit, H. D., Marcal, P. V., and Rice, J. R. "A Finite Element Formulation for Problems of Large Strain and Large Displacement." International Journal of Solids and Structures, 6, No. 8 (August 1970), 1069-1086.

48. Fung, Y. C. Foundations of Solid Mechanics. Englewood Cliffs, N.J.: Prentice-Hall, Inc., 1965.

49. Bathe, K. J., Ozdemir, H., and Wilson, E. L. "Static and Dynamic Geometric and Material Nonlinear Analysis." Division of Structural Engineering and Structural Mechanics, Department of Civil Engineering, University of California, Berkeley, California, SESM Report No. 74-4, 1974.

50. Mondkar, D. P. "Static and Dynamic Analysis of Nonlinear Structures." Earthquake Engineering Research Center, College of Engineering, University of California, Berkeley, California, EERC 75-10, 1975.

51. Rajasekaran, S., and Murray, D. W. "Incremental Finite Element Matrices." Journal of the Structural Division, American Society of Civil Engineers, Proceedings, 99, ST12 (December 1973), 2423-2438.

52. Felippa, C. A. (Discussion) "Incremental Finite Element Matrices." Journal of the Structural Division, American Society of Civil Engineers, Proceedings, 100, ST12 (December 1974), 2521-2523.

53. Sabir, A. B., and Lock, A. C. "The Application of Finite Elements to the Large Deflection Geometrically Nonlinear Behavior of Cylindrical Shells." In Variational Methods in Engineering, Vol. 2, C. A. Brebbia and H. Tottenham, Eds. Southampton, England: Southampton University Press, 1973, pp. 7.66-7.75.

54. Gallagher, R. H., Gellatly, R. A., Padlog, J., and Mallet, R. H. "A Discrete Element Procedure for Thin Shell Instability Analysis." American Institute of Aeronautics and Astronautics Journal, 5, No. 1 (January 1967), 138-145.

55. International Mathematical and Statistical Libraries Inc., IMSL Subroutine Library. Ames, Iowa: Iowa State University Computation Center, 1975.

56. Janney, J. R., Hognestad, E., and McHenry, D. "Ultimate Flexural Strength of Prestressed and Conventionally Reinforced Concrete Beams." American Concrete Institute Journal, Proceedings, 27, No. 6 (February 1956), 601-620.

57. Scordelis, A. C., Ngo, D., and Franklin, H. A. "Finite Element Study of Reinforced Concrete Beams with Diagonal Tension Cracks." In Shear in Reinforced Concrete, Vol. 1, American Concrete Institute, Publication SP-42, Detroit, Michigan: 1974, 79-102.

58. Houde, J. and Mirza, M. S. "A Finite Element Analysis of Shear Strength of Reinforced Concrete Beams." In Shear in Reinforced Concrete, Vol. 1, American Concrete Institute, Publication SP-42, Detroit, Michigan: 1974, 103-108.

59. Cardenas, A., and Sozen, M. A. "Strength and Behavior of Isotropically and Nonisotropically Reinforced Concrete Slabs Subjected to Combination of Flexural and Torsional Moments." Department of Civil Engineering, University of Illinois, Urbana, Illinois, Structural Research Series No. 336, 1968.

60. Jofriet, J. C., and McNeice, G. M. "Finite Element Analysis of Reinforced Concrete Slabs." Journal of the Structural Division, American Society of Civil Engineers, Proceedings, 97, No. 3 (March 1971), 785-805.

61. Davies, J. D. "Analysis of Corner Supported Rectangular Slabs." The Structural Engineer, 48, No. 2 (February 1970), 75-82.

62. McNeice, G. M., and Kemp, K. O. "Comparison of Finite Element and Unique Limit Analysis Solutions for Certain Reinforced Concrete Slabs." Institution of Civil Engineers, England, Proceedings, 43, (August 1969), 629-640.

63. Taylor, R., Maher, D. R. H., and Hayes, B. "Effect of the Arrangement of Reinforcement on the Behavior of Reinforced Concrete Slabs." Magazine of Concrete Research, 18, No. 55 (June 1966), 85-94.

64. Timoshenko, S., and Woinowsky-Krieger, S. Theory of Plates and Shells. 2nd Edition, New York: McGraw-Hill Book Company, Inc., 1959.

65. Brebbia, C., and Connor, J. "Geometrically Nonlinear Finite Element Analysis." Journal of the Engineering Mechanics Division, American Society of Civil Engineers, Proceedings, 95, No. EM2 (April 1969), 463-483.

66. Adotte, G. "Second Order Theory in Orthotropic Plates." Journal of the Structural Division, American Society of Civil Engineers, Proceedings, 93, No. ST5 (October 1967),

67. McGregor, J. G., Breen, J. E., and Pfrang, E. O. "Design of Slender Concrete Columns." American Concrete Institute Journal, Proceedings, 67, No. 1 (January 1970), 6-28.

68. Martin, I., and Olivieri, E. "Test of Slender Reinforced Concrete Columns Bent in Double Curvature." In Symposium on Reinforced Concrete Columns, American Concrete Institute, Publication SP-13, Detroit, Michigan: 1966, 121-138.

69. Breen, J. E., and Ferguson, P. M. "Long Cantilever Columns Subjected to Lateral Forces." Part 1 and Part 2. American Concrete Institute Journal, Proceedings, 66, No. 11 (November 1969), 884-893.

ACKNOWLEDGMENTS

APPENDIX: EXPLICIT FORMS OF THE MATRICES IN THE FINITE ELEMENT FORMULATION

Explicit forms for a number of expressions for the rectangular finite element used in this study are presented in this Appendix. The rectangular finite element has both membrane and bending stiffness. The assumed displacement functions for the inplane displacements u and v are as follows:

$$
\begin{array}{cc}
1 \cdot \alpha_1 & 1 \cdot \alpha_5 \\
x \cdot \alpha_2 \qquad y \cdot \alpha_3 & x \cdot \alpha_6 \qquad y \cdot \alpha_7 \qquad (A.1) \\
xy \cdot \alpha_4 & xy \cdot \alpha_8
\end{array}
$$

u-displacement   v-displacement

The assumed displacement function for the out of plane displacement w is given by

$$
\begin{array}{c}
1 \cdot \alpha_9 \\
x \cdot \alpha_{10} \qquad y \cdot \alpha_{11} \\
x^2 \cdot \alpha_{12} \qquad xy \cdot \alpha_{13} \qquad y^2 \cdot \alpha_{14} \qquad (A.2) \\
x^3 \cdot \alpha_{15} \qquad x^2 y \cdot \alpha_{16} \qquad xy^2 \cdot \alpha_{17} \qquad y^3 \cdot \alpha_{18} \\
x^3 y \cdot \alpha_{19} \qquad xy^3 \cdot \alpha_{20}
\end{array}
$$

where the α's are the generalized displacement parameters. The relation between α's and the nodal displacements r is given by,

$$
\alpha = C^{-1} r \qquad (A.3)
$$

where C^{-1} is a function only of element dimensions. For con-

venience the explicit forms of C^{-1} for inplane displacements and out of plane displacements are given in two separate tables, Table 1 and Table 2, respectively. The matrices given in Table 1 and Table 2 are combined to form a single C^{-1} matrix. The actual form of the combined C^{-1} matrix will depend upon the order of the listing of nodal displacements. In the numerical calculations all of the nodal displacements were listed in the order as given by equations 3.4 and 3.5.

The relationship between the displacement gradient vector d and the generalized displacement parameters α is given by the relation

$$d = D\alpha \qquad (A.4)$$

The explicit form of equation A.4 is given in Table 3. The expression for the basic stiffness matrix as given by equation 3.32 is

$$K_0 = \int_V C^{-1^T} D^T (c_{ij} L_1 L_j^m) \, D \, C^{-1} \cdot dv \qquad (A.5)$$

Equation A.5 can be rewritten as,

$$K_0 = C^{-1^T} \int_{Area} [D^T \int_z (c_{ij} L_i L_j^T) \cdot dz \cdot D \cdot dA] \, C^{-1} \qquad (A.6)$$

The innermost integral over the depth is replaced by an integration of the individual layer and a summation of all the layers. Defining a $\hat{K}_0$ matrix for the innermost integral we get

$$\hat{K}_0 = \sum_{\substack{All \\ layers}} \int_{h_j}^{h_{j+1}} (c_{ij} L_i L_j^T) \, dz \qquad (A.7)$$

The explicit form of the $\hat{K}_0$ matrix is given in Table 4. Pre and post multiplying $\hat{K}_0$ matrix by D^T and D, respectively, and integrating over the area according to equation A.6 we get

$$K1 = \int_{Area} D^T \hat{K}_0 D \cdot dA \tag{A.8}$$

where K1 is a 20 x 20 matrix. The explicit form of K1 is lengthy and is given in Fortran Code form in Table 5. The basic stiffness matrix K_0 (equation A.6) was obtained by pre and post multiplying K1 by C^{-1^T} and C^{-1}, respectively, during the course of numerical calculations. In the computer coding K1(20 x 20) was treated as a work space and the same space was used in the generation of the initial stress and the initial displacement matrices. Hence, the use of the same notations for K1 in Tables 5, 7 and 9.

The initial stress matrix as defined by equation 3.29 is

$$K_\sigma = \int_V C^{-1^T} D^T H_i D C^{-1} \cdot \sigma_i \cdot dv \tag{A.9}$$

Equation A.9 can be rewritten as

$$K_\sigma = C^{-1^T} \int_{Area} D^T \int_z (H_i \sigma_i) \, dz \cdot D \cdot dA \cdot C^{-1} \tag{A.10}$$

Defining the innermost integral as $\hat{K}_\sigma$, we get

$$\hat{K}_\sigma = \int_z H_i \sigma_i \cdot dz \tag{A.11}$$

Equation A.11 is integrated using the layered discretization and the $\hat{K}_\sigma$ matrix is given in Table 6. Assuming that the stress resultants N_x, N_y and N_{xy} evaluated at the centroid are

constant over the area we get,

$$K_\sigma = C^{-1^T} K1 C^{-1} \tag{A.12}$$

where K1 is defined by the following equation,

$$K1 = \int_{Area} D^T \hat{K}_\sigma D \cdot dA \tag{A.13}$$

The K1 matrix defined by equation A.13 is given in Table 7 in Fortran Code form. The premultiplication and the postmultiplication of K1 by C^{-1^T} and C^{-1} was done during the course of the numerical calculations.

The initial displacement matrix is given by

$$K_D = K_1 + K_1^T + K_2 \tag{A.14}$$

where

$$K_1 = \int_v C^{-1^T} D^T c_{ij} L_i \, {}^1r^T C^{-1^T} D^T H_j D C^{-1} \cdot dv \tag{A.15}$$

$$K_2 = \int_v C^{-1^T} D^T H_i D C^{-1} \, {}^1r \, c_{ij} \, {}^1r^T C^{-1^T} D^T H_j D C^{-1} \cdot dv \tag{A.16}$$

From equation 3.17, equations A.15 and A.16 can be rewritten as

$$K_1 = \int_v C^{-1^T} D^T c_{ij} L_i \, {}^1d^T H_j D C^{-1} \cdot dv \tag{A.17}$$

$$K_2 = \int_v C^{-1^T} D^T H_i \, {}^1d \, c_{ij} \, {}^1d^T H_j D C^{-1} \cdot dv \tag{A.18}$$

where ${}^1d^T$ is the total displacement gradient vector at the start of the increment.

Considering first the K_1 matrix and defining a $\hat{K}_1$ matrix

we get

$$K_1 = C^{-1^T} \int_{Area} D^T \hat{K}_1 D \cdot dA \cdot C^{-1} \qquad (A.19)$$

where,

$$\hat{K}_1 = \int_z L_i c_{ij}{}^{-1} d^T H_j \cdot dz \qquad (A.20)$$

The $\hat{K}_1$ matrix is given in Table 8. The quantities $w,_x$ and $w,_y$ in Table 8 are evaluated at the centroid of the element.

Equation A.19 can be rewritten as

$$K_1 = C^{-1^T} K1 \, C^{-1} \qquad (A.21)$$

where,

$$K1 = \int_{Area} D^T \hat{K}_1 D \cdot dA \qquad (A.22)$$

K1 matrix is given in Table 9 in Fortran Code form.

Considering next the K_2 matrix, equation A.18 can be rewritten as

$$K_2 = C^{-1^T} \int_{Area} D^T \hat{K}_2 D \cdot dA \qquad (A.23)$$

where,

$$\hat{K}_2 = \int_z H_i{}^{-1} d \, c_{ij}{}^{-1} d^T H_j \cdot dz \qquad (A.24)$$

The $\hat{K}_2$ matrix is given in Table 10. The quantities $w,_x$ and $w,_y$ in Table 10 are evaluated at the centroid of the element. Equation A.23 can be rewritten as,

$$K_2 = C^{-1^T} K1 \, C^{-1} \qquad (A.25)$$

where

$$K1 = \int_{Area} D^T \hat{K}_2 D \cdot dA \qquad (A.26)$$

The matrix K1 is the same as that given in Table 7 except that the values of KA, KB and KC are those for the $\hat{K}_2$ matrix given in Table 10. The K_D matrix is obtained using equation A.14.

Table 1. C^{-1} matrix for inplane displacements

$$\alpha = C^{-1} r$$

	1	2	3	4	5	6	7	8	
α_1	1	·	·	·	·	·	·	·	u_1
α_2	$-\dfrac{1}{a}$	·	$\dfrac{1}{a}$	·	·	·	·	·	v_1
α_3	$-\dfrac{1}{b}$	·	·	·	·	·	$\dfrac{1}{b}$	·	u_2
α_4	$\dfrac{1}{ab}$	·	$-\dfrac{1}{ab}$	·	$\dfrac{1}{ab}$	·	$-\dfrac{1}{ab}$	·	v_2
α_5	·	1	·	·	·	·	·	·	u_3
α_6	·	$-\dfrac{1}{a}$	·	$\dfrac{1}{a}$	·	·	·	·	v_3
α_7	·	$-\dfrac{1}{b}$	·	·	·	·	·	$\dfrac{1}{b}$	u_4
α_8	·	$\dfrac{1}{ab}$	·	$-\dfrac{1}{ab}$	·	$\dfrac{1}{ab}$	·	$-\dfrac{1}{ab}$	v_4

where $\alpha = $ (left column vector) and the right column vector $\cdot$ (u, v terms).

Table 2. C^{-1} matrix for out of plane displacements

$$\alpha = C^{-1} r$$

	1	2	3	4	5	6	7	8	9	10	11	12
α_9	1	·	·	·	·	·	·	·	·	·	·	·
α_{10}	·	1	·	·	·	·	·	·	·	·	·	·
α_{11}	·	·	1	·	·	·	·	·	·	·	·	·
α_{12}	$-\dfrac{3}{a^2}$	$-\dfrac{2}{a}$	·	$\dfrac{3}{a^2}$	$-\dfrac{1}{a}$	·	·	·	·	·	·	·
α_{13}	$-\dfrac{1}{ab}$	$-\dfrac{1}{b}$	$-\dfrac{1}{a}$	$\dfrac{1}{ab}$	·	$\dfrac{1}{a}$	$-\dfrac{1}{ab}$	·	·	$\dfrac{1}{ab}$	$\dfrac{1}{b}$	·

Right-hand side vector: w_1, $w,_{x1}$, $w,_{y1}$, w_2, $w,_{x2}$

$$
\begin{bmatrix} \alpha_{14} \\ \alpha_{15} \\ \alpha_{16} \\ \alpha_{17} \\ \alpha_{18} \\ \alpha_{19} \\ \alpha_{20} \end{bmatrix}
=
\begin{bmatrix}
-\dfrac{3}{b^2} & \cdot & -\dfrac{2}{b} & \cdot & \cdot & \cdot & \cdot & \cdot & \cdot & \dfrac{3}{b^2} & \cdot & -\dfrac{1}{b} \\[2ex]
\dfrac{2}{a^3} & \dfrac{1}{a^2} & \cdot & -\dfrac{2}{a^3} & \dfrac{1}{a^2} & \cdot & \cdot & \cdot & \cdot & \cdot & \cdot & \cdot \\[2ex]
\dfrac{3}{a^2 b} & \dfrac{2}{ab} & \cdot & -\dfrac{3}{a^2 b} & \dfrac{1}{ab} & \cdot & \dfrac{3}{a^2 b} & -\dfrac{1}{ab} & \cdot & -\dfrac{3}{a^2 b} & -\dfrac{2}{ab} & \cdot \\[2ex]
\dfrac{3}{ab^2} & \cdot & \dfrac{2}{ab} & -\dfrac{3}{ab^2} & \cdot & -\dfrac{2}{ab} & \dfrac{3}{ab^2} & \cdot & -\dfrac{1}{ab} & -\dfrac{3}{ab^2} & \cdot & \dfrac{1}{ab} \\[2ex]
\dfrac{2}{b^3} & \cdot & \dfrac{1}{b^2} & \cdot & \cdot & \cdot & \cdot & \cdot & \cdot & -\dfrac{2}{b^3} & \cdot & \dfrac{1}{b^2} \\[2ex]
-\dfrac{2}{a^3 b} & -\dfrac{1}{a^2 b} & \cdot & \dfrac{2}{a^3 b} & -\dfrac{1}{a^2 b} & \cdot & -\dfrac{2}{a^3 b} & \dfrac{1}{a^2 b} & \cdot & \dfrac{2}{a^3 b} & \dfrac{1}{a^2 b} & \cdot \\[2ex]
-\dfrac{2}{ab^3} & \cdot & -\dfrac{1}{ab^2} & \dfrac{2}{ab^3} & \cdot & \dfrac{1}{ab^2} & -\dfrac{2}{ab^3} & \cdot & \dfrac{1}{ab^2} & \dfrac{2}{ab^3} & \cdot & -\dfrac{1}{ab^2}
\end{bmatrix}
\cdot
\begin{bmatrix} w,_{y2} \\ w_3 \\ w,_{x3} \\ w,_{y3} \\ w_4 \\ w,_{x4} \\ w,_{y4} \end{bmatrix}
$$

Table 3. D matrix

	1	2	3	4	5	6	7	8	9	10
$u,_x$	·	1	·	y	·	·	·	·	·	·
$u,_y$	·	·	1	x	·	·	·	·	·	·
$v,_x$	·	·	·	·	·	1	·	y	·	·
$v,_y$	·	·	·	·	·	·	1	x	·	·
$w,_x$	·	·	·	·	·	·	·	·	·	1
$w,_y$	·	·	·	·	·	·	·	·	·	·
$w,_{xx}$	·	·	·	·	·	·	·	·	·	·
$w,_{yy}$	·	·	·	·	·	·	·	·	·	·
$w._{xy}$	·	·	·	·	·	·	·	·	·	·

d   D

11	12	13	14	15	16	17	18	19	20
·	·	·	·	·	·	·	·	·	·
·	·	·	·	·	·	·	·	·	·
·	·	·	·	·	·	·	·	·	·
·	·	·	·	·	·	·	·	·	·
·	$2x$	y	·	$3x^2$	$2xy$	y^2	·	$3x^2y$	y^3
1	·	x	$2y$	·	x^2	$2xy$	$3y^2$	x^3	$3xy^2$
·	2	·	·	$6x$	$2y$	·	·	$6xy$	·
·	·	·	2	·	·	$2x$	$6y$	·	$6xy$
·	·	1	·	·	$2x$	$2y$	·	$3x^2$	$3y^2$

$$
\begin{bmatrix} \alpha_1 \\ \alpha_2 \\ \alpha_3 \\ \alpha_4 \\ \vdots \\ \alpha_{20} \end{bmatrix}
$$

α

Table 4. $\hat{K}_0$ matrix (summation of all layers)

1	2	3	4	5	6	7	8	9	
$c_{11}\cdot t_j$ (K11)	$c_{13}\cdot t_j$ (K12)	$c_{13}\cdot t_j$ (K13)	$c_{12}\cdot t_j$ (K14)	.	.	$-c_{11}\cdot HJS$ (K17)	$-c_{12}\cdot HJS$ (K18)	$-c_{13}\cdot\frac{HJS}{2}$ (K19)	1
	$c_{33}\cdot t_j$ (K22)	$c_{33}\cdot t_j$ (K23)	$c_{23}\cdot t_j$ (K24)	.	.	$-c_{13}\cdot HJS$ (K27)	$-c_{23}\cdot HJS$ (K28)	$-c_{33}\cdot\frac{HJS}{2}$ (K29)	2
		$c_{33}\cdot t_j$ (K33)	$c_{23}\cdot t_j$ (K34)	.	.	$-c_{13}\cdot HJS$ (K37)	$-c_{23}\cdot HJS$ (K38)	$-c_{33}\cdot\frac{HJS}{2}$ (K39)	3
			$c_{22}\cdot t_j$ (K44)	.	.	$-c_{21}\cdot HJS$ (K47)	$-c_{22}\cdot HJS$ (K48)	$-c_{23}\cdot\frac{HJS}{2}$ (K49)	4
Symmetric				.	.	.	.	.	5
					.	.	.	.	6
						$c_{11}\cdot HJC$ (K77)	$c_{12}\cdot HJC$ (K78)	$c_{13}\cdot\frac{HJC}{2}$ (K79)	7
							$c_{22}\cdot HJC$ (K88)	$c_{23}\cdot\frac{HJC}{2}$ (K89)	8
								$c_{33}\cdot\frac{HJC}{4}$ (K99)	9

$$HJS = \frac{h_{j+1}^2 - h_j^2}{2} \quad ; \quad HJC = \frac{h_{j+1}^3 - h_j^3}{3}$$

Table 5. K1 matrix in the development of basic stiffness matrix

```
*********************************************************************

IMPLICIT REAL * 8 (A-H,K,O-Z)

A- X DIMENSION OF THE ELEMENT
B- Y DIMENSION OF THE ELEMENT
AR- AREA OF THE ELEMENT
ARA=AR*A
ARB=AR*B
AR2=AR*AR
ARA2=AR*A*A
ARB2=AR*B*B
AR2B=AR2*B
AR2A=AR2*A
ARA3=ARA2*A
ARB3=ARB2*B
AR2A2=AR*ARA2
AR2B2=AR*ARB2
A2=A*A
B2=B*B
A3=A2*A
B3=B2*B
K11,K12,K13 . . . .K99 ETC. ARE DEFINED IN TABLE 4.
*********************************************************************

    DO 15 I=1,20
    DO 15 J=1,20
15  K1(I,J)=0.D0

    K1(2,2)   =K11*AR
    K1(2,3)   =K12*AR
    K1(2,4)   =(K11*ARB+K12*ARA)*0.5D0
```

Table 5. (Continued)

```
K1(2,6)   =K12*AR
K1(2,7)   =K14*AR
K1(2,8)   =(K12*ARB+K14*ARA)*0.5D0
K1(2,12)  =K17*AR*2.D0
K1(2,13)  =K19*AR
K1(2,14)  =K18*AR*2.D0
K1(2,15)  =K17*ARA*3.D0
K1(2,16)  = K17*ARB+K19*ARA
K1(2,17)  =K18*ARA+K19*ARB
K1(2,18)  =K18*ARB*3.D0
K1(2,19)  =K17*AR2*1.5D0+K19*ARA2
K1(2,20)  =K18*AR2*1.5D0+K19*ARB2
K1(3,3)   =K22*AR
K1(3,4)   =(K12*ARB+K22*ARA)*0.5D0
K1(3,6)   =K22*AR
K1(3,7)   =K24*AR
K1(3,8)   =(K22*ARB+K24*ARA)*0.5D0
K1(3,12)  =K27*AR*2.D0
K1(3,13)  =K29*AR
K1(3,14)  =K28*AR*2.D0
K1(3,15)  =K27*ARA*3.D0
K1(3,16)  = K27*ARB+K29*ARA
K1(3,17)  =K28*ARA+K29*ARB
K1(3,18)  =K28*ARB*3.D0
K1(3,19)  =K27*AR2*1.5D0+K29*ARA2
K1(3,20)  =K28*AR2*1.5D0+K29*ARB2
K1(4,4)   =(K11*ARB2+K22*ARA2+K12*AR2*1.5D0)/3.D0
K1(4,6)   =(K12*ARB+K22*ARA)*0.5D0
K1(4,7)   =(K14*ARB+K24*ARA)*0.5D0
K1(4,8)   =K12*ARB2/3.D0+K14*ARA2/4.D0+K22*ARA2/4.D0+K24*ARA2/3.D0
K1(4,12)  =K17*ARB+K27*ARA
K1(4,13)  =(K19*ARB+K29*ARA)*0.5D0
```

Table 5. (Continued)

```
K1(4,14)  =K18*ARB+K28*ARA
K1(4,15)  =K17*AR2*1.5D0+K27*ARA2*2.D0
FRAC=2.D0/3.D0
K1(4,16)  =K17*ARB2*FRAC+K19*AR2*0.5D0+K27*AR2*0.5D0+K29*ARA2*FRAC
K1(4,17)  =K18*AR2*0.5D0+K19*ARB2*FRAC+K28*ARA2*FRAC+K29*AR2*0.5D0
K1(4,18)  =K18*ARB2*2.D0+K28*AR2*1.5D0
K1(4,19)  =K17*AR2B+K19*AR2A*0.5D0+K27*AR2A+K29*ARA3*0.75D0
K1(4,20)  =K18*AR2B+K19*ARB3*0.75D0+K28*AR2A+K29*AR2B*0.5D0
K1(6,6)   =K22*AR
K1(6,7)   =K24*AR
K1(6,8)   =(K22*ARB+K24*ARA)*0.5D0
K1(6,12)  =K27*AR*2.D0
K1(6,13)  =K29*AR
K1(6,14)  =K28*AR*2.D0
K1(6,15)  =K27*ARA*3.D0
K1(6,16)  =K27*ARB+K29*ARA
K1(6,17)  =K28*ARA+K29*ARB
K1(6,18)  =K28*ARB*3.D0
K1(6,19)  =K27*AR2*1.5D0+K29*ARA2
K1(6,20)  =K28*AR2*1.5D0+K29*ARB2
K1(7,7)   =K44*AR
K1(7,8)   =(K24*ARB+K44*ARA)*0.5
K1(7,12)  =K18*AR*2.D0
K1(7,13)  =K49*AR
K1(7,14)  =K48*AR*2.D0
K1(7,15)  =K18*ARA*3.D0
K1(7,16)  =K18*ARB+K49*ARA
K1(7,17)  =K48*ARA+K49*ARB
K1(7,18)  =K48*ARB*3.D0
K1(7,19)  =K18*AR2*1.5D0+K49*ARA2
K1(7,20)  =K48*AR2*1.5D0+K49*ARB2
K1(8,8)   =(K22*ARB2+K44*ARA2+K24*AR2*1.5D0)/3.D0
```

Table 5. (Continued)

```
KI(8,12)  =K27*ARB+K18*ARA
KI(8,13)  =(K29*ARB+K49*ARA)*0.5D0
KI(8,14)  =K28*ARB+K48*ARA
KI(8,15)  =K27*AR2*1.5D0+K18*ARA2*2.D0
KI(8,16)  =K27*ARB2*FRAC+K29*AR2*0.5D0+K18*AR2*.5D0+K49*ARA2*FRAC
KI(8,17)  =K28*AR2*0.5D0+K29*ARB2*FRAC+K48*ARA2*FRAC+K49*AR2*0.5D0
KI(8,18)  =K28*ARB2*2.0D0+K48*AR2*1.5D0
KI(8,19)  =K27*AR2B+K29*AR2A*0.5D0+K18*AR2A+K49*ARA3*0.75D0
KI(8,20)  =K28*AR2B+K29*ARB3*0.75D0+K48*AR2A+K49*AR2B*0.5D0
KI(12,12)=K77*AR*4.D0
KI(12,13)=K79*AR*2.D0
KI(12,14)=K78*AR*4.D0
KI(12,15)=K77*ARA*6.D0
KI(12,16)=K77*ARB*2.D0+K79*ARA*2.D0
KI(12,17)=K78*ARA*2.D0+K79*ARB*2.D0
KI(12,18)=K78*ARB*6.D0
KI(12,19)=K77*AR2*3.D0+K79*ARA2*2.D0
KI(12,20)=K78*AR2*3.D0+K79*ARB2*2.D0
KI(13,13)=K99*AR
KI(13,14)=K89*AR*2.D0
KI(13,15)=K79*ARA*3.D0
KI(13,16)=K79*ARB+K99*ARA
KI(13,17)=K89*ARA+K99*ARB
KI(13,18)=K89*ARB*3.D0
KI(13,19)=K79*AR2*1.5D0+K99*ARA2
KI(13,20)=K89*AR2*1.5D0+K99*ARB2
KI(14,14)=K88*AR*4.D0
KI(14,15)=K78*ARA*6.D0
KI(14,16)=K78*ARB*2.D0+K89*ARA*2.D0
KI(14,17)=(K88*ARA+K89*ARB)*2.D0
KI(14,18)=K88*ARB*6.D0
KI(14,19)=K78*AR2*3.D0+K89*ARA2*2.D0
```

Table 5. (Continued)

```
K1(14,20)=K88*AR2*3.D0+K89*ARB2*2.D0
K1(15,15)=K77*ARA2*12.D0
K1(15,16)=K77*AR2*3.D0+K79*ARA2*4.D0
K1(15,17)=K78*ARA2*4.D0+K79*AR2*3.D0
K1(15,18)=K78*AR2*9.D0
K1(15,19)=K77*AR2A*6.D0+K79*ARA3*4.5D0
K1(15,20)=K78*AR2A*6.D0+K79*AR2B*3.D0
K1(16,16)=K77*ARB2*2.D0*FRAC+K79*AR2*2.D0+K99*ARA2*2.D0*FRAC
K1(16,17)=K78*AR2+K79*ARB2*2.D0*FRAC+K89*ARA2*2.D0*FRAC+K99*AR2
K1(16,18)=K78*ARB2*4.D0+K89*AR2*3.D0
K1(16,19)=K77*AR2B*2.D0+K79*AR2A*3.D0+K99*ARA3*1.5D0
K1(16,20)=K78*AR2B*2.D0+K79*ARB3*1.5D0+K89*AR2A*2.D0+K99*AR2B
K1(17,17)=K88*ARA2*2.D0*FRAC+K89*AR2*2.D0+K99*ARB2*2.D0*FRAC
K1(17,18)=K88*AR2*3.D0+K89*ARB2*4.D0
K1(17,19)=K78*AR2A*2.D0+K89*ARA3*1.5D0+K79*AR2B*2.D0+K99*AR2A
K1(17,20)=K88*AR2A*2.D0+K89*ARB3*3.D0+K89*AR2B*2.D0+K99*AR2A
K1(18,18)=K88*ARB2*12.D0
K1(18,19)=K78*AR2B*6.D0+K89*AR2A*3.D0
K1(18,20)=K88*AR2B*6.D0+K89*ARB3*4.5D0
K1(19,19)=K77*AR2*AR*4.D0+K79*AR2A2*4.5D0+K99*ARA3*A*9.D0/5.D0
K1(19,20)=K78*AR2*AR*4.D0+K79*AR2B2*2.25D0+K89*AR2A2*2.25D0+K99*AR
1*AR2
K1(20,20)=K88*AR2*AR*4.D0+K89*AR2B2*4.5D0+K99*ARB3*B*9.D0/5.D0

      DO 16 I=2,20
      J1=I-1
      DO 16 J=1,J1
   16 K1(I,J)=K1(J,I)
```

Table 6. $\widehat{K}_\sigma$ matrix

	1	2	3	4	5	6	7	8	9	
	·	·	·	·	·	·	·	·	·	1
	·	·	·	·	·	·	·	·	·	2
	·	·	·	·	·	·	·	·	·	3
	·	·	·	·	·	·	·	·	·	4
	·	·	·	·	N_x (KA)	N_{xy} (KC)	·	·	·	5
	·	·	·	·	N_{xy} (KC)	N_y (KB)	·	·	·	6
	·	·	·	·	·	·	·	·	·	7
	·	·	·	·	·	·	·	·	·	8
	·	·	·	·	·	·	·	·	·	9

Table 7. K1 matrix in the development of initial stress matrix

```
***************************************************************

IMPLICIT REAL * 8 (A-F,K,C-Z)

A- X DIMENSICN OF THE ELEMENT
B- Y DIMENSICN OF THE ELEMENT
AR- AREA OF THE ELEMENT
ARA=AR*A
ARB=AR*B
AR2=AR*AR
ARA2=AR*A*A
ARB2=AR*B*B
AR2B=AR2*B
AR2A=AR2*A
ARA3=ARA2*A
ARB3=ARB2*B
AR2A2=AR*ARA2
AR2B2=AR*ARB2
A2=A*A
B2=B*B
A3=A2*A
B3=B2*B
AR3=AR2*AR
AR4=AR3*AR
ARA4=ARA3*A
ARB4=ARB3*B
ARA5=ARA4*A
ARB5=ARB4*B
ARA6=ARA5*A
ARB6=ARB5*B
AR3A=AR2A*AR
AR3B=AR2B*AR
```

Table 7. (Continued)

───

```
AR3A2=AR3A*A
AR3B2=AR3B*B
AR2A3=AR2A2*A
AR2B3=AR2B2*B
AR2A4=AR2A3*A
AR2B4=AR2B3*B
KA,KB,AND KC ARE DEFINED IN TABLE 6.
*****************************************************************

      DO 100   I=1,20
      DO 100   J=1,20
100   K1(I,J)=0.D0

      K1(10,10)  =  KA*AR
      K1(10,11)  =  KC*AR
      K1(10,12)  =  KA*ARA
      K1(10,13)  =  KA*ARB*.5D0+KC*ARA*.5D0
      K1(10,14)  =  KC*ARB
      K1(10,15)  =  KA*ARA2
      K1(10,16)  =  KA*AR2*.5D0+KC*ARA2/3.D0
      K1(10,17)  =  KA*ARB2/3.D0+KC*AR2*.5D0
      K1(10,18)  =  KC*ARB2
      K1(10,19)  =  KA*AR2A*.5D0+KC*ARA3*.25D0
      K1(10,20)  =  KA*ARB3*.25D0+KC*AR2B*0.5D0
      K1(11,11)  =  KB*AR
      K1(11,12)  =  KC*ARA
      K1(11,13)=KC*ARB*.5D0+KB*ARA*.5D0
      K1(11,14)=KB*ARB
      K1(11,15)=KC*ARA2
      K1(11,16)=KC*AR2*.5D0+KB*ARA2/3.D0
      K1(11,17)=KC*ARB2/3.D0+KB*AR2*.5D0
      K1(11,18)=KB*ARB2
```

Table 7. (Continued)

```
K1(11,19)=KC*AR2A*.5D0+KB*AR3A3*.25D0
K1(11,20)=KC*ARB3/4.D0+KB*AR2B*.5D0
K1(12,12)=KA*ARA2*4.D0/3.D0
K1(12,13)=KA*AR2*.5D0+KC*ARA2*2.D0/3.D0
K1(12,14)=KC*AR2
K1(12,15)=KA*ARA3*1.5D0
K1(12,16)=KA*ARZA*2.D0/3.D0+KC*ARA3*.5D0
K1(12,17)=KA*AR2B/3.D0+KC*AR2A*2.D0/3.D0
K1(12,18)=KC*AR2B
K1(12,19)=KA*AR2A2*.75D0+KC*ARA4*.4D0
K1(12,20)=KA*AR2B2*.25D0+KC*AR3*2.D0/3.D0
K1(13,13)=KA*ARB2/3.D0+KC*AR2*.5D0+KB*ARA2/3.D0
K1(13,14)=KC*ARB2*2.D0/3.D0+KB*AR2*0.5D0
K1(13,15)=KA*AR2A*0.5D0+KC*ARA3*0.75D0
K1(13,16)=KA*AR2B/3.D0+KC*AR2A*C.5D0+KB*ARA3*.25D0
K1(13,17)=KA*ARB3*.25D0+KC*AR2B*0.5D0+KB*AR2A/3.D0
K1(13,18)=KC*ARB3*0.75D0+KB*AR2B*0.5D0
K1(13,19)=KA*AR3/3.D0+KC*AR2A2*0.5D0+KB*ARA4*0.2D0
K1(13,20)=KA*ARB4*.2D0+KC*AR2B2*.5D0+KB*AR3/3.D0
K1(14,14)=KB*ARB2*4.D0/3.D0
K1(14,15)=KC*AR2A
K1(14,16)=KC*AR2B*2.D0/3.D0+KB*AR2A/3.D0
K1(14,17)=KC*ARB3*.5D0+KB*AR2B*2.D0/3.D0
K1(14,18)=KB*ARB3*1.5D0
K1(14,19)=KC*AR3*2.D0/3.D0+KB*AR2A2*0.25D0
K1(14,20)=KC*ARB4*.4D0+KB*AR2B2*0.75D0
K1(15,15)=KA*ARA4*9.D0/5.D0
K1(15,16)=KA*AR2A2*0.75D0+KC*ARA4*0.6D0
K1(15,17)=KA*AR3/3.D0+KC*AR2A2*0.75D0
K1(15,18)=KC*AR3
K1(15,19)=KA*AR2A3*0.6D0+KC*ARA5*0.5D0
K1(15,20)=KA*AR3B*0.25D0+KC*AR3A*0.75D0
```

Table 7. (Continued)

```
K1(16,16)=KA*AR3*4.D0/9.D0+KC*AR2A2*0.5D0+KB*ARA4*0.2D0
K1(15,17)=KA*AR2B2*0.25D0+KC*AR3*5.D0/9.D0+KB*AR2A2*0.25D0
K1(16,18)=KC*AR2B2*0.75D0+KB*AR3/3.D0
K1(16,19)=KA*AR3A*0.5D0+KC*AR2A3*0.5D0+KB*ARA5/6.D0
K1(16,20)=KA*AR2B3*0.2D0+KC*AR3B*7.D0/12.D0+KB*AR3A*0.25D0
K1(17,17)=KA*ARB4*0.2D0+KC*AR2B2*0.5D0+KB*AR3*4.D0/9.D0
K1(17,18)=KC*ARB4*0.6D0+KB*AR2B2*0.75D0
K1(17,19)=KA*AR3B*0.25D0+KC*AR3A*7.D0/12.D0+KB*AR2A3*0.2D0
K1(17,20)=KA*AR85/6.D0+KC*AR2B3*0.5D0+KB*AR3B*0.5D0
K1(18,18)=KE*ARB4*9.D0/5.D0
K1(18,19)=KC*AR3B*0.75D0+KB*AR3A*0.25D0
K1(18,20)=KC*ARB5*0.5D0+KB*AR2B3*0.9D0
K1(19,19)=KA*AR3A2*0.6D0+KC*AR2A4*0.5D0+KB*ARA6/7.D0
K1(19,20)=KA*AR3B2*0.2D0+KC*AR4/16.D0+KB*AR3A2*0.2D0
K1(20,20)=KA*ARB6/7.D0+KC*AR2B4*0.5D0+KB*AR3B2*0.6D0

    DO 110 I=2,20
    J1=I-1
    DO 110 J=1,J1
110 K1(I,J)=K1(J,I)
```

Table 8. $\hat{K}_1$ matrix (summation of all layers)[a]

1	2	3	4	5	6	7	8	9	
·	·	·	·	$(c_{11} \cdot w,_x + c_{13} \cdot w,_y)$ $\cdot t_j$ (K15)	$(c_{12} \cdot w,_y + c_{13} \cdot w,_x)$ $\cdot t_j$ (K16)	·	·	·	1
·	·	·	·	$(c_{13} \cdot w,_x + c_{33} \cdot w,_y)$ $\cdot t_j$ (K25)	$(c_{23} \cdot w,_y + c_{33} \cdot w,_x)$ $\cdot t_j$ ((K26)	·	·	·	2
·	·	·	·	$(c_{13} \cdot w,_x + c_{33} \cdot w,_y)$ $\cdot t_j$ (K35)	$(c_{23} \cdot w,_y + c_{33}\, w,_x)$ $\cdot t_j$ (K36)	·	·	·	3
·	·	·	·	$(c_{12} \cdot w,_x + c_{23} \cdot w,_y)$ $\cdot t_j$ (K45)	$(c_{22} \cdot w,_y + c_{23} \cdot w,_x)$ $\cdot t_j$ (K46)	·	·	·	4
·	·	·	·	·	·	·	·	·	5
·	·	·	·	·	·	·	·	·	6
·	·	·	·	$(c_{11} \cdot w,_x + c_{13} \cdot w,_y)$ $.HJS.(-1)$ (K75)	$(c_{12} \cdot w,_y + c_{13} \cdot w,_x)$ $.HJS.(-1)$ (K76)	·	·	·	7

$$(c_{12} \cdot w,_x + c_{23} \cdot w,_y) \quad (c_{22} \cdot w,_y + c_{23} \cdot w,_x)$$

$$\cdots \quad \cdots \quad \cdot \quad \cdot \qquad .HJS.(-1) \qquad\qquad .HJS.(-1) \qquad \cdot \quad \cdot \quad \cdot \qquad 8$$

$$(K85) \qquad\qquad\qquad (K86)$$

$$(c_{13} \cdot w,_x + c_{33} \cdot w,_y) \quad (c_{23} \cdot w,_y + c_{33} \cdot w,_x)$$

$$\cdots \quad \cdots \quad \cdot \quad \cdot \qquad .(-2).HJS \qquad\qquad .(-2).HJS \qquad \cdot \quad \cdot \quad \cdot \qquad 9$$

$$(K95) \qquad\qquad\qquad (K96)$$

$^a t_j$ = thickness of the jth layer; HJS = $\dfrac{h_{j+1}^2 - h_j^2}{2}$.

Table 9. (Continued)

```
AR3A2=AR3A*A
AR3B2=AR3B*B
AR2A3=AR2A2*A
AR2B3=AR2B2*B
AR2A4=AR2A3*A
AR2B4=AR2B3*B
K15,K16,K25,K26......K96 ETC. ARE DEFINED IN TABLE 8.
*************************************************************************

      DO 110 I=1,20
      DO 110 J=1,20
110   K1(I,J)=0.D0

K1(2,10)=K15*AR
K1(2,11)=K16*AR
K1(2,12)=K15*ARA
K1(2,13)=(K15*ARB+K15*ARA)*0.5D0
K1(2,14)=K16*ARB
K1(2,15)=K15*ARA2
K1(2,16)=K15*AR2*.5D0+K16*ARA2/3.D0
K1(2,17)=K15*ARB2/3.D0+K16*AR2*0.5D0
K1(2,18)=K16*ARB2
K1(2,19)=K15*AR2A*0.5D0+K16*ARA3/4.D0
K1(2,20)=K15*ARB3*0.25D0+K15*AR2B*0.5D0
K1(3,10)=K25*AR
K1(3,11)=K26*AR
K1(3,12)=K25*ARA
K1(3,13)=(K25*ARB+K26*ARA)*0.5D0
K1(3,14)=K26*ARB
K1(3,15)=K25*ARA2
K1(3,16)=K25*AR2*.5D0+K26*ARA2/3.D0
K1(3,17)=K25*ARB2/3.D0+K26*AR2*0.5D0
```

Table 9. (Continued)

```
K1(3,18)=K26*ARB2
K1(3,19)=K25*AR2A*0.5D0+K26*ARA3/4.D0
K1(3,20)=K25*ARB3*0.25D0+K26*AR2B*0.5D0
K1(4,10)=(K15*ARB+K25*ARA)*.5D0
K1(4,11)=(K16*ARB+K26*ARA)*.5D0
K1(4,12)=K15*AR2*.5D0+K25*AR2A2*2.D0/3.D0
K1(4,13)=K15*ARB2/3.D0+(K16-K25)*AR2*.25D0+K26*ARA2/3.D0
K1(4,14)=K16*ARB2*2.D0/3.D0+K26*AR2*0.5D0
K1(4,15)=K15*AR2A*.5D0+K25*ARA3*.75D0
K1(4,16)=K15*AR2B/3.D0+(K16/6.D0+K25/3.D0)*AR2A+K26*ARA3*.25D0
K1(4,17)=K15*ARB3*.25D0+(K15/3.D0+K25/6.D0)*AR2B+K26*AR2A/3.D0
K1(4,18)=K16*ARB3*.75D0+K26*AR2B*.5D0
K1(4,19)=K15*AR3/3.D0+(K16/3.D0+K25*3.D0/8.D0)*AR2A2+K26*ARA4*.2D0
K1(4,20)=K15*ARB4*.2D0+(K16*.375D0+K25*.125D0)*AR2B2+K26*AR3/3.D0
K1(6,10)=K35*AR
K1(6,11)=K36*AR
K1(6,12)=K35*ARA
K1(6,13)=(K35*ARB+K36*ARA)*.5D0
K1(6,14)=K36*ARB
K1(6,15)=K35*ARA2
K1(6,16)=K35*AR2*.5D0+K36*ARA2/3.D0
K1(6,17)=K35*ARB2/3.D0+K36*AR2*0.5D0
K1(6,18)=K36*ARB2
K1(6,19)=K35*AR2A*0.5D0+K36*ARA3/4.D0
K1(6,20)=K35*ARB3*0.25D0+K36*AR2B*.5D0
K1(7,10)=K45*AR
K1(7,11)=K46*AR
K1(7,12)=K45*ARA
K1(7,13)=(K45*ARB+K46*ARA)*0.5D0
K1(7,14)=K46*ARB
K1(7,15)=K45*ARA2
K1(7,16)=K45*AR2*.5D0+K46*ARA2/3.D0
```

Table 9.   (Continued)

```
K1(13,16)=K95*AR2*.5D0+K96*ARA2/3.D0
K1(13,17)=K95*ARB2/3.D0+K96*AR2*.5D0
K1(13,18)=K96*ARB2
K1(13,19)=K95*AR2A*.5D0+K96*ARA3/4.D0
K1(13,20)=K95*ARB3*.25D0+K96*AR2B*.5D0
K1(14,10)=K85*AR*2.D0
K1(14,11)=K86*AR*2.D0
K1(14,12)=K85*ARA*2.D0
K1(14,13)=K85*ARB+K86*ARA
K1(14,14)=K86*ARB*2.D0
K1(14,15)=K85*ARA2*2.D0
K1(14,16)=(K85*AR2*.5D0+K86*ARA2/3.D0)*2.D0
K1(14,17)=(K85*ARB2/3.D0+K86*AR2*.5D0)*2.D0
K1(14,18)=K86*ARB2*2.D0
K1(14,19)=(K85*AR2A*.5D0+K86*ARA3/4.D0)*2.D0
K1(14,20)=K85*ARB3*.5D0+K86*AR2B
K1(15,10)=K75*ARA*3.D0
K1(15,11)=K76*ARA*3.D0
K1(15,12)=K75*ARA2*4.D0
K1(15,13)=K75*AR2*1.5D0+K76*ARA2*2.D0
K1(15,14)=K76*AR2*3.D0
K1(15,15)=K75*ARA3*4.5D0
K1(15,16)=K75*AR2A*2.D0+K76*ARA3*1.5D0
K1(15,17)=K75*AR2B+K76*AR2A*2.D0
K1(15,18)=K76*AR2B*3.D0
K1(15,19)=K75*AR2A2*2.25D0+K76*ARA4*1.2D0
K1(15,20)=K75*AR2B2*.75D0+K76*AR3*2.D0
K1(16,10)=K75*ARB+K95*ARA
K1(16,11)=K76*ARB+K96*ARA
K1(16,12)=K75*AR2+K95*ARA2*4.D0/3.D0
K1(16,13)=K75*ARB2*2.D0/3.D0+(K76+K95)*AR2*.5D0+K96*ARA2*2.D0/3.D0
K1(16,14)=K76*ARB2*4.D0/3.D0+K96*AR2
```

Table 9. (Continued)

```
K1(16,15)=K75*AR2A+K95*ARA3*1.5D0
K1(16,16)=K75*AR2B*2.D0/3.D0+(K76/3.D0+K95*2.D0/3.D0)*AR2A+K96*
1 ARA3*.5D0
K1(16,17)=K75*ARB3*.5D0+(K75*2.D0/3.D0+K95/3.D0)*AR2B+K96*AR2A*
12.D0/3.D0
K1(16,18)=K75*ARB3*1.5D0+K95*AR2B
K1(16,19)=K75*AR3*2.D0/3.D0+(K76*.25D0+K95*.75D0)*AR2A2+K96*ARA4*
1.4D0
K1(16,20)=K75*ARB4*.4D0+(K75*.75D0+K95*.25D0)*AR2B2+K96*AR3*2.D0/
13.D0
K1(17,10)=K85*ARA+K95*ARB.
K1(17,11)=K85*ARA+K96*ARB
K1(17,12)=K85*ARA2*4.D0/3.D0+K95*AR2
K1(17,13)=K85*AR2*.5D0+K86*ARA2*2.D0/3.D0+K95*ARB2*2.D0/3.D0+K96*
1AR2*.5D0
K1(17,14)=K86*AR2+K96*ARB2*4.D0/3.D0
K1(17,15)=K85*ARA3*1.5D0+K95*AR2A
K1(17,16)=K85*AR2A*2.D0/3.D0+K86*ARA3*.5D0+K95*AR2B*2.D0/3.D0+K96*
1AR2A/3.D0
K1(17,17)=K85*AR2B/3.D0+K86*AR2A*2.D0/3.D0+K95*ARB3*.5D0+K96*AR2B
1*2.D0/3.D0
K1(17,18)=K86*AR2B+K96*ARB3*1.5D0
K1(17,19)=K85*AR2A2*.75D0+K86*ARA4*.4D0+K95*AR3*2.D0/3.D0+K96*
2AR2A2*.25D0
K1(17,20)=K85*AR2B2*.25D0+K86*AR3*2.D0/3.D0+K95*ARB4*.4D0+K96*AR2B
12*.75D0
K1(18,10)=K85*ARB*3.D0
K1(18,11)=K85*ARB*3.D0
K1(18,12)=K85*AR2*3.D0
K1(18,13)=K85*ARB2*2.D0+K86*AR2*1.5D0
K1(18,14)=K86*ARB2*4.D0
K1(18,15)=K85*AR2A*3.D0
```

Table 9. (Continued)

K1(18,16)=K85*AR2B*2.D0+K86*AR2A
K1(18,17)=K85*ARB3*1.5D0+K85*AR2B*2.D0
K1(18,18)=K85*ARB3*4.5D0
K1(18,19)=K85*AR3*2.D0+K36*AR2A2*.75D0
K1(18,20)=K85*ARB4*1.2D0+K86*AR2B2*2.25D0
K1(19,10)=K75*AR2*1.5D0+K95*ARA2
K1(19,11)=K76*AR2*1.5D0+K96*ARA2
K1(19,12)=K75*AR2A*2.D0+K95*ARA3*1.5D0
K1(19,13)=K75*AR2B+(K76+K95*.5D0)*AR2A+K96*ARA3*.75D0
K1(19,14)=K76*AR2B*2.D0+K96*ARA2
K1(19,15)=K75*AR2A2*2.25D0+K95*ARA4*1.8D0
K1(19,16)=K75*AR3*4.D0/3.D0+(K76+K95)*AR2A2*.75D0+K96*ARA4*.6D0
K1(19,17)=K75*AR2B2*.75D0+(K76*4.D0+K95/3.D0)*AR3+K96*AR2A2*
1.75D0
K1(19,18)=K76*AR2B2*2.25D0+K96*AR3
K1(19,19)=K75*AR3A*1.5D0+(K76*.6D0+K95*.9D0)*AR2A3+K96*ARA5*.5D0
K1(19,20)=K75*AR2B3*.6D0+(K76*1.5D0+K95*.25D0)*AR3B+K96*AR3A*.75D0
K1(20,10)=K85*AR2*1.5D0+K95*ARB2
K1(20,11)=K86*AR2*1.5D0+K96*ARB2
K1(20,12)=K85*AR2A*2.D0+K95*AR2B
K1(20,13)=K85*AR2B+K86*AR2A+K95*ARB3*.75D0+K96*AR2B*.5D0
K1(20,14)=K86*AR2B*2.D0+K96*ARB3*1.5D0
K1(20,15)=K85*AR2A2*2.25D0+K95*AR3
K1(20,16)=K85*AR3*4.D0/3.D0+K86*AR2A2*.75D0+K95*AR2B2*.75D0+K96*
1AR3/3.D0
K1(20,17)=K85*AR2B2*.75D0+K86*AR3*4.D0/3.D0+K95*ARB4*.6D0+K96*
1AR2B2*.75D0
K1(20,18)=K86*AR2B2*2.25D0+K96*ARB4*1.8D0
K1(20,19)=K85*AR3A*1.5D0+K36*AR2A3*.6D0+K95*AR3B*.75D0+K96*AR3A*
1.25D0
K1(20,20)=K85*AR2B3*.6D0+K36*AR3B*1.5D0+K95*ARB5*.5D0+K96*AR2B3*
1.9D0

Table 10. $\hat{\mathcal{R}}_2$ matrix (summation of all layers)[a]

	1	2	3	4	5	6	7	8	9	
	·	·	·	·	·	·	·	·	·	1
	·	·	·	·	·	·	·	·	·	2
	·	·	·	·	·	·	·	·	·	3
	·	·	·	·	·	·	·	·	·	4
	·	·	·	·	KA	KC	·	·	·	5
	·	·	·	·	KC	KB	·	·	·	6
	·	·	·	·	·	·	·	·	·	7
	·	·	·	·	·	·	·	·	·	8
	·	·	·	·	·	·	·	·	·	9

[a] $KA = [c_{11} \cdot (w,_x)^2 + 2 \cdot c_{13} \cdot (w,_x \cdot w,_y) + c_{33} \cdot (w,_y)^2] t_j;$

$KB = [c_{22} \cdot (w,_y)^2 + 2 \cdot c_{23} \cdot (w,_x \cdot w,_y) + c_{33} \cdot (w,_x)^2] t_j;$

$KC = [c_{12} \cdot (w,_x \cdot w,_y) + c_{13} \cdot (w,_x)^2 + c_{23} \cdot (w,_y)^2 + c_{33} \cdot (w,_x \cdot w,_y)] t_j.$